Potential-dependent real-time multidrug sensing with screen printed manganese oxide electrode platform

by

Pheladi Lizzy Mokaba

submitted in accordance with the requirements for
the degree of

MASTER OF SCIENCE

in the subject

CHEMISTRY

at the

UNIVERSITY OF SOUTH AFRICA

SUPERVISOR: PROF USISIPHO FELENI

CO-SUPERVISOR: PROF TITUS A.M. MSAGATI
PROF HLENGILIZWE NYONI

February 2024

Declaration

Name: Pheladi Lizzy Mokaba

Student number: 65975588

Degree: Master of Science: Chemistry

Exact wording of the title of the dissertation as appearing on the electronic copy submitted for examination:

POTENTIAL DEPENDENT REAL TIME MULTIDRUG SENSING WITH SCREEN PRINTED MANGANESE OXIDE ELECTRODE PLATFORM

I declare that the above dissertation is my own work and that all the sources that I have used or quoted have been indicated and acknowledged by means of complete references.

I further declare that I submitted the dissertation to originality checking software and that it falls within the accepted requirements for originality.

I further declare that I have not previously submitted this work, or part of it, for examination at Unisa for another qualification or at any other higher education institution.

(The dissertation will not be examined unless this statement has been submitted.)

SIGNATURE

23 /02/2024

DATE

Acknowledgement

I want to thank the God of Mount Zion from the bottom of my heart for giving me the chance to begin and finish my academic path. Throughout the challenges and triumphs, it has been the divine strength and unwavering support that has sustained me. To the God of Mount Zion, I offer all honour and glory. Your guidance has been a constant presence, providing me with the fortitude to persevere and the resilience to overcome obstacles. In moments of doubt, your grace has been my inspiration to keep going and never give up.

I want to express my sincere gratitude to the supervisor, Prof. Usisipho Feleni, for her outstanding advice, constant assistance, and remarkable knowledge over the whole study process. Her dedication to quality has been the main factor in this work's successful completion. My academic experience has been greatly enhanced by Prof. Feleni's commitment to creating a collaborative and intellectually exciting research environment. I am particularly grateful for the insightful discussions, constructive feedback, and encouragement provided by Prof Feleni. Her mentorship has not only shaped the direction of this research but has also played a pivotal role in my overall academic and professional growth. I have been greatly inspired by Prof. Usisipho Feleni's contributions to the field of electrochemistry and her remarkable career as a woman in science.

My profound gratitude goes out to John Mahlangu, my partner, whose steadfast support has been a pillar of strength during the highs and lows of this scholastic pursuit. Mahlangu’s constant encouragement and understanding have been instrumental in my perseverance and success. In moments of challenge, John's willingness to listen and provide valuable advice has been a beacon of positivity, turning obstacles into opportunities for growth. Their steadfast belief in my abilities and their shared commitment to this journey has made the challenges more surmountable and the victories more meaningful. Beyond the confines of academia, John's presence has brought balance and joy to my life. The sacrifices made and the shared celebrations have created a supportive foundation upon which this academic achievement rests.

I want to thank my mother from the bottom of my heart for her steadfast support during my academic career. Her support has consistently been a source of bravery. In loving memory of my late grandmother, who passed away during my academic journey. I dedicate this work to her, and may her soul continue to rest in peace. Her memory remains a guiding force in my aspirations. I am grateful for my siblings' unwavering support, especially that of my sister. Your support has been as a source of inspiration. My friend deserves special recognition for her steadfast support during this adventure. My success has been greatly aided by our friendship.

My sincere appreciation goes out to the Institute for Nanotechnology and Water Sustainability (iNanoWS) and its hardworking employees for establishing such a welcoming academic setting. Their unwavering support and provision of essential resources have been integral to the successful completion of this research project. A special note of appreciation goes to the institute for the invaluable financial support provided. This support has not only facilitated the execution of this research but has also underscored iNanoWS’ s commitment to fostering meaningful contributions in the field. I want to express my heartfelt gratitude to the iNanoWS lab team for their fantastic support during the trial. Their expertise, guidance, and collaborative spirit have significantly enriched the depth and quality of this work. The collective effort of the lab team has been a driving force behind the successful outcomes of this endeavour.

I would like to thank the Applied Electrochemistry (AEC) Thematic Area for making a significant contribution to my research. Their input, particularly during presentations, has provided essential perspectives and enhanced the overall quality of this research. The engagement and support from the members of the thematic area have been instrumental in refining the ideas presented in this work.

Dedication

This work is dedicated to my mother, Johannah Mmatlala Mokaba, and my late grandmother, Thaitha Mapitsi Mokaba. May her soul rest in peace, Mahlako.

Publications

Pheladi Lizzy Mokaba, Titus A.M. Msagati, Hlengilizwe Nyoni, Bhekie B. Mamba, Usisipho Feleni, Electro-Oxidation of Ibuprofen and Metoprolol using Manganese Oxide Platform, *ChemistrySelect*, accepted 2024.

Pheladi Lizzy Mokaba, Titus A.M. Msagati, Ntuthuko W. Hlongwa, Usisipho Feleni, Manganese oxide based electrochemical sensor for signaling carbamazepine and sulfamethoxazole in wastewater samples, *Electrocatalysis,* under review 2024.

Pheladi Lizzy Mokaba, Titus A.M. Msagati, Usisipho Feleni, Manganese oxide applications in sulfonamides electrochemical sensors: a short review, *Electroanalysis,* submitted 2024.

Pheladi Lizzy Mokaba, Titus A.M. Msagati, Usisipho Feleni, Tin selenide quantum dots application in energy and enzyme- based biosensor for environmental monitoring endocrine disruptors, to be submitted in *Electrochimica Acta*.

Presentations

Pheladi Lizzy Mokaba, Hlengilizwe Nyoni, Titus Msagati, Usisipho Feleni, Integrating passive sampling and electrochemical sensing techniques to monitor developing contaminants in the aquatic environment. **Oral presentation**. April 2021, FameLab SA heat, University of South Africa, South Africa.

Pheladi Lizzy Mokaba, Hlengilizwe Nyoni, Titus A.M. Msagati, Usisipho Feleni, Electro-oxidation of carbamazepine and sulfamethoxazole using a manganese oxide platform. **Oral presentation**. iNanoWS, University of South Africa, South Africa, June 2023.

Pheladi Lizzy Mokaba, Hlengilizwe Nyoni, Titus A.M. Msagati, Usisipho Feleni, Metal oxide electrochemical reactor for the determination of carbamazepine and sulfamethoxazole. **Oral presentation.** The International Water Association Particle Separation Conference, Boksburg, South Africa; Birchwood Hotel and OR Tambo Conference Centre; December 6–8, 2023.

Participation of the enrichment project

Black Women in Science 2023 Fellowship Program, South Africa, completion date: October 2023.

Abstract

Emerging pollutants (EPs) provide a new global water quality concern, potentially posing a major damage to human health and the surrounding. Pharmaceuticals, extensively used in both human and veterinary medicine, have become pervasive environmental contaminants due to their continual release into sewage systems and subsequent ubiquity in various ecosystems. In the ambient matrix, they are often present in small amounts (ng/L to g/L) due to their stable composition and slightly elevated polarization. Traditional methods for detecting pharmaceutical compounds in water have long been hindered by their expense and complexity, making widespread implementation challenging. However, electrochemical sensors offer a promising solution to this problem. These sensors provide a cost-effective, portable, and user-friendly alternative to traditional analytical techniques. This research focuses on the development an electrochemical sensor using a screen-printed manganese oxide electrode platform for the potential-dependent analysis of multiple drugs, including sulfamethoxazole, carbamazepine, metoprolol, and ibuprofen. These substances are critical to monitor due to their widespread presence and potential health implications. The study leveraged the unique properties of MnO_2 nanoparticles, such as their electrochemical activity, large surface area, and catalytic qualities, to enhance the sensitivity and functionality of screen-printed electrodes for the detection of these drugs. The MnO_2 nanoparticles were characterized using a suite of techniques including Fourier-transform infrared spectroscopy (FTIR), X-ray diffraction (XRD), scanning electron microscopy (SEM), UV-visible spectroscopy, small-angle X-ray scattering (SAXS), and Raman spectroscopy. The optical properties of MnO_2NPs were investigated using UV/Vis spectroscopy, covering a wavelength range from 280 to 800 nm. This analysis revealed crucial information about the behaviour of MnO_2NPs in response to light across different wavelengths. Specifically, the band gap of the MnO_2NPs was determined to be 1.14 electron volts (eV) suggests that these nanoparticles possess favourable electrical and optical characteristics. A band gap of this magnitude indicates that MnO_2NPs can effectively absorb light within a certain energy range, making them potentially useful in various applications such as photocatalysis, photovoltaics, and optical sensing. Electrochemical impedance spectroscopy (EIS) and cyclic voltammetry (CV) were employed to investigate the electrochemical behavior of both bare and MnO_2NPs-modified screen-printed electrodes. A comparison between the two revealed significant differences in electron transfer kinetics. In the case of the bare electrode, EIS and CV analyses indicated slower electron transfer kinetics, as evidenced by a peak potential separation of 0.249 V in the CV curve. This separation reflects the energy barrier that electrons must overcome during the redox process. Conversely, for the MnO_2NPs-modified SPCE, the peak potential dispersion was reduced to 0.269 V, suggesting faster electron transfer kinetics. This reduction in peak potential separation indicates a more efficient and rapid reaction occurring at the electrode surface, likely facilitated by the presence of MnO_2NPs. The study investigated the influence of pH, scan speed, and electrolytes to identify optimal experimental conditions. Subsequently, under these ideal circumstances, the electrochemical characteristics of carbamazepine, sulfamethoxazole, ibuprofen, and metoprolol were assessed using differential pulse voltammetry. Calibration curves were constructed for each analyte of interest, enabling the determination of limit of detection. The results revealed limit of detection 0.0005 μM for CBZ, 0.0002 μM for SMX, 0.0004 μM for IBU, and 0.005 μM for MP. These values were derived from the extrapolation of calibration curves, which demonstrated linearity within the range of 0.010 to 0.006 μM. These limits of detection signify the lowest concentrations of each analyte that can be reliably detected and quantified using the DPV technique under the specified experimental conditions. Furthermore, the study conducted stability and interference investigations to evaluate the performance of the MnO_2NPs/SPCE sensor under optimal conditions. These investigations demonstrated satisfactory performance, indicating the sensor's robustness and reliability in real-world applications. The effectiveness of the suggested sensor was validated through its successful application in analysing wastewater samples. This practical testing confirmed the sensor's ability to detect multiple drugs, highlighting its potential accurately and selectively. In conclusion, the study successfully developed an extremely accurate, precise, and selective MnO_2NPs/SPCE sensor for the multidrug detection. By combining the advantages of MnO_2 nanoparticles and screen-printed electrode technology, this sensor offers a cost-effective and efficient solution for environmental monitoring and pharmaceutical analysis.

Keywords

Carbamazepine
Electrochemical sensor
Ibuprofen
Manganese oxide nanoparticle
Metoprolol
Pharmaceuticals
Screen printed electrode.
Sulfamethoxazole

Abbreviations

A	Absorbance
AA	Ascorbic acid
Ag/AgCl	Silver/Silver chloride
APIs	Active pharmaceutical ingredients
BR	Britton robinson
C_2H_5OH	Ethanol
CV	Cyclic voltammetry
CD	Carbon dots
CBZ	Carbamazepine
CE	Counter electrode
DPV	Differential pulse voltammetry
DNA	Deoxyribonucleic acid
ED	Electrochemical deposition
EIS	Electrochemical impedance spectroscopy
EPs	Emerging pollutants
FBS	Fetal bovine serum
FTIR	Fourier transform infrared spectroscopy.
$[Fe\ (CN)_6]^{4-}$	Ferrocyanide
Ga_2O_3	Gallium oxide
GCE	Glassy carbon electrode
GC-MS	Gas chromatography coupled with mass spectroscopy.
GIFT	Generalized indirect fourier transformation.
H_2NaPO_4	disodium hydrogen phosphate dibasic
H_2O	Water
H_2O_2	Hydrogen peroxide
H_2SO_4	Sulphuric acid
HCl	Hydrochloric acid
HEK	Human embryonic kidney
HPLC	High-performance liquid chromatography
HT	Hydrothermal
IBU	Ibuprofen
K^+	Potassium cation
K_2SO_4	Potassium sulphate
KBr	Potassium bromide
$KMnO_4$	Potassium permanganate
kΩ	Kiloohm
LC-MS	Liquid chromatography coupled with mass spectroscopy.
LDH	Lactate dehydrogenase
LLE	Liquid-liquid extraction
LOD	Limit of detection
LSV	Linear sweep voltammetry
M	Molar
mg/L	Milligrams per liter

MIPs	Molecularly imprinted polymers
MnO_2	Manganese oxide
MnO_2NPs	Manganese oxide nanoparticle
$MnSO_4$	Manganese sulphate
MON	Metal-oxide nanoparticle
MRI	Magnetic resonance imaging
MP	Metoprolol
Na^+	Sodium cation
NaOH	Sodium hydroxide
ng/L	Nanogram per liter
NPs	Nanoparticles
NRs	Nanorods
NSAID	Non-steroidal anti-inflammatory drugs
NWs	Nanowires
1D	One dimension
-OH	Hydroxyl
OTC	Over the counter
PBS	Phosphate buffer solution
PDDF	Pair distance distribution function
pH	Potential of hydrogen
Pharm	Pharmaceuticals
Rct	Charge transfer resistance
RE	Reference electrode
RNA	Ribonucleic acid
Rs	Solution resistance
RSD	Relative standard deviation
RT	Room temperature
SAXS	Small angle x-ray scattering spectroscopy.
SEM	Scanning electron microscopy
SERS	Surface-enhanced Raman scattering
SMX	Sulfamethoxazole
SLS	Sodium lauryl sulfate
SnO_2	Tin oxide
SOS	Second-order scattering
SPCE	Screen-printed carbon electrode.
SPE	Solid-phase extraction
SPEs	Screen-printed electrodes.
SPME	Solid phase microextraction
SWV	Square wave voltammetry
2D	Two dimension
3D	Three dimension
TMS	Tetramethoxysilane
TOP	Trioctylphosphine
TSC	Trisodium citrate
UV/Vis	Ultraviolet-visible spectroscopy
µA	Microampere
µg/L	Microgram per liter
µL	Microliter
WE	Working electrode.
WO_2	Tungsten oxide
WWTP	Wastewater treatment plant
XRD	X-Ray diffraction
ZnO	Zinc oxide
Zw	Warburg impedance
α MnO_2	Alpha manganese oxide
β MnO_2	Beta manganese oxide
γ MnO_2	Gamma manganese oxide
δ MnO_2	Delta manganese oxide

Ω Ohm

Table of contents

Contents

List of figures

List of tables

Chapter 1: Introduction

Summary

This section provides a review of new pollutants: medicines, as well as how they infiltrate the environment. The negative consequences of this medicine on both humans and aquatic life. The negative implications of this medicine on both human health and the surrounding. A quick description of the four medications of importance in this investigation, namely carbamazepine, sulfamethoxazole, ibuprofen, and metoprolol, as well as the concentrations recorded in the water bodies. The section also includes the issue description and motivation, goals and objectives, and the thesis summary.

1.1 Emerging pollutants: pharmaceutical pollutants

Emerging pollutants (EPs) provide a new worldwide water safety concern, potentially posing a major damage to human health and the surrounding [1]. EPs are organic and inorganic substances prevalent in the surrounding that may be detrimental to the health of people and animals and are not controlled [2,3]. Insecticides, pharmaceuticals, and personal care products are all examples for developing contaminants [4]. Pharmaceuticals (Pharm) play a crucial role in maintaining human and animal health. However, their widespread use and consumption patterns have resulted in their presence in the aquatic environment [5]. Pharm enter aquatic ecosystems through various pathways, including treated sewage effluent discharge, landfill leaching, and direct discharge from pharmaceutical manufacturing plants as shown in Figure 1.1. Due to their high solubility in water, as well as their chemical stability and low biodegradability, many Pharm persist in the environment once released [6]. The spectrum of Pharm found in aquatic environments is diverse, encompassing antibiotics, antipyretics, analgesics, anti-inflammatories, antimicrobials, and hormones [7]. These contaminants pose risks to both human health and the aquatic environment [8]. For instance, antibiotics can contribute to the development of antibiotic-resistant bacteria, while hormones may disrupt the endocrine systems of aquatic organisms, leading to infertility and developmental issues [9]. The presence of these pollutants in water is typically detected at low concentrations, ranging from µg/L to ng/L [10].

Traditional wastewater treatment methods often fail to fully eliminate pharmaceutical pollutants, leaving them to persist in the environment over time [11]. To address this issue, various quantitative analytical strategies have been developed for the identification of specific pharmaceuticals like carbamazepine, sulfamethoxazole, metoprolol, and ibuprofen in environmental samples [12]. These approaches encompass a range of techniques including spectrofluorimetry, gas chromatography (GC), spectrophotometry, planar chromatography, electrokinetic chromatography, liquid chromatography-tandem mass spectrometry (LC-MS/MS), and high-performance liquid chromatography (HPLC). However, many of these methods rely on expensive instruments, involve high costs, and utilize environmentally unfriendly and toxic solvents [13]. In response to these limitations, there has been a growing emphasis on the development of innovative, cost-effective, and environmentally friendly techniques for identifying and quantifying pharmaceutical contaminants in the environment [14]. Electrochemical sensors have emerged as a promising alternative to traditional methods for pollutant identification, including pharmaceuticals [15]. These sensors offer several advantages, including affordability, portability, ease of use, and the ability to detect contaminants in real-time, making them well-suited for environmental monitoring applications [16].

A promising strategy for enhancing the capability of electrochemical sensors to detect pharmaceutical contaminants in the environment is their modification [17]. This involves incorporating novel materials or altering the sensor's surface to improve its strength, specificity, and responsiveness[18]. Manganese oxide nanoparticles have emerged as a potential modification for electrochemical sensors in the identification of pharmaceutical contaminants [19]. MnO_2NPs offer several desirable properties for use in such sensors, including a large surface area, chemical resistance, and excellent conductivity [20,21]. Overall, the aim of this research is to develop a sensor that can quickly and accurately identify

the presence of pharmaceuticals in wastewater samples. Such a sensor could significantly contribute to the improved management and treatment of wastewater, ultimately helping to mitigate the impact of pharmaceutical contaminants on the environment and human health [22].

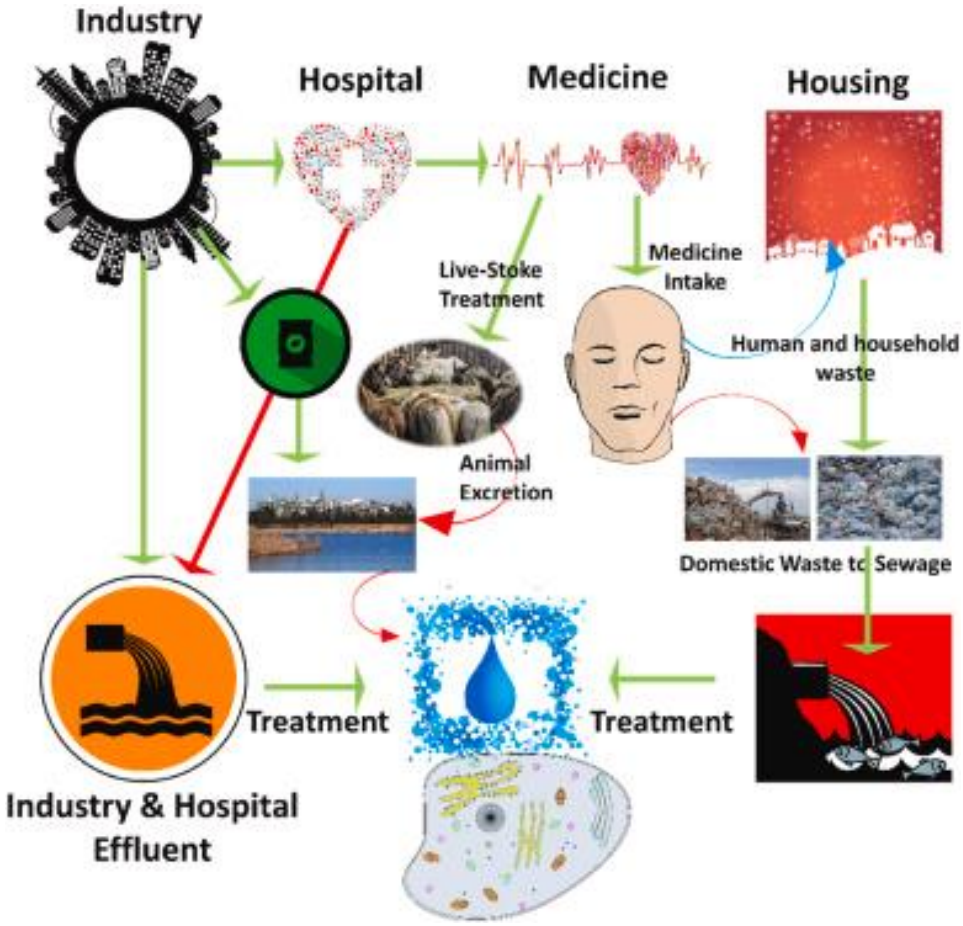

Figure 1.1: *The manner in which medications enter the environment. Reprinted with permission [16].*

1.2 Negative impact of pharmaceuticals on the health of human and aquatic life.

The simple fact that South Africa is considered a country with a water scarcity exacerbates the problem because the country has so few water resources [23,24]. Wood et al. (2017) state that South Africa faces significant difficulties such as poor wastewater treatment, a high prevalence of tuberculosis, drug resistance to the disease, and restricted access to drinkable water, especially in rural areas [25]. Pharmaceuticals may exist in aquatic ecosystems in low concentrations, but because to their broad usage, high biological reactivity, continual release, and relatively slow breakdown, they are pseudo-persistent in aquatic environments [6]. One of the most enduring categories of environmental pollutants, pharmaceuticals have the potential to seriously endanger both aquatic life and human health [26]. The first of the biggest risks to global health and food security is the high potential of antibiotic emergent pollutants posing antibiotic resistance [27]. Bacteria resistance can cause medications to fail in both people and animals [28]. Furthermore, bacteria can ingest antibiotics and impact biological approach, resulting in ecological consequences when soil is treated with antibiotic-containing dung. As a result, the growth of seeds and output yield can be dramatically influenced [29]. Table 1.1 lists numerous antibiotic leftovers discovered in different water matrix, involves their health effects [16]. Beta-blockers are a hormone disruptive chemical that has been demonstrated to affect androgen levels in male creatures [30,31]. Furthermore, metabolic buildup in marine organisms can change the functioning of their circulatory systems [32]. Bioaccumulation studies, for example, have shown that these chemicals reside in a range of fish tissues, including the brain, liver, blood plasma, gills, muscles, and gills [16]. Long-term exposure to these substances encourages antibiotic resistance, which has a significant impact on public health. Even though pharmaceuticals are present in lower concentrations in diverse water matrix [4]. Resistance to

antibiotics genes, which reach the surrounding via wastewater treatment plants and manure, are expected to have an indirect but significant impact on human health. It is difficult to determine the over-time impacts of medications on the surrounding and human health because there is still a dearth of knowledge about their behaviour and hazards/ecological threats [33].

Table 1.1: Pharmaceutical pollutants and their toxicity effects.

Chemical	Adverse effect	Reference
Anti-biotics (e.g sulfamethoxazole, Penicillin)	Humans can develop antibiotic resistance; though healthy people may be at a lesser risk. causes of bacterial pathogen resistance that change the makeup of microbial communities in nature and have an impact on the higher food chain. Using organic fertilizers (sludge or manure) high in antibiotics can impede plant growth because they interfere with root formation.	[34,16,24]
Anti-epileptics (e.g carbamazepine, gabapentin)	Carcinogenicity in mice Reduces thyroid, hormones, oestrogen, and testosterone, which reduces fertility by impairing the endocrine system and people and aquatic creatures may experience developmental problems. Drowsiness and visual difficulties are just two of the negative impacts on the neurological system that have been recorded.	[35,16]
Beta- Blocker (e.g Metoprolol)	They also reduce the amount of testosterone and the rate at which aquatic species reproduce. Zooplankton and benthic creatures may be impacted by beta-blockers.	[16]
Analgesics (e.g Ibuprofen, naproxen)	Kidney and gill injury in fish, such as rainbow trout Toxic to phytoplankton and benthos	[36,16]

1.3 Pollutants from pharmaceutical products

Pharmaceuticals often include over the counter (OTC) or prescription pharmaceuticals for humans, animals, and plants, as well as nutraceuticals used for prophylaxis, therapy, and health supplements [6]. Antibiotics, painkillers, anti-allergic pharmaceuticals, hormones, non-steroidal anti-inflammatory drugs, beta-blockers, cholesterol regulators, and antiepileptics discovered in aquatic habitats at amounts ranging from (usually ng/L to μg/L) [24].

1.3.1 Carbamazepine

Carbamazepine (5 H-dibenzo [b, f] azepine-5-carboxamide), (CBZ), is a prevalent anti-epileptic medicine with a high durability in the surroundings and insufficient removal by typical sewage treatments, as illustrated in Figure 1.2 [24]. When other medications have failed to control bipolar disorder, carbamazepine may be administered. It affects the brain's aberrant electrical activity by lowering it. Depression, psychological disorders, illicit substance departure, PTSD, disorder of the legs, mellitus insipidus, certain painful disorders, and chorea among kids are all controlled by carbamazepine [37]. According to Madikizela et al.,2017, the maximum detected value of carbamazepine in South African wastewater was 2.2 g/L. Furthermore, wastewater contains up to 0.052 ng/L of two carbamazepine metabolites (carbamazepine-10, 11-epoxide, and carbamazepine-10, 11-dihydroxycarbamazepine).

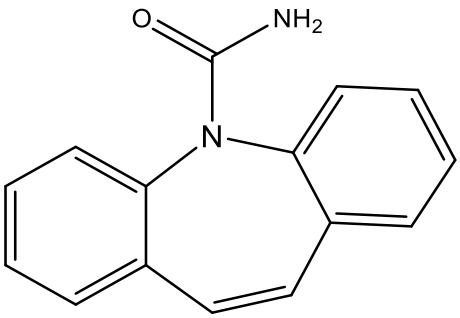

Figure 1.2: Carbamazepine

1.3.2 Sulfamethoxazole

Sulfamethoxazole (4-Amino-N-(5-methylisoxazole-3-yl)-benzene sulfonamide) is a popular antibiotic involve alleviating illnesses by preventing the synthesis of dihydrofolic acid. (a necessary component for bacterial proliferation), as shown in Figure 1.2 [38]. Antibacterial resistance genes being discovered because of chronic exposure to antibiotics is one of the main issues surrounding their consumption, hence it is important to check for them in environmental samples [37]. Sulfamethoxazole is a medication used to treat viral illnesses in humans, including urinary tract infections, asthma, and prostate cancer. SMX is efficient against both involve utilized for relieving illnesses caused by bacterial strains that are gram-positive as well as gram negative in the animal husbandry and aquaculture industries [39]. In African wastewater effluents, sulfamethoxazole concentrations ranged from 0.15 to 10 g/L [40]. According to Madikizela et al.,2020 and Faleye et al.,2018, the antibiotic sulfamethoxazole has been found to be at higher concentrations in Africa than anyplace else in the globe, with a concentration of 0.0868 g/L being observed.

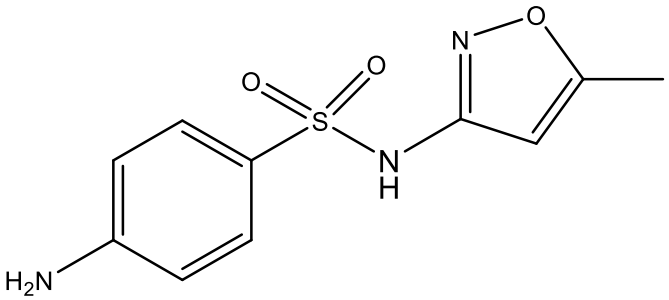

Figure 1.3: Sulfamethoxazole

1.3.3 Ibuprofen

Ibuprofen is an analgesic and NSAID [24]. It can be found in water bodies either completely or partially as metabolites, such as hydroxy ibuprofen and carboxy ibuprofen as shown in figure 1.4. Ibuprofen was detected in water samples from South Africa at levels of 278.261, and 170 ng/L [41]. Madikizela et al demonstrated the detection of the concentration of NSAID compounds such as Ibuprofen, which was found to be higher in African wastewater than in developing countries such as Europe. This observation is the result of inadequate hygiene. For instance, ibuprofen was discovered to have an average level of 111.9 mg/L in the Northern WWTP influent in the Gauteng region and a peak level of 221 mg/L in a WWTP influent in the KwaZulu-Nata region of South Africa. In trials done in Europe, the highest recorded ibuprofen influent values were 22.8, 1.36, and 20.2 mg/L. As a result, One of the NSAIDs that is often observed in surface and wastewater in Africa is ibuprofen [34].

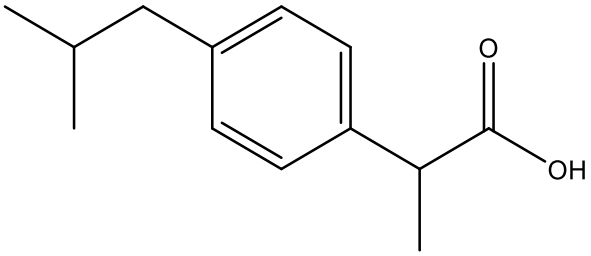

Figure 1.4: Ibuprofen

1.3.4 Metoprolol

Metoprolol is the most frequently administered antihypertensive drug in the world, and it belongs to the beta-blocker ((1)-adrenergic receptor antagonist) family, as illustrated in Figure 1.5. MP involves medication to treat hyperthyroidism, angina, arrhythmia, hypertension, and myocardial infarction [42]. The beta-blocker metabolites in surface water with the greatest proportions of environmental toxicity data, according to Letsoalo et al. 2023, suggested a possible over time danger of persistent contamination and neurotoxic consequences on marine and terrestrial creatures that are not intended recipients. Furthermore, metoprolol has been determined to be among the drugs most frequently found in fish specimens from the shores of Europe. [24]. Five ng/L was the most significant amount of metoprolol identified in Canada. Metoprolol, propranolol, and atenolol—three -blockers—were identified in Egypt's and Cameroon's water bodies in amounts of less than 17 ng/L. High concentrations have been recognized as a warning sign that beta-blockers should be evaluated on a regular basis in developing nations [9].

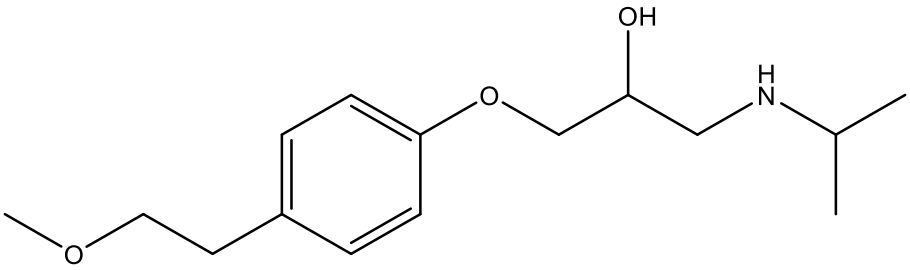

Figure 1.5: Metoprolol

1.4 Problem statement

The presence of emergent organic contaminants, particularly pharmaceutical pollutants, in water sources is a growing concern globally, including in South Africa [43]. These substances, which include hormones, antibiotics, and various other pharmaceutical compounds, are not effectively removed by conventional wastewater treatment processes. Their presence in the water cycle poses significant risks to human health and the environment [44]. For instance, exposure to certain pharmaceuticals in water can lead to the development of diseases in humans and can disrupt aquatic ecosystems,

affecting the health and behavior of aquatic organisms [33]. The detection and quantification of these contaminants in water bodies are crucial for assessing the extent of pollution and for implementing strategies to mitigate their impacts [43]. Advanced analytical techniques such as Liquid Chromatography-Mass Spectrometry (LC-MS), High-Performance Liquid Chromatography (HPLC) with various detectors, Gas Chromatography-Mass Spectrometry (GC-MS), Ultraviolet (UV) detection, and Capillary Electrophoresis have been employed to identify and measure the concentrations of pharmaceutical compounds in water. These methods offer sensitivity and specificity in detecting a wide range of contaminants at low concentrations. However, the application of these techniques faces several challenges such as specialized personnel, high costs, use harmful solvents, infrastructure requirements and time-consuming procedures [45]. Given these challenges, there is a pressing need to develop more accessible, cost-effective, and environmentally friendly methods for detecting pharmaceutical pollutants in water [46]. Emerging technologies and innovations could offer solutions that are less reliant on specialized skills and infrastructure, reduce the use of hazardous chemicals, and provide faster results. Electrochemical sensors emerge as a promising solution to these challenges, leveraging advancements in material science, nanotechnology, and electrochemistry [47].

1.5 Justification

The justification for developing an electrochemical sensor specifically designed for detecting pharmaceutical contaminants in water samples is compelling, especially considering the pressing need for effective, efficient, and accessible water monitoring solutions [45]. The increasing prevalence of pharmaceutical pollutants in water bodies worldwide poses significant risks to both human health and environmental sustainability [44]. Traditional methods for detecting these contaminants, while effective, often come with significant drawbacks, including high costs, complexity, and the need for specialized equipment and personnel [48]. Electrochemical detection presents a promising alternative, offering several advantages that align with the needs for broader, more accessible water quality monitoring such as affordability, dependability, portability, and simplicity of use [49]. The challenge of electrochemical fouling, where bare electrodes may suffer from reduced sensitivity due to surface interactions with the sample matrix, is a significant hurdle. However, this can be overcome by modifying the electrode surface to enhance its sensitivity and selectivity towards specific contaminants [46].

The use of nanotechnology, specifically the incorporation of MnO_2 nanoparticles, represents a sophisticated approach to this problem. MnO_2 nanoparticles offer several benefits such as enhanced electrocatalytic reactivity, increased surface area, good selectivity, and sensitivity [50]. The proposed use of MnO_2 nanoparticles to modify screen-printed carbon electrodes (SPCE) for the detection of compounds such as carbamazepine, ibuprofen, metoprolol, and sulfamethoxazole introduces a method that is not only potentially more effective but also more sustainable and accessible. Transition metal nanoparticles like MnO_2 serve as multifunctional catalysts due to their environmental friendliness, cost-effectiveness, and versatile application across nanoscience fields, including photocatalysis, energy storage, and now, electrochemical sensing [51]. The unique properties, several synthesis routes, and applications of MnO_2 nanoparticle will be discussed thoroughly in chapter 2. The use of SPCE represents a significant advancement in electrochemical sensor technology, offering a platform that challenges traditional three-electrode systems [52]. This shift is motivated by the need for more accessible, cost-effective, and versatile methods for monitoring water quality, especially given the increasing concern over pharmaceutical pollutants in aquatic environments [53].

The Mn (VI) of the precursor was reduced by a potassium permanganate utilizing cathodic reduction, resulting in the formation of MnO_2 nanorods [54]. Potassium permanganate ($KMnO_4$) serve as an oxidizing agent [55]. A research gap exists in the simultaneous detection using electrochemical sensor of pharmaceutical determination in application of wastewater samples. Most electrochemical sensors that have been developed are used in application of serum, urine, and saliva samples [56]. In summary, the development of an electrochemical detector leveraging MnO_2 nanoparticles for the enhancement of SPCE represents a forward-looking approach to water quality monitoring [57]. It addresses key challenges in the detection of pharmaceutical pollutants, offering a method that is both practical and aligned with the needs for sustainable, global environmental health initiatives.

Despite the advances in electrochemical sensing, there is a significant gap in comprehensive studies focusing on the simultaneous detection of multidrug using manganese oxide nanoparticles (MnO_2) on

screen-printed electrodes (SPEs). The existing literature often addresses individual drug detection or uses other electrode materials, leaving a gap in the exploration of MnO_2 nanoparticles as a multifunctional sensing platform for these specific drugs. According to Dawadi et al. (2020), their review covers the synthesis methods, applications, and challenges associated with MnO_2 nanoparticles in various sensing applications, including electrochemical sensors. However, it does not specifically address the simultaneous detection of multiple pharmaceuticals. Motoc et al. (2013) explored the use of modified electrodes for the detection of ibuprofen, highlighting the potential of different nanomaterials but not including MnO_2 nanoparticles or the simultaneous detection of multiple drugs. Apetrei et al. (2017) discussed the application of SPEs for detecting various pharmaceuticals in water, focusing primarily on carbon-based materials and not addressing MnO_2 nanoparticles or the detection of multiple drugs. Addressing this gap could significantly advance the field of environmental and pharmaceutical monitoring by offering a robust and sensitive method for detecting multiple contaminants simultaneously.

1.6 Aims and objectives.

Aim

This study focussed on the development of a potential dependent real time multidrug sensor systems using screen printed manganese oxide electrode platform in water samples.

Objectives of the study

- Synthesis of manganese oxide nanoparticles (MnO_2NPs).
- Characterization of MnO_2NPs using FTIR, XRD, SEM, SAXS spectroscopy, UV/Vis spectrophotometer, Raman spectroscopy, CV and DPV.
- Development, optimisation, evaluation and testing of MnO_2NPs on a screen-printed electrode for sulfamethoxazole, metoprolol, ibuprofen, and carbamazepine.
- Application of the developed MnO_2NPs sensors in monitoring target drugs in real- water samples.

1.7 Outline for a thesis

The research is divided into six chapters:

Introduction to chapter one: This chapter introduces the topic of developing contaminants, with a particular emphasis on medicines. Describes how drugs reach the environment, which could be through wastewater discharge, inappropriate disposal, or other means. Describes the negative consequences of drugs on both human health and the surrounding. The study focuses on four specific pharmaceuticals: carbamazepine, sulfamethoxazole, ibuprofen, and metoprolol. Provides data on the reported concentrations of the indicated medicines in bodies of water. The problem or concerns addressed in the study should be stated. Clearly states the study's goal and objectives. Provides a summary of how the thesis is organized, as well as a road map for what the reader can expect in the next chapters.

Chapter two: Literature review; this part is anticipated to provide a detailed summary of recent electrochemical sensor research. It may cover different types of sensors, their principles of operation, and their applications, with a specific emphasis on their relevance to the detection or analysis of pharmaceutical compounds. This section of the literature review would go over several strategies for creating metal-based nanoparticles. It could involve procedures like chemical reduction, sol-gel, or

green synthesis. The review may highlight the benefits and drawbacks of each method, with an emphasis on their applicability to the setting of your study. This section would likely explore recent studies and applications of manganese oxide. The review might emphasize any applications related to sensing or detection, considering the electrochemical context mentioned in the introduction.

Chapter three: Methodology; describes the substances and equipment used in the characterization of MnO_2 nanoparticles. This could include precursor materials, solvents, and other necessary reagents. Lists the instruments employed for characterization, such as FTIR, Raman spectroscopy, SEM, XRD, UV/vis spectroscopy, and SAXS. These tools help analyze the physical and chemical features of the MnO_2 nanoparticles. Electrochemical techniques for sensing, CV involve measuring the electrochemical behaviour of the MnO_2 nanoparticles. This technique provides information about redox reactions and can be valuable for characterizing the sensor's electrochemical features. EIS describes the application of EIS for studying the electrical response of the MnO_2 nanoparticle sensor. Differential pulse voltammetry (DPV) provides information on how this technique is employed in the study. It is often used for sensitive and selective analysis in electrochemical sensing. Details the process used to fabricate the MnO_2 nanoparticles on a SPCE. This step involves crucial for creating a functional sensor platform. Describes how the MnO_2 nanoparticle sensor is applied in wastewater.

Chapter four: Results and discussion: Summarizes the data obtained from FTIR, SEM, XRD and Raman spectroscopy, providing insights into the structural and morphological properties of the MnO_2 nanoparticles. CV, EIS, and DPV presents the results of electrochemical characterization, including the detection of carbamazepine and sulfamethoxazole. Discuss the optimization process for parameters such as pH and scan rate in the context of improving the sensor's performance. Discusses how the sensor responds to potential interfering substances. Addresses the stability of the MnO_2 nanoparticle sensor over time and under various conditions. Describes the application of the MnO_2 nanoparticle sensor in detecting specific pharmaceutical compounds in wastewater.

Chapter five: This chapter summarizes the data obtained from UV/Vis spectroscopy and SAXS. This section provides insights into the optical traits and structural traits of the MnO_2 nanoparticles. CV, EIS, and DPV presents the results of electrochemical characterization, emphasizing the identification of Ibuprofen and metoprolol. Discusses the electrochemical behaviour of MnO_2NPs concerning these pharmaceutical compounds such as Ibuprofen and metoprolol. Interference and stability studies evaluates how the sensor responds to potential interfering substances and its stability over time and varying conditions. These studies contribute to assessing the sensor's reliability and specificity. Describes the application of the MnO_2 nanoparticle sensor in detecting specific pharmaceutical compounds (Ibuprofen and metoprolol) in wastewater.

Chapter six: This section draws insights from the research study's overall outcomes and gives suggestions for further research.

References

[1] M. Vasilachi, Ionela Cătălina Asimini, Dana Mihaela Fertu, Daniela Ionela Gavrilescu, “Occurrence and fate of emerging pollutants in water environment and options for their removal,” *Water (Switzerland)*, vol. 13, no. 2, pp. 1–34, 2021, doi: 10.3390/w13020181.

[2] D. S. Bilal, Muhammad, Bagheri, Ahmad Reza, Vilar, S. S. Aramesh, Nahal, Eguiluz, Katlin Ivon Barrios, Ferreira, Luiz Fernando Romanholo, Ashraf, and H. M. N. Iqbal, “Oxidoreductases as a versatile biocatalytic tool to tackle pollutants for clean environment – a review,” *J. Chem. Technol. Biotechnol.*, vol. 97, no. 2, pp. 420–435, 2022, doi: 10.1002/jctb.6743.

[3] Y. Jari, N. Roche, M. C. Necibi, S. El Hajjaji, D. Dhiba, and A. Chehbouni, “Emerging Pollutants in Moroccan Wastewater: Occurrence, Impact, and Removal Technologies,” *J. Chem.*, vol. 2022, 2022, doi: 10.1155/2022/9727857.

[4] R. Álvarez-Ruiz, Y. Picó, and J. Campo, “Bioaccumulation of emerging contaminants in mussel (Mytilus galloprovincialis): Influence of microplastics,” *Sci. Total Environ.*, vol. 796, 2021, doi: 10.1016/j.scitotenv.2021.149006.

[5] A. Chaturvedi, Preeti, Shukla, Parul, Shekher, Balendu, Chowdhary, Pankaj, Chandra, RamGupta, Pratima Pandey, “Prevalence and hazardous impact of pharmaceutical and personal care products and antibiotics in environment : A review on emerging contaminants,” *Environ. Res.*, vol. 194, no. December 2020, p. 110664, 2021, doi: 10.1016/j.envres.2020.110664.

[6] A. Gogoi, P. Mazumder, V. K. Tyagi, G. G. Tushara Chaminda, A. K. An, and M. Kumar, “Occurrence and fate of emerging contaminants in water environment: A review,” *Groundw. Sustain. Dev.*, vol. 6, no. January, pp. 169–180, 2018, doi: 10.1016/j.gsd.2017.12.009.

[7] A. C. D. Maanen, I. Wilting, and P. A. F. Jansen, “Prescribing medicines to older people — How to consider the impact of ageing on human organ and body functions,” no. July 2019, pp. 1921–1930, 2020, doi: 10.1111/bcp.14094.

[8] N. Rai, Mansi, Paudel, I. A. Sakhrie, Mesevilhou, Gemmati, Donato, Khan, and A. V. Tisato, Veronica, Kanase, Anurag Schulz, Armin Singh, “Perspective on Quantitative Structure – Toxicity Relationship (QSTR) Models to Predict Hepatic Biotransformation of Xenobiotics,” pp. 448–462, 2023.

[9] L. M. Madikizela, S. Ncube, and L. Chimuka, “Analysis, occurrence and removal of pharmaceuticals in African water resources: A current status,” *J. Environ. Manage.*, vol. 253, no. October 2019, p. 109741, 2020, doi: 10.1016/j.jenvman.2019.109741.

[10] A. Olasupo and F. B. M. Suah, “Recent advances in the removal of pharmaceuticals and endocrine-disrupting compounds in the aquatic system: A case of polymer inclusion membranes,” *J. Hazard. Mater.*, vol. 406, no. June 2020, p. 124317, 2021, doi: 10.1016/j.jhazmat.2020.124317.

[11] H. J. Lee, K. Y. Kim, S. Y. Hamm, M. S. Kim, H. K. Kim, and J. E. Oh, “Occurrence and distribution of pharmaceutical and personal care products, artificial sweeteners, and pesticides in groundwater from an agricultural area in Korea,” *Sci. Total Environ.*, vol. 659, pp. 168–176, 2019, doi: 10.1016/j.scitotenv.2018.12.258.

[12] I. Tariq, Muhammad Ali, Izaz Ihsanullah, S. Naushad, Mu, Ali, A. Hassan, Syed Shah, and A. Wahab, “Journal of Water Process Engineering Hospital wastewater as a source of environmental contamination : An overview of management practices , environmental risks , and treatment processes,” *J. Water Process Eng.*, vol. 41, no. February, p. 101990, 2021, doi: 10.1016/j.jwpe.2021.101990.

[13] R. Gaballah, Mohamed S Guo, Jianbin Sun, Hui Aboagye, Dominic Sobhi, Mostafa Muhmood, Atif Dong, “Bioresource Technology A review targeting veterinary antibiotics removal from livestock manure management systems and future outlook,” *Bioresour. Technol.*, vol. 333, no. March, p. 125069, 2021, doi: 10.1016/j.biortech.2021.125069.

[14] E. Czatzkowska, Małgorzata Wolak, Izabela Harnisz, Monika Korzeniewska, “Impact of Anthropogenic Activities on the Dissemination of ARGs in the Environment — A Review,” 2022.

[15] D. Michael, I. Rizzo, L. McArdell, C. S. Manaia, C. M. Merlin, C. Schwartz, T. Dagot, C. Fatta-Kassinos, “Urban wastewater treatment plants as hotspots for the release of antibiotics in the environment: A review,” *Water Res.*, vol. 47, no. 3, pp. 957–995, 2013, doi: 10.1016/j.watres.2012.11.027.

[16] S. Letsoalo Mokgehle R. Sithole, Thandiwe Mufamadi and T. Mazhandu Zvanaka, Sillanpaa, Mika Kaushik, Ajeet Mashifana, “Efficient detection and treatment of pharmaceutical contaminants to produce clean water for better health and environmental,” *J. Clean. Prod.*, vol. 387, no. September 2022, p. 135798, 2023, doi: 10.1016/j.jclepro.2022.135798.

[17] M. C. Necibi and D. Dhiba, “Contaminants of Emerging Concern in African Wastewater Effluents : Occurrence , Impact and Removal Technologies,” pp. 1–12, 2021.

[18] S. Rizzo, Luigi, Malato, I. Antakyali, Demet Beretsou, Vasiliki G, Maja, B Đ Gernjak, Wolfgang Heath, Ester Ivancev-tumbas, A. R. Karaolia, Popi, Lado, H. Mascolo, Giuseppe, Mcardell,

Christa S Schaar, and D. Silva, Adrián M T Fatta-kassinos, “Science of the Total Environment Consolidated vs new advanced treatment methods for the removal of contaminants of emerging concern from urban wastewater,” vol. 655, no. October 2018, pp. 986–1008, 2019, doi: 10.1016/j.scitotenv.2018.11.265.

[19] C. Lee, Bao Cheen, P. Shuaib, Mohamed Saheed, Mohamed Show, and J. Chang, Jo-shu Chuan, Tau Shiung, Su Ching, “Conventional and emerging technologies for removal of antibiotics from wastewater,” *J. Hazard. Mater.*, vol. 400, no. April, p. 122961, 2020, doi: 10.1016/j.jhazmat.2020.122961.

[20] E. Makuwa, S, Tlou, M Green, “The effects of dry versus wet season on the performance of a wastewater treatment plant in North West Province , South Africa,” vol. 48, no. 1, pp. 40–49, 2022.

[21] R. Kruger, Annika Pieters, C. Van Horn, Suranie Zijl, and N. Aneck, “The role of effect - based methods to address water quality monitoring in South Africa : a developing country ’ s struggle,” *Environ. Sci. Pollut. Res.*, pp. 84049–84055, 2022, doi: 10.1007/s11356-022-23534-3.

[22] N. Jones, O A H Voulvoulis and J. N. Lester, “Human Pharmaceuticals in the Aquatic Environment a Review,” vol. 3330, no. May, 2010, doi: 10.1080/09593332208618186.

[23] B. Ryu, Heejeong Li and Y. Guise, Sylvain De Mccutcheon, Jeffrey Lei, “Recent progress in the detection of emerging contaminants PFASs,” *J. Hazard. Mater.*, vol. 408, no. August 2020, p. 124437, 2021, doi: 10.1016/j.jhazmat.2020.124437.

[24] S. Madikizela, Lawrence M.Rimayi, Cornelius Khulu, Sinegugu Chimuka, Luke Ncube, *Pharmaceuticals and personal care products*. Elsevier Inc., 2022. doi: 10.1016/B978-0-12-822850-0.00009-0.

[25] A. Wood, Timothy Paul, Du Preez, Christiaan Steenkamp and E. R. Duvenage, Cornelia Rohwer, “Database-driven screening of South African surface water and the targeted detection of pharmaceuticals using liquid chromatography - High resolution mass spectrometry,” *Environ. Pollut.*, vol. 230, pp. 453–462, 2017, doi: 10.1016/j.envpol.2017.06.043.

[26] K. Samal, S. Mahapatra, and M. Hibzur Ali, “Pharmaceutical wastewater as Emerging Contaminants (EC): Treatment technologies, impact on environment and human health,” *Energy Nexus*, vol. 6, no. April, p. 100076, 2022, doi: 10.1016/j.nexus.2022.100076.

[27] M. Milić, Nataša, Milanović and M. V. Letić, Nevena Grujić, Sekulić, Maja Turk, Radonić, Jelena Mihajlović, Ivana Miloradov, “Occurrence of antibiotics as emerging contaminant substances in aquatic environment,” *Int. J. Environ. Health Res.*, vol. 23, no. 4, pp. 296–310, 2013, doi: 10.1080/09603123.2012.733934.

[28] W. Aslam, Bilal, Wang, M. I. Arshad, M. A. Khurshid, Mohsin Muzammil, Saima Rasool, Muhammad Hidayat Nisar, and Z. Alvi, Ruman Farooq Aslam, Muhammad Aamir Qamar, Muhammad Usman Salamat, Muhammad Khalid Farooq Baloch, “Antibiotic resistance: a rundown of a global crisis,” *Infect. Drug Resist.*, vol. 11, pp. 1645–1658, 2018, doi: 10.2147/IDR.S173867.

[29] N. J. Waleng and P. N. Nomngongo, “Occurrence of pharmaceuticals in the environmental waters: African and Asian perspectives,” *Environ. Chem. Ecotoxicol.*, vol. 4, no. November 2021, pp. 50–66, 2022, doi: 10.1016/j.enceco.2021.11.002.

[30] V. I. Iancu, G. L. Radu, and R. Scutariu, “A new analytical method for the determination of beta-blockers and one metabolite in the influents and effluents of three urban wastewater treatment plants,” *Anal. Methods*, vol. 11, no. 36, pp. 4668–4680, 2019, doi: 10.1039/c9ay01597c.

[31] T. Henriques, Jorge F. Almeida, Ana Rita Andrade, O. Koba, Olga Golovko, and I. Soares, Amadeu M.V.M. Oliveira, Miguel Domingues, “Effects of the lipid regulator drug gemfibrozil: A toxicological and behavioral perspective,” *Aquat. Toxicol.*, vol. 170, pp. 355–364, 2016, doi:

10.1016/j.aquatox.2015.09.017.

[32] K. Zhang, Y. Zhao, and K. Fent, “Cardiovascular drugs and lipid regulating agents in surface waters at global scale: Occurrence, ecotoxicity and risk assessment,” *Sci. Total Environ.*, vol. 729, p. 138770, 2020, doi: 10.1016/j.scitotenv.2020.138770.

[33] L. M. Madikizela and S. Ncube, “Health effects and risks associated with the occurrence of pharmaceuticals and their metabolites in marine organisms and seafood,” *Sci. Total Environ.*, vol. 837, no. March, p. 155780, 2022, doi: 10.1016/j.scitotenv.2022.155780.

[34] L. M. Madikizela, N. T. Tavengwa, and L. Chimuka, “Status of pharmaceuticals in African water bodies: Occurrence, removal and analytical methods,” *J. Environ. Manage.*, vol. 193, pp. 211–220, 2017, doi: 10.1016/j.jenvman.2017.02.022.

[35] A. Bellino, G. Lofrano, M. Carotenuto, G. Libralato, and D. Baldantoni, “Antibiotic effects on seed germination and root development of tomato (Solanum lycopersicum L),” *Ecotoxicol. Environ. Saf.*, vol. 148, no. October 2017, pp. 135–141, 2018, doi: 10.1016/j.ecoenv.2017.10.006.

[36] L. M. Madikizela, Y. B. Nuapia, L. Chimuka, S. Ncube, and A. Etale, “Target and Suspect Screening of Pharmaceuticals and their Transformation Products in the Klip River, South Africa, using Ultra-High–Performance Liquid Chromatography–Mass Spectrometry,” *Environ. Toxicol. Chem.*, vol. 41, no. 2, pp. 437–447, 2022, doi: 10.1002/etc.5265.

[37] A. Pierpaoli, Mattia Dettlaff and R. Szopińska, Małgorzata Karpienko, Katarzyna Wróbel, Maciej Łuczkiewicz, Aneta Fudala-Książek, Sylwia Bogdanowicz, “Simultaneous opto-electrochemical monitoring of carbamazepine and its electro-oxidation by-products in wastewater,” *J. Hazard. Mater.*, vol. 419, 2021, doi: 10.1016/j.jhazmat.2021.126509.

[38] X. Zhang, Yi, Wu, Yanqing, Su, Lishen Zhu, Chunlin, Wu, “An ultrasensitive electrochemical sensor based on in situ synthesized manganese dioxide/gold nanoparticles nanocomposites for rapid detection of methylmercury in foodstuffs,” *Anal. Methods*, vol. 14, no. 23, pp. 2329–2336, 2022, doi: 10.1039/d2ay00417h.

[39] M. Ramya, P. S. Kumar, G. Rangasamy, V. U. Shankar, G. Rajesh, and K. Nirmala, “Experimental investigation of the electrochemical detection of sulfamethoxazole using copper oxide-MoS2 modified glassy carbon electrodes,” *Environ. Res.*, vol. 216, no. P1, p. 114463, 2023, doi: 10.1016/j.envres.2022.114463.

[40] J. Melo Henrique, J. Rocha Camargo, G. Gabriel de Oliveira, J. Santos Stefano, and B. Campos Janegitz, “Disposable electrochemical sensor based on shellac and graphite for sulfamethoxazole detection,” *Microchem. J.*, vol. 170, no. May, 2021, doi: 10.1016/j.microc.2021.106701.

[41] N. P. Ngubane, D. Naicker, S. Ncube, L. Chimuka, and L. M. Madikizela, “Determination of naproxen, diclofenac and ibuprofen in Umgeni estuary and seawater: A case of northern Durban in KwaZulu–Natal Province of South Africa,” *Reg. Stud. Mar. Sci.*, vol. 29, p. 100675, 2019, doi: 10.1016/j.rsma.2019.100675.

[42] B. Mutharani, P. Ranganathan, S. M. Chen, T. W. Chen, M. A. Ali, and A. H. Mahmoud, “Sonochemical synthesis of novel thermo-responsive polymer and tungsten dioxide composite for the temperature-controlled reversible ‘on-off’ electrochemical detection of β-Blocker metoprolol,” *Ultrason. Sonochem.*, vol. 64, no. October 2019, p. 105008, 2020, doi: 10.1016/j.ultsonch.2020.105008.

[43] K. M. Gani, N. Hlongwa, T. Abunama, S. Kumari, and F. Bux, “Emerging contaminants in South African water environment- a critical review of their occurrence, sources and ecotoxicological risks,” *Chemosphere*, vol. 269, p. 128737, 2021, doi: 10.1016/j.chemosphere.2020.128737.

[44] S. Letsoalo, Mokgehle R. Sithole, Thandiwe Mufamadi and T. Mazhandu, Zvanaka Sillanpaa, Mika Kaushik, Ajeet Mashifana, “Efficient detection and treatment of pharmaceutical contaminants to produce clean water for better health and environmental,” *J. Clean. Prod.*,

vol. 387, no. September 2022, p. 135798, 2023, doi: 10.1016/j.jclepro.2022.135798.

[45] P. Karthik, V. Selvakumar and K. Senthil Kumar, P. Satheeskumar, V. Godwin Vijaysunder, M. Hariharan, S. Antony, “Recent advances in electrochemical sensor developments for detecting emerging pollutant in water environment,” *Chemosphere*, vol. 304, no. March, p. 135331, 2022, doi: 10.1016/j.chemosphere.2022.135331.

[46] M. J. Blanco, M C, Guti, S, Lobo and P. Miranda, A J, Tu, “Electrochemical sensing with electrodes modified with molecularly imprinted polymer films,” pp. 1922–1928, 2004, doi: 10.1007/s00216-003-2330-2.

[47] Y. Liu, Dagang, Zhang and P. R. Sun, Xun, Chang, “Recent Advances in Bio-Sourced Polymeric Carbohydrate / Nanotube Composites,” vol. 40359, 2014, doi: 10.1002/app.40359.

[48] B. T. Continuous and M. Paloma, Y, Pingarr, “Beyond Sensitive and Selective Electrochemical Biosensors: Towards Continuous, Real-Time, Antibiofouling and Calibration-Free Devices,” 2020.

[49] L. F. Sgobbi, C. A. Razzino, and S. A. S. Machado, “A disposable electrochemical sensor for simultaneous detection of sulfamethoxazole and trimethoprim antibiotics in urine based on multiwalled nanotubes decorated with Prussian blue nanocubes modified screen-printed electrode,” *Electrochim. Acta*, vol. 191, pp. 1010–1017, 2016, doi: 10.1016/j.electacta.2015.11.151.

[50] Q. Zhu and Q. Xu, “Immobilization of Ultrafine Metal Nanoparticles to High-Surface-Area Materials and Their Catalytic Applications,” *Chem*, vol. 1, no. 2, pp. 220–245, 2016, doi: 10.1016/j.chempr.2016.07.005.

[51] B. Mutharani, P. Ranganathan, S. M. Chen, T. W. Chen, M. A. Ali, and A. H. Mahmoud, “Sonochemical synthesis of novel thermo-responsive polymer and tungsten dioxide composite for the temperature-controlled reversible ‘on-off’ electrochemical detection of β-Blocker metoprolol,” *Ultrason. Sonochem.*, vol. 64, no. February, p. 105008, 2020, doi: 10.1016/j.ultsonch.2020.105008.

[52] L. Hui, Zengyu, Zhang, G. Ren, Guozhang, Sun, and H. Yu, “Green Flexible Electronics : Natural Materials , Fabrication , and Applications,” vol. 2211202, pp. 1–29, 2023, doi: 10.1002/adma.202211202.

[53] Y. Luo, “Preparation of MnO2 nanoparticles by directly mixing potassium permanganate and polyelectrolyte aqueous solutions,” *Mater. Lett.*, vol. 61, no. 8–9, pp. 1893–1895, 2007, doi: 10.1016/j.matlet.2006.07.165.

[54] X. Liu, Xingyue, Liang, J. Yu, Jing, Xu, Keying, Shen, and W. Duan, “Trends in Analytical Chemistry Recent development of noble metal-based bimetallic nanoparticles for colorimetric sensing,” *Trends Anal. Chem.*, vol. 169, no. October, p. 117386, 2023, doi: 10.1016/j.trac.2023.117386.

[55] L. John, Anjali, Benny, C. Rose, Anila, Sudhakar, and A. Narahari, Yethadka, Varghese, *Electrochemical sensors using conducting polymer / noble metal nanoparticle nanocomposites for the detection of various analytes : a review*, vol. 11, no. 1. Springer Berlin Heidelberg, 2021. doi: 10.1007/s40097-020-00372-8.

[56] S. S. Kalanur, S. Jaldappagari, and S. Balakrishnan, “Enhanced electrochemical response of carbamazepine at a nano-structured sensing film of fullerene-C60 and its analytical applications,” *Electrochim. Acta*, vol. 56, no. 15, pp. 5295–5301, 2011, doi: 10.1016/j.electacta.2010.08.071.

[57] N. Jaiswal, I. Tiwari, C. W. Foster, and C. E. Banks, “Highly sensitive amperometric sensing of nitrite utilizing bulk-modified MnO2 decorated Graphene oxide nanocomposite screen-printed electrodes,” *Electrochim. Acta*, vol. 227, pp. 255–266, 2017, doi: 10.1016/j.electacta.2017.01.007.

Chapter 2: Literature review

Synthesis and application of metal oxide-based nanoparticles in sensors

Summary

The section addresses recent research that is deemed significant to the current study. This could include findings, methodologies, or advancements in the field that have direct relevance to the ongoing investigation. Various synthesis techniques used to create metal-based nanoparticles are mentioned. Metal-based nanoparticles may involve the use due to the importance of synthesis procedures in modifying their properties and features. A brief overview of conventional detection techniques is provided. This could include traditional methods used for detecting certain substances, serving as a baseline for comparing the performance of the electrochemical sensors under investigation. Numerous electrochemical sensors that have previously been used to identify pharmaceuticals, including carbamazepine, ibuprofen, sulfamethoxazole, and metoprolol. This highlights the relevance of the current study to electrochemical approaches are used to detect these medicinal substances.

2.1 Introduction

Sensors have garnered significant attention in scientific, environmental, and medical fields due to their extensive use over the years and their remarkable characteristics [1]. In everyday life, a wide variety of sensors are used, which are classified based on the quantities and qualities they detect [2]. Sensors come in a variety of forms, including magnetic, chemical, thermal, and radiation sensors [3]. A device that finds and gauges the concentration of chemical substances in its surroundings is called a "chemical sensor". Chemical devices are capable of sensing by a range of methods, such as optical, acoustic, and electrochemical ones [4].. This highlights the versatility of chemical sensors in terms of the mechanisms they employ for detecting chemical substances [5]. Electrochemical sensors have been more desirable than other sensors. This preference is attributed to their significant experimental simplification, detectability, and affordability [6].

The area of electrochemistry has grown to appreciate electrochemical sensors owing to their exceptional qualities [7]. Electrochemical sensors are a powerful tool and well established to gain real-time analysis [8]. In addition to simultaneously detecting several analytes, organic, inorganic, neutral, and ionic molecules are among the many chemicals that electrochemical sensors are frequently able to detect [9]. Target analytes in an electrolyte on a working electrode are used in electrochemical sensors to conduct a redox reaction that resulting in variations in an electrical signal proportional to the amount of the analyte [4]. A voltammetry electrochemical sensor is a type of electrochemical sensor that operates based on the principles of voltammetry. Voltammetry involve approach of changing potential is applied to an electrode and measuring the resulting current [7].

The basic principle of an electrochemical sensor involves the use of electrochemical reactions to detect and quantify the presence of a specific analyte in a sample. Electrochemical sensors operate based on redox reactions, where electrons are transferred between molecules [10]. These reactions can involve the oxidation (loss of electrons) and reduction (gain of electrons) of chemical species. The working electrode is where the electrochemical reaction takes place [8]. The working electrode is often made of a material that facilitates the redox process. A transducer and a solidified sensing element (recognition system) make up most of an electrochemical sensor (conversion system) [5]. Figure 2.1 depicts its fundamental design and principles.

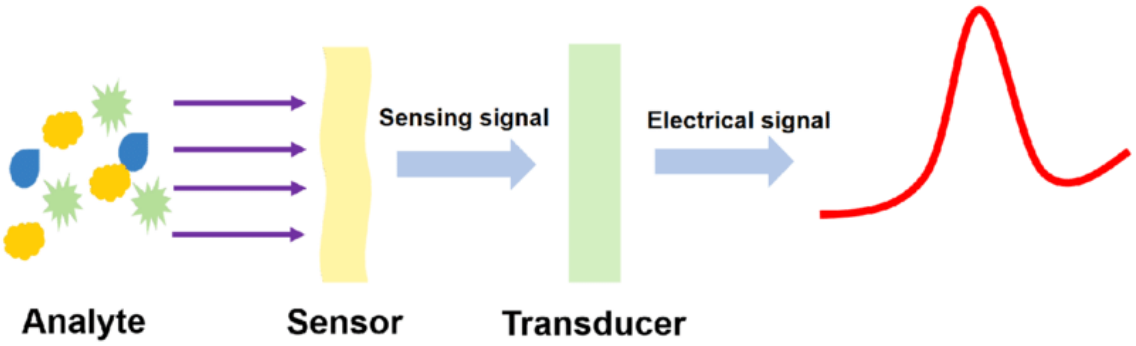

Figure 2.1: Overview basic principle of the electrochemical sensor [11].

When it comes to electrochemical identification techniques, noticing instruments that use SPCE are preferred across additional electrode forms due to the convenience of preparation, simple of manufacture, and ability to be readily made from an array of substances, as Figure 2.2 illustrates [9]. These circumstances allow for the mass production of SPEs at minimal production costs. Furthermore, due to their quick and linear responses, high sensitivity, low power consumption, and capacity to function at room temperature, SPEs are the most extensive electrochemical sensors to be employed for in-situ examination [10]. Screen-printed electrodes make progress toward decentralized analysis by addressing the cost-effectiveness problem as well as the portability need. It is possible to create extremely specialized and ultimately calibrated electrodes for target analytes by simply modifying the reference, counter, and working electrodes with different accessible inks. In the realm of research, screen-printed electrodes' versatility is essential [9].

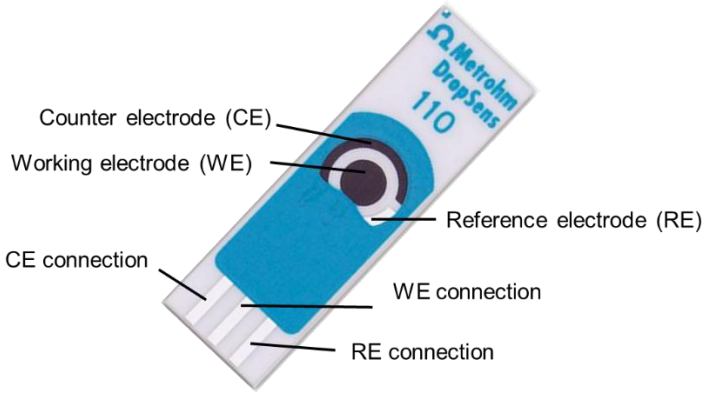

Figure 2.2: Diagram of a screen-printed electrode (SPE) [12].

2.2 Modification of the electrochemical sensor

The impact of the characteristics of the working electrode (WE) on sensor performance in detecting environmental pollutants [5]. The fabrication of electrodes has become increasingly important due to the disadvantages of bare electrodes. Bare electrodes refer to electrodes that do not have any surface modification or coating. These electrodes have several disadvantages, includes superficial passivation displacement, significant noise levels, uneven surface, non-repeatability of surface act, excessive potential need, and sluggish rates of electrochemical responses of particular substances on the electrode's surface [13]. These issues limit their applicability for analytical purposes and typically result in low sensitivity and selectivity for detecting environmental pollutants. To overcome these limitations, various surface modifications or coatings can be applied to the electrodes to enhance their performance. Modified electrodes are an increasingly popular approach to enhancing the performance of electrochemical sensors. The responsiveness, specificity, and speed of response of the sensor can be increased by altering the electrode surface with new substances, such as metal-based nanoparticles [14]. One key advantage of metal-based nanoparticles is their high electrical conductivity, which can facilitate the transmission of electrons between the desired analytes and electrode surface [15]. This can lead to more accurate and precise measurements. Additionally, metal-

based nanoparticles have low charge transfer resistance, which enables the rapid and efficient transfer of electrons [16]. This property allows for faster response times and measurements that are more reliable. Overall, using metal-based nanoparticles as mediators for modified electrodes is a promising approach to improving the performance of electrochemical sensors [17].

2.3 Introduction to the metal oxide-based nanoparticle.

Metal nanoparticles are distinguished by their tiny dimensions and substantial surface area as counterparts [18]. These traits are outcome of quantum confinement effects, surface plasmon resonance, and surface energy. Quantum confinement effects arise when the size of the nanoparticle is smaller than the electron wavelength. In this case, the electronic properties of the particle are no longer governed by the bulk properties of the metal, but rather by the confinement of electrons within the nanoparticle [19]. Surface plasmon resonance involve the metal nanoparticles exposed to light. The high surface area of the nanoparticle allows for collective oscillations of the electrons, resulting in strong absorption and scattering of light at specific wavelengths [20]. The high surface energy of metal nanoparticles involves a significant character in their unique properties. The high proportion of surface atoms counterparts leads to increased reactivity and catalytic activity, making them useful in a variety of applications such as catalysis, sensing, and biomedical imaging [21]. Overall, metal-based nanoparticles have significant potential for use in various fields due to their unique properties resulting from their nanometer size and high surface area. Metal and metal oxide nanoparticles, which are non-toxic inorganic particles. Inorganic nanoparticles are generally more stable and hydrophilic than organic nanoparticles [17]. The rapid advancement of nanotechnology has led to the development of various types of nanoparticles, including metal oxides, for use in various industries. Metal oxide nanoparticles can be synthesized in various morphologies, including spheres, rods, tubes, and wires, using a variety of techniques [19]. These techniques include sol-gel, hydrothermal, thermal decomposition, and co-precipitation methods. Metal oxide nanoparticles' distinctive characteristics and diverse morphologies make them appealing for use in a variety of applications, including catalysis, energy storage, electronics, and medicine. [22].

2.3.1 Synthesis of metal oxide-based nanoparticle

Metal nanoparticles are prepared and stabilized using an array of chemical as well as physical methods. Some of these methods include electrochemical changes, chemical reduction, and photochemical reduction [23]. The selection of a metal nanoparticle preparation technique is crucial because different techniques can affect the stability, physicochemical properties, and morphology of the nanoparticles. For example, the kinetics of metal ions' interactions with reducing agents and the process by which stabilizing agents adhere to metal nanoparticles can impact the properties of the resulting nanoparticles [24]. Approaches for preparing metal nanoparticles fall into two distinct groups: bottom-up methods and upward methods. Bottom-up methods involve building up the nanoparticles from small precursor molecules or atoms, while top-down methods involve breaking down larger materials into smaller nanoparticles [25]. Examples of bottom-up methods include chemical reduction, which involves the reduction of metal ions in solution to form nanoparticles, and sol-gel synthesis, which involves the hydrolysis and condensation of metal alkoxides to form nanoparticles [26]. Examples of top-down methods include laser ablation, which involves the use of lasers to break down bulk metal into nanoparticles, and milling, which involves the mechanical grinding of bulk metal to form nanoparticles. Each of these approaches has its advantages and disadvantages, and the choice of method depends on factors such as the desired nanoparticle properties and the available resources [25]. Whereas atoms or molecules are the starting material in bottom-up approaches, top-down methods start with bulk material and use various physical, chemical, and mechanical processes to reduce the particle size to nanoparticles illustrated in Figure 2.3.

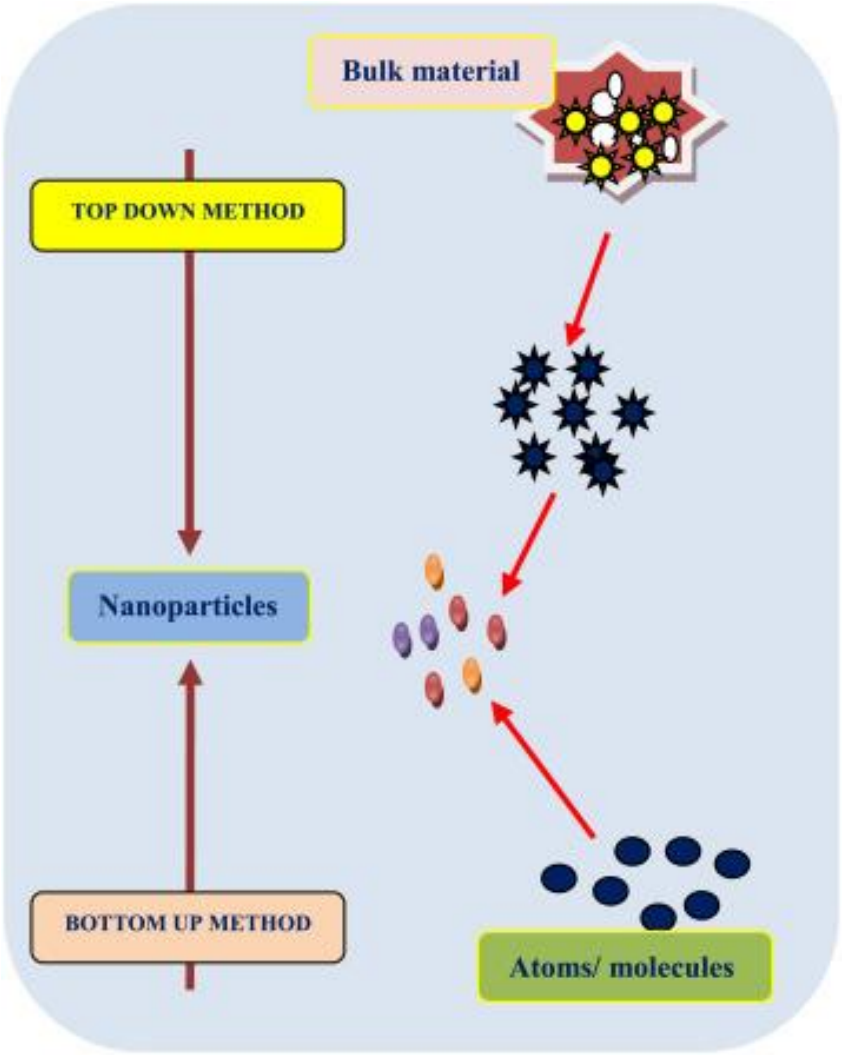

Figure 2.3: A diagram of top and bottom approaches [26].

The upward technique entails breaking down bulk materials into smaller nanoparticles via various physical and chemical processes such as thermal, laser, and mechanical milling [27]. Although this method is simple, it is not ideal for creating very small and irregularly shaped particles, and it can alter the surface chemistry and physicochemical characteristics of the nanoparticles. In contrast, the bottom-up approach involves creating nanoparticles from smaller molecules like atoms, molecules, or small particles [26]. This approach starts by producing nanostructured building pieces that are then combined to form the final nanoparticle. The bottom-up approach can produce very small and precisely shaped nanoparticles without altering their surface chemistry or physicochemical characteristics. Both approaches have advantages and limitations, and the choice of approach depends on the specific application and requirements [27].

2.3.2 Physical vapour deposition method

The physical deposition method, which involves depositing a material onto a surface as a thin film or nanoparticle. This process is achieved by vaporizing the material using controlled vacuum techniques, such as thermal evaporation and sputtering deposition, and then condensing it onto a substrate. The fabrication of lanthanum strontium cobalt thin films frequently uses physical vapour deposition techniques, such as pulsed vapour deposition. In this process, a solid target is ablated using a laser, which creates ablated species in plasma [28]. These ablated species are then deposited onto a substrate to create a film. Carbon nanotubes are also coated using this technique with thin films and metal nanoparticles. However, the physical deposition method has some drawbacks. It can be expensive and generate a low volume of material. Therefore, this method may not be suitable for large-scale production or applications that require large quantities of material [24].

2.3.3 Sol-gel method

The sol-gel method is a technique for synthesizing nanoparticles, which involves mixing metal or metal oxide particles with a pre-hydrolysed silica sol or a sol containing the matrix-forming species, followed by gel formation [29]. The method can be carried out in different ways, including direct mixing of metal or metal oxide particles with the pre-hydrolysed silica sol, or mixing prefabricated colloids of metal or metal oxide with a sol containing the matrix-forming species [30]. The process of synthesizing nanoparticles using the sol-gel method typically involves four main phases: hydrolysis, condensation, particle growth, and particle agglomeration. In the direct precipitation approach, silica sol is heated at a low temperature to precipitate the metal oxide particles. Gelatin and colloidal suspension are used to create a network in a continuous liquid phase (gel). Silanes, such as tetramethoxysilane (TMS) and tetraethoxysilane, are commonly used to create silica gel. Metal alkoxides, which are organo-metallic precursors for numerous metals including titanium, silica, and aluminium, are also used in the sol-gel method [31]. This approach involves producing a homogeneous solution of one or more chosen alkoxides and then adding a catalyst to start a reaction at a specific pH. By carefully controlling the reaction conditions, it is possible to manage the particle size and morphology, making the sol-gel method a useful technique for synthesizing nanoparticles with specific properties [32]. Bach et al., [33] produced lamellar type birnessite MnO_2 from combined, using a sol-gel technique. MnO_2 gels were created by reducing water permanganate solutions with biological reducing substances, with fumaric acid yielding the best results. It was discovered that cations are alkaline interacted with manganese oxide to form tertiary oxides. Hydrothermal and sol-gel processes were used to create various crystal states of MnO_2 nanostructures. The hydrothermal approach was used to create α-MnO_2, β-MnO_2, and δ-MnO_2 nanorods, whereas the sol-gel method was used to create γ-MnO_2 [34]. Overall, these studies demonstrate that different methods can be used to synthesize MnO_2 nanostructures with different crystal phases and morphologies. The choice of method depends on the desired properties and applications of the MnO_2 [27] .The sol-gel process, which is a simple technique used for the synthesis of oxide films with controlled thickness, morphology, and crystal structure. The sol-gel process involves the conversion of a liquid "sol" into a solid "gel" phase, which can be further processed into thin films as shown in Figure 2.4. The sol-gel process's key advantage is its ability to control the reaction at the molecular level, resulting in very pure products with homogeneous form and structure as crystals [33]. One of the main drawbacks is the relatively long time required for the synthesis, which can be a hindrance in large-scale production. Additionally, there is a risk of agglomeration, where the nanoparticles clump together, leading to reduced purity and uniformity of the resulting oxide films. Despite its limitations, the sol-gel process remains a powerful tool for the synthesis of oxide films with controlled properties. Ongoing research continues to refine the sol-gel process and address its limitations, leading to the development of new and improved techniques for the synthesis of oxide films [32].

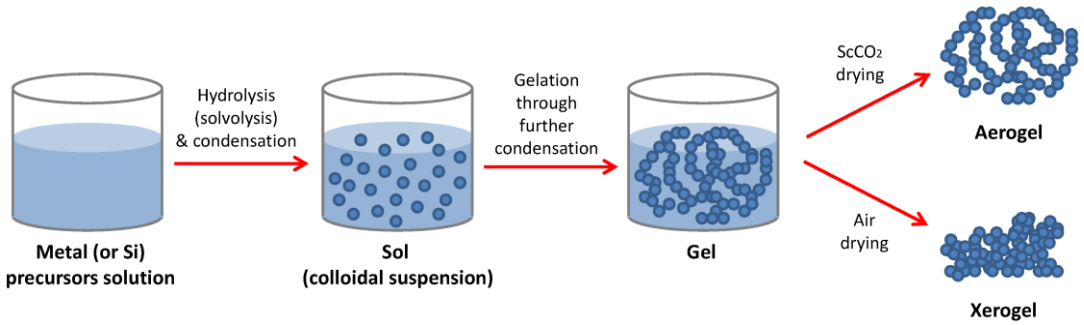

Figure 2.4: Schematic representation for the synthesis of sol gel method [33].

2.3.4 Hydrothermal Method

The hydrothermal method is a chemical synthesis technique that involves the reaction of a solid material with aqueous solution vapour at high pressure and temperature. The process leads to the deposition of small particles [35]. In this method, cations precipitate in a polymeric hydroxide form, and these hydroxides further undergo dehydration, which accelerates the formation of metal oxide crystal structures. The presence of a second metal cation is beneficial in controlling the particle formation process, as it prevents the formation of complex hydroxides when a base is added to a metal salt solution [25]. Overall, the hydrothermal method is a useful technique for synthesizing small

particles with controlled structures and properties, and it has many applications in fields such as materials science, catalysis, and nanotechnology [36]. The high pressure and temperature conditions in the hydrothermal process promote the formation of well-crystallized nanoparticles with a narrow size distribution. Additionally, the process can be carried out in a closed system, which reduces the risk of contamination and allows for precise control of reaction conditions as demonstrated in Figure 2.5. The resultant nanoparticles may possess particular chemical and physical characteristics that enable a variety of uses in industries like healthcare, electronics, and energy [35]. Kwak et al. [37] reported a single-step method for achieving homogeneous and controlled crystal growth, allowing the phase and product ratio to be controlled. Wei et al. [38] used a hydrothermal process to prepare α- and β-MnO_2 nanowires from commercially available γ-MnO_2 and proposed a mechanism for nanoparticle formation. Wang et al. [34] explored the effects of inorganic cation concentrations on the reaction media and provided a regulated hydrothermal method for creating α-, β-, γ-, and δ-MnO_2. The hydrothermal reactions may regulate the chemical response as illustrated by Cheng et al, allowing for the reasonable formation of manganese dioxide with various geometries and appealing crystal forms.

Figure 2.5: Schematic representation for the synthesis of MnO_2 using hydrothermal method. *Reprinted with permission* [39].

The following are the chemical processes that are used in this method:

$$MnSO_{4\ (s)} + 2KMnO_{4\ (s)} + 2H_2O_{\ (l)} \longrightarrow K_2SO_{4(aq)} + 2H_2SO_{4\ (aq)} + 5MnO_{2\ (s)}$$

Hydrothermal process has become increasingly popular in recent years due to their many advantages over traditional synthesis methods. One of the primary advantages of hydrothermal processes is their ability to produce NPs with controlled sizes and shapes. Another advantage of hydrothermal processes is that they can be used to create uniform, integrated crystal structures. Overall, the advantages of hydrothermal processes make them an attractive method for the preparation of nanoparticles, and their use is likely to continue to grow in popularity in the coming years [35].

2.3.5 Chemical reduction method

The chemical reduction method is a popular technique used to synthesize metal nanoparticles [40]. The process involves the reduction of an ionic salt in an appropriate medium in the presence of a surfactant using different reducing agents. For example, sodium borohydride can be used as a reducing agent in an aqueous solution to prepare metal nanoparticles. During the process, the formed metal nanoparticles are capped using a stabilizing agent, such as trisodium citrate (TSC) or sodium lauryl sulfate (SLS), to prevent their aggregation [41]. The stability of the metal nanoparticles in the dispersion is monitored by analysing the absorbance. Other reducing agents that can be used to synthesize metal nanoparticles include glucose, ethylene glycol, ethanol, citrate of sodium, and hydrazine hydrate, among others. The choice of reducing agent depends on the type of metal being synthesized and the desired properties of the resulting nanoparticles [42]. For example, sodium borohydride is commonly used for the synthesis of silver nanoparticles due to its high reduction potential and ability to produce stable nanoparticles. Chemical reduction methods are often used in

various fields, including metallurgy, chemistry, and materials science. However, they have several disadvantages, which include [40]:

- Environmental impact: Many chemical reduction methods require the use of hazardous chemicals that can be harmful to the environment. The production of these chemicals can also be energy-intensive and contribute to greenhouse gas emissions.
- Safety hazards: Chemical reduction processes can also pose safety hazards to workers, especially if they involve the use of highly reactive or flammable chemicals.
- Cost: Chemical reduction methods can be expensive due to the high cost of raw materials and energy required to produce them.
- Complexity: Many chemical reduction methods are complex and require specialized equipment and skilled operators. This can make them difficult to implement on a large scale.
- Product purity: Chemical reduction methods may not always produce high-purity products, as impurities can be introduced during the reduction process.
- Overall, chemical reduction methods have several disadvantages that need to be considered when selecting a suitable method for a particular application. Alternatives such as electrochemical or bio reduction may provide more sustainable and safer alternatives [43].

2.3.6 Solvothermal method

The solvothermal method is a chemical synthesis technique used to produce nanoscale materials, such as nanoparticles or nanocrystals, by using a solvent under high temperature and pressure conditions [44]. This method is commonly used to prepare inorganic materials, such as metal oxides, sulphides, and nitrides. The presence of water or organic solvents, such as methanol, ethanol, or polyols, in the reaction mixture is crucial for the solvothermal method to work effectively. The solvent plays a critical role in controlling the reaction rate, reducing the particle size, and enhancing the purity of the resulting nanomaterials. The solvothermal reaction is typically performed in a pressure vessel that can withstand high temperatures and pressures. The solvent is heated above its boiling point, and the reactants are added to the mixture [41]. The pressure vessel is then sealed and heated to the desired temperature and pressure conditions, which can range from a few hours to several days. Microwave-assisted reactions can be employed to increase the kinetics of crystallization by one to two orders of magnitude. This is achieved by applying electromagnetic radiation in the microwave frequency range to the reaction mixture, which can induce rapid heating and enhance the reaction rate [45]. Microwave-assisted solvothermal synthesis is a promising technique for the rapid and efficient production of nanomaterials with controlled size, morphology, and composition [41].

2.3.7 Other methods of metal-nanoparticle synthesis

2.3.7.1 Microwave-assisted nanoparticle preparation

Microwave-assisted nanoparticle preparation is a technique that involves using microwave radiation to synthesize and prepare nanoparticles [41]. This method is a quick and efficient way to produce nanoparticles with a narrow size distribution and controlled morphology. The process typically involves the use of a precursor solution containing the desired metal ions or other chemicals. This solution is then exposed to microwave radiation, which heats the solution rapidly and promotes the formation of nanoparticles [46]. By adjusting the amount of each component of the initial solution, microwave energy, and response time, the dimensions, form, and makeup of the nanoparticles can be adjusted. However, as compared to traditional methods of nanoparticle synthesis, microwave-assisted preparation offers several advantages [25]. It is a fast process, often taking only a few minutes, and requires less energy and fewer chemicals. The resulting nanoparticles are also more consistent in size and shape, making them suitable for an array of purposes such as catalysis, biomedical imaging, and drug delivery [21]. MnO was produced on nickel-based graphene by Bello et al., [47] using a thermal microwave heating approach. The prepared materials were then investigated for their electrochemical applications. Zhang et al., MnO_2 was synthesized using a microwave-assisted reflux condenser. When the reaction was carried out under neutral conditions, the researchers discovered

that the results consisted of both small plates and tiny wires are two types of nanomaterials. fortunately as the response time increased from 5 to 30 minutes, so did the nanowire-to-nanoplate ratio, as did the length of the nanowires [48]. The preferential development of crystal planes under specified conditions explained the change in morphology with microwave irradiation period [47]. Both studies demonstrate the potential of microwave-assisted methods for the synthesis of MnO and MnO_2 with different morphologies and properties. The use of microwave irradiation can promote rapid and efficient heating, resulting in the formation of nanoparticles with unique morphologies and crystal structures. Such methods can offer several advantages over traditional synthesis methods, such as shorter reaction times and improved product yields [41].

2.3.7.2 Biological method

The biological methods for synthesizing nanoparticles involve the use of biological organisms or their components, such as enzymes or proteins, to produce nanoparticles. These approaches have a number of benefits over conventional chemical procedures, including lower costs, softer conditions for reaction, and lesser environmental effect [29]. One approach to biological synthesis of nanoparticles involves the use of microorganisms such as bacteria, fungi, and algae. These organisms produce enzymes and other biomolecules that can be used to reduce metal ions into nanoparticles. For example, some bacteria can reduce silver ions into silver nanoparticles, while certain fungi can produce gold nanoparticles. Another method involves using plant extracts or proteins to synthesize nanoparticles. Plant extracts contain a variety of biomolecules such as flavonoids, terpenoids, and phenolics, which can be used as reducing and stabilizing agents in nanoparticle synthesis [49]. Proteins, such as bovine serum albumin and gelatine, biological can also be used to synthesize nanoparticles by acting as both reducing and capping agent methods for nanoparticle synthesis have various possibilities in health, technology, and catalysis. For example, nanoparticles produced by biological methods have shown promise in drug delivery, imaging, and cancer therapy [41].

2.3.7.3 Electrochemical deposition

Electrochemical deposition (ED) is one such method used to produce metal nanoparticles, which involves the use of an electrolytic bath containing metal salts and a three-terminal potentiostat [50]. In this technique, a cathode electrode is used for the deposition of metal nanoparticles, while an anode electrode and a reference electrode such as Ag/AgCl or calomel are also used. A slight voltage is applied for a suitable time in the electrolytic bath, which helps in the deposition of the metal nanoparticles. This technique is widely employed for different purposes such as cyclic voltammetry, double pulse, and potential step deposition. Other methods like electrodeposition synthesis or template synthesis are also used to produce nanomaterials, while ion etching is preferred to produce porous alumina membranes [41]. Manganese oxide is electrochemically deposited from several manufactured minerals, including manganese chloride, manganese acetate, and manganese sulfate, and the conditions under which this process is carried out can affect the characteristics of the substance that is produced. The electrochemical deposition process involves applying an electric potential to a solution containing the manganese salt and a suitable electrode [40]. Manganese oxide material performance is largely dependent on its oxidation state, structure, surface area, and other deposition possibilities and circumstances, including workload cycle, rate, and current density. Ghaemi and Binder used both quick current and regular direct current to explore the electrochemical features of manganese dioxide coated. A variety of anode peak current densities, pulse frequencies, and duty cycles were used throughout the electrodeposition process. The resulting manganese dioxide material was then characterized to determine its properties and performance [38]. Overall, electrochemical deposition is a promising approach for the synthesis of manganese dioxide materials with controlled properties. Better materials for electrodes for use in devices that store energy and other purposes might result from additional studies in this area of study [49]. There are several ways to improve the electrode's surface, such as the doping process, which, when referring to metal-based nanoparticles, is the deliberate addition of impurities or foreign atoms to the particles' crystal lattice. Doping is a widely used technique to alter the characteristics of nanoparticles for certain uses. Dopant compounds are added during the synthesis or post-synthesis stages of the doping process.

2.4 Introduction of the doping method for metal-based nanoparticle

Doping is the process of introducing small amounts of foreign materials (dopants) into a material to modify its properties. The doping synthesis method for metal nanoparticles involves the addition of dopants during the nanoparticle synthesis process. One common doping method for metal nanoparticles is the chemical reduction method. In this method, a reducing agent is added to a solution containing the metal precursor and dopant precursor. The reducing agent reduces the metal precursor, forming nanoparticles, while the dopant precursor is incorporated into the nanoparticle structure [51]. The dopant can be introduced in different ways, for example, by adding it to the solution before or after the metal precursor, or by co-reducing both precursors. Another method is the thermal decomposition method, where metal precursors and dopants are heated in a solvent or in the presence of a surfactant, causing the precursors to decompose and form nanoparticles. The dopant can be introduced by adding it to the precursor mixture before heating, or by adding it during the heating process. Doping can also be achieved by surface modification of the nanoparticles. This involves coating the surface of the nanoparticles with a dopant material [52]. The dopant can be introduced by adding it to the solution during or after the nanoparticle synthesis, or by using a dopant-modified surfactant. The choice of doping method depends on the specific dopant and metal nanoparticle system, as well as the desired properties of the doped nanoparticles. Careful control of the doping process is crucial to achieving uniform doping and desired nanoparticle properties [53].

2.4.1 Chemical reduction method

The chemical reduction method is a commonly used technique for doping metal nanoparticles. In this method, a reducing agent is used to convert metal ions into their corresponding metal nanoparticles. The reducing agent also serves as the dopant source, which is incorporated into the metal nanoparticles during their formation. One example of this method is the synthesis of silver nanoparticles doped with copper [52]. In this case, a reducing agent such as sodium borohydride is added to a solution containing silver ions and copper ions. The reducing agent reduces both the silver and copper ions to form silver-copper alloy nanoparticles. The amount of copper in the resulting nanoparticles can be controlled by adjusting the ratio of copper ions to silver ions in the solution. This method has several advantages over other doping techniques, such as high efficiency, low cost, and easy control over the dopant concentration. However, it also has some limitations, such as limited control over the size and shape of the nanoparticles and the need for careful handling of the reducing agent [7].

2.4.2 Thermal decomposition method

The thermal decomposition method for doping of metal nanoparticles is a technique used to prepare metal nanoparticles with controlled doping. In this method, a metal precursor is thermally decomposed in the presence of a doping agent to create metal nanoparticles with the desired dopant concentration [41]. The process involves the heating of a metal precursor in a solvent, usually a high-boiling point organic solvent such as oleyl amine or trioctylphosphine (TOP). The doping agent is then introduced into the reaction mixture, which can either be a metal salt or an organometallic compound. The mixture is then heated to a high temperature, typically around 200-300°C, which causes the metal precursor to decompose and form nanoparticles. The doping agent reacts with the metal precursor during the decomposition process, resulting in the incorporation of the dopant into the metal nanoparticles. The dopant concentration can be controlled by adjusting the amount of doping agent added to the reaction mixture [54]. The thermal decomposition method for doping of metal nanoparticles has several advantages over other doping methods, such as chemical reduction and co-precipitation. It allows for precise control of the dopant concentration, resulting in nanoparticles with a uniform distribution of dopants. The method also allows for the preparation of nanoparticles with a wide range of sizes and shapes. Overall, the thermal decomposition method for doping of metal nanoparticles is a powerful technique for the preparation of doped nanoparticles with controlled properties for a variety of applications, including catalysis, electronics, and biomedicine [51].

2.5 Stabilising agent for metal-based nanoparticle.

A stabilizing agent for metal nanoparticles is a substance that is added to a metal nanoparticle solution to prevent the particles from agglomerating or clumping together. Because of their strong sensitivity and propensity to aggregate, metal nanoparticles may lose some of their special qualities and become brittle [55]. Stabilizing agents can be organic or inorganic and work by forming a protective layer around the nanoparticles, which prevents them from encountering each other. This layer can be formed through various mechanisms, including electrostatic interactions, steric hindrance, and chemical bonding. Commonly used stabilizing agents for metal nanoparticles include surfactants, polymers, and inorganic compounds such as silica or gold [35]. The choice of stabilizing agent depends on the specific properties of the metal nanoparticle being used and the application for which it is intended. Overall, the use of a stabilizing agent is crucial for maintaining the stability and functionality of metal nanoparticles, making them suitable for a wide range of applications in fields such as electronics, biotechnology, and medicine [56].

2.6 Manganese oxide nanoparticle material

Manganese oxide nanoparticles are a type of small particle with diameters ranging from 1 to 100 nanometer. They have unique physical and chemical properties that make them useful in a wide range of applications [57]. Their enormous area to volume ratio, which makes them extremely reactive and capable of catalysing a variety of chemical reactions, is one of their essential characteristics. Manganese oxide nanoparticles are also magnetic and have potential applications in magnetic resonance imaging (MRI) and drug delivery. They have been studied for their potential use in environmental remediation, such as the removal of heavy metals and detection of pollutants in polluted water [58]. Additionally, they have been investigated for their use in energy storage devices such as batteries and supercapacitors. Manganese oxide nanoparticles can have various oxidation numbers (+2, +3, +4), resulting in different structural forms such as MnO, MnO_2, Mn_2O_3, and Mn_3O_4 nanostructures. This versatility makes manganese oxide an attractive area of research. MnO_2 nanoparticle is of great interest due to its unique properties. It has a low band gap and high optical constant, which may have potential applications in areas such as solar cells, catalysis, and sensors [59].

2.6.1 Crystal structure of manganese oxide nanoparticle material

Manganese oxide refers to a family of compounds made up of manganese and oxygen atoms. The crystal structure of manganese oxide can vary depending on the specific compound, as there are several different types of manganese oxide with different crystal structures [60]. The various polymorphic forms of MnO_2, which include α-, β-, γ-, δ-, and λ-types, and are shown in Figure 2.6. These different polymorphs are formed by the arrangement of basic MnO_6 octahedron units with different connectivity, resulting in layer structures or chain/tunnel structures. For example, the most common form of manganese oxide is MnO, which has a rock salt crystal structure. This means that the manganese and oxygen atoms form a regular pattern of alternating layers, like the structure of common table salt. MnO_2, on the other hand, has a rutile crystal structure, with the manganese and oxygen atoms forming a tetragonal arrangement. Other manganese oxide compounds, such as Mn_2O_3 and Mn_3O_4, have different crystal structures such as cubic and spinel, respectively [61]. These crystal structures are determined by the arrangement of the atoms in the compound, which can affect its properties such as its electrical conductivity, magnetic properties, and catalytic activity [62]. MnO6 octahedrons combine with further MnO_6 octahedra to form links along to the c-axis and holes between these links. The difference between the polymorphs lies in the arrangements of Mn^{4+} within the octahedral sites, as each polymorph is comprised of a hexagonally close-packed lattice structure made up of O^{2-} anions and Mn^{4+} cations, as shown in the Figure 2.7 [60]. These different polymorphic forms can exhibit different physical and chemical properties, such as their electrochemical performance or catalytic activity, due to their unique crystal structures and arrangements of Mn^{4+} ions. Therefore, understanding the synthesis and characterization of these polymorphic forms is important for tailoring their properties for various applications [63].

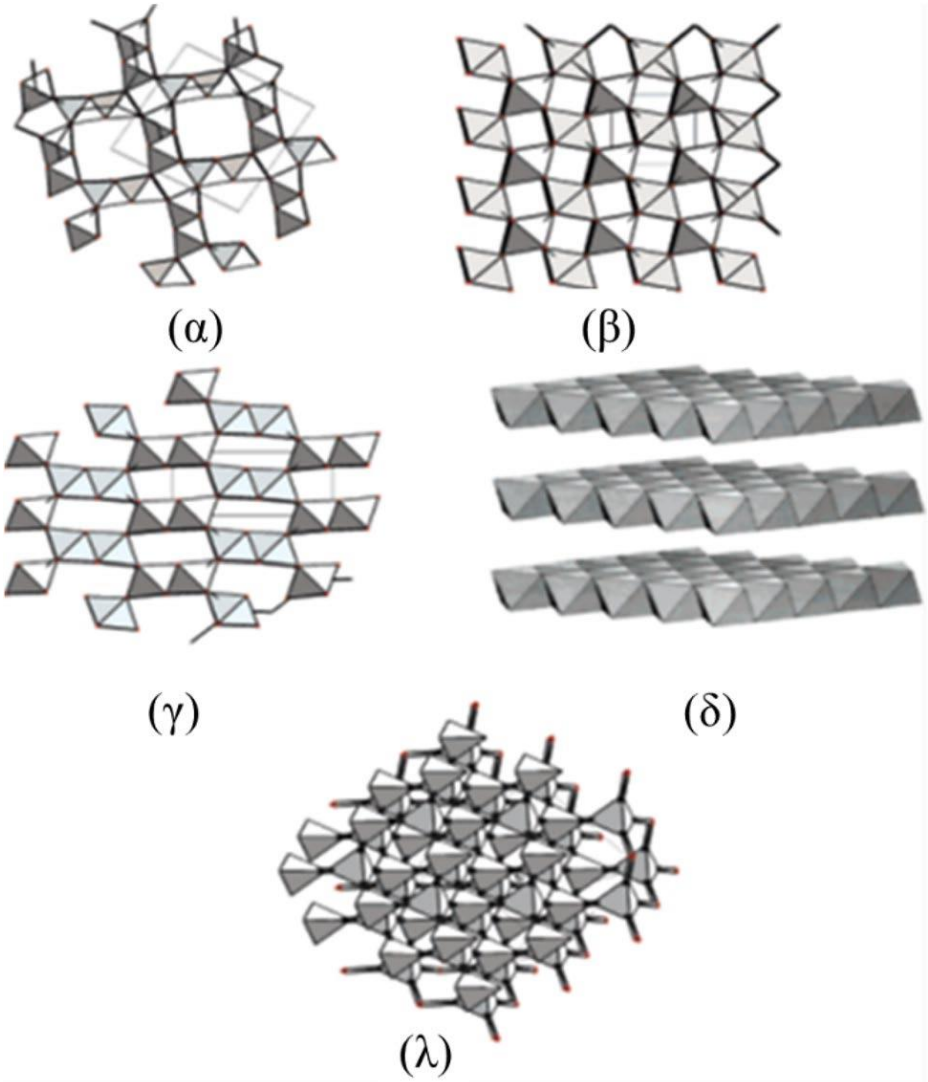

Figure 2.6: Crystal structures of α-, β-, γ-, δ-, λ-MnO_2. *Reprinted with permission* [56].

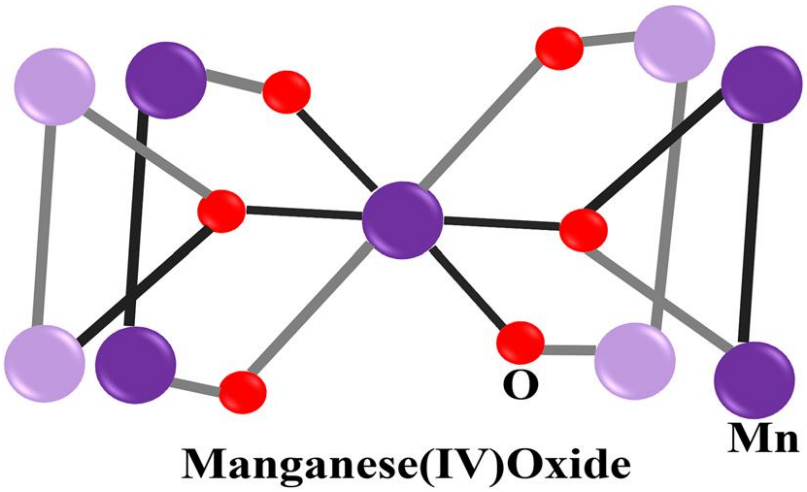

Figure 2.7*:* MnO_2 unit cell model in the form of a ball and stick (manganese atoms are violet, while oxygen atoms are red). Reprinted with permission [56].

2.6.2 Different types of manganese oxide nanoparticle

There is a rising interest in synthesizing manganese oxide with appealing forms, including urchin-like, three-dimensional (3D) helices, and narrow-minded (1D) nanowires, nanorods, and nanotubes, as well as multifaceted (2D) nanoflakes and nanosheets. These different morphologies can significantly affect the properties of MnO_2, and researchers are exploring various methods to produce these structures as shown in Figure 2.8 [64]. For example, Yang et al. [65] synthesised different MnO_2 crystal structures and investigated their orange methyl binding capabilities. They showed that the geometries and crystalline structures had a significant influence on the adsorption capabilities, with amorphous MnO_2 exhibiting the maximum activity. Using a soft-chemical method, Zang et al. [48] created 1D α-MnO_2 nanowires/nanorods and 2D δ-MnO_2 nanoplates with extremely stable pseudo capacitance characteristics. produced 2D δ-MnO_2 nanoplates and 1D α-MnO_2 nanowires/nanorods. Baral et al. [56] used the hard template method to create 2D and 3D-MnO_2 and the hydrothermal method to create 1D-MnO_2 nanorods. The 3D MnO_2 hierarchical structures often produce more active sites or possess more interesting properties compared to 1D/2D nanostructures. The best performing polymorphs were found to be those with an open three-dimensional microporous and mesoporous morphology, which have higher BET surface areas. The improved surface area allowed for more adsorption of oxygen to lattice oxygen, leading to a higher Oads/Olatt molar ratio and faster reducibility. Catalytic activity was observed only in certain MnO_2 polymorphs, specifically those with a distorted cubic phase containing Mn (III). These phases include Mn_2O_3 (bixbyite), Mn_3O_4 (hausmannite), and λ-MnO_2 (spinel). The longer Mn-O bonds between edge-sharing MnO_2 octahedra in these phases contribute to lattice distortions due to the Jahn-Teller effect [25]. This effect, combined with the antibonding electronic configuration of degenerate Mn (III) electrons, is hypothesized to contribute to the structural flexibility that is important for catalytic turnover in moist conditions at the surface. The relationship between the morphology and surface area of MnO_2 polymorphs and their catalytic activity, highlighting the importance of specific phases containing Mn (III) and the role of lattice distortions due to the Jahn-Teller effect. Therefore, understanding the morphology of manganese oxide is crucial for designing and optimizing its properties for specific applications [60]. Manganese oxide's morphology can be affected by its manufacturing procedure and environmental factors like pH and temperature, which can be used to modify and customize the material's characteristics for a range of uses [21].

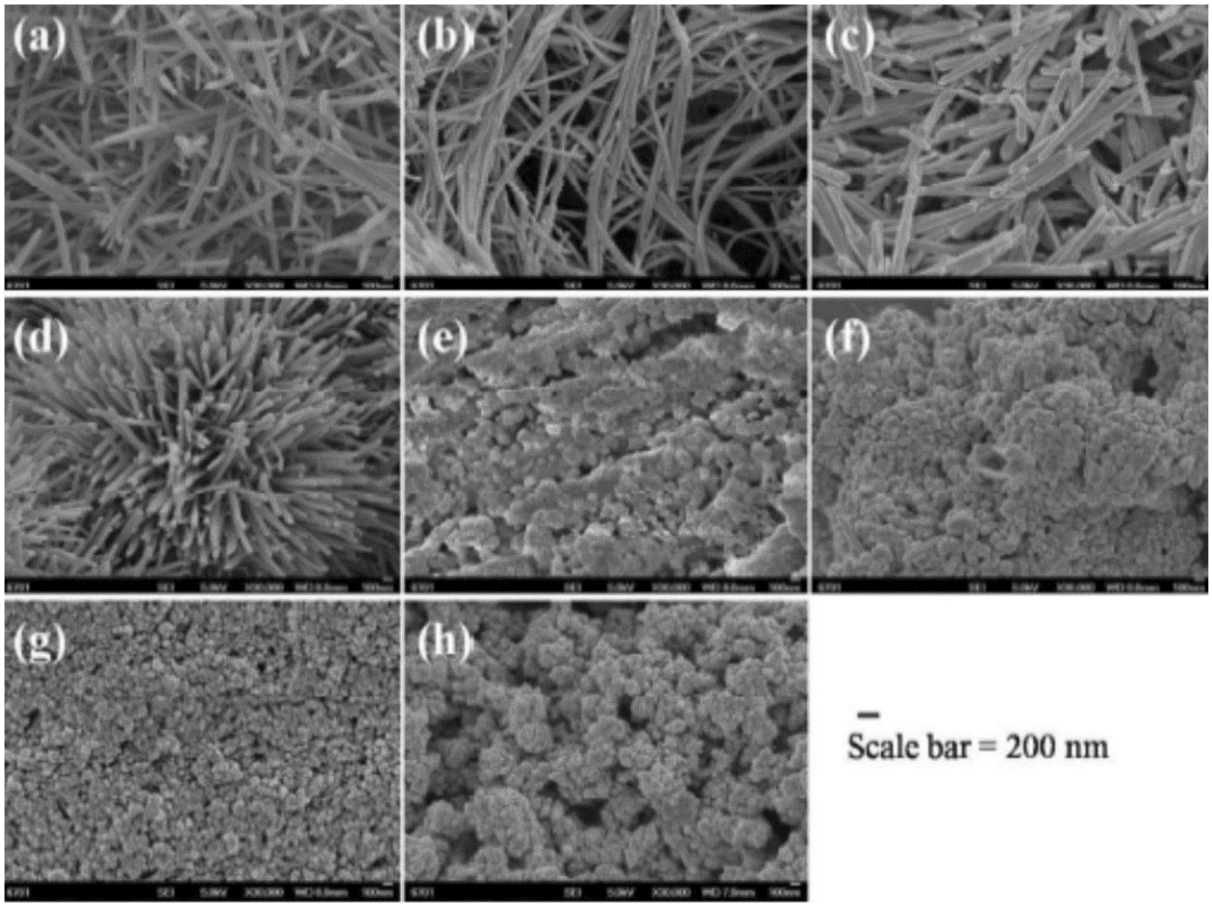

Figure 2.8: a α-MnO_2 nanotubes, **b** α-MnO_2 nanowires, **c** β-MnO_2, **d** γ-MnO_2, **e** δ-MnO_2, **f** Mn_2O_3, **g** Mn_3O_4 and **h** A-MnO_2 for SEM pictures. Reprinted with permission [66].

2.6.3 Synthesis of manganese oxide nanoparticle

The synthesis of MnO_2 nanoparticles can be achieved through several methods, including chemical precipitation, hydrothermal method (HT), sol-gel process, and sonochemical method [45]. These methods can result in the synthesis of MnO_2 nanoparticles with different properties, such as particle size, crystallinity, and morphology, depending on the specific synthesis conditions. The properties of manganese oxide can be affected by the method used to synthesize it, as well as the starting materials that are used. The specific phases of the resulting manganese oxide can vary depending on these factors [19]. Additionally, the conditions under which the synthesis reaction takes place, such as temperature and pH, can also have a significant impact on the final product. Therefore, controlling these factors during the synthesis process is important for achieving desired properties and characteristics of the manganese oxide product. A summary is provided on the shape, stoichiometry, and process of synthesis of the several manganese oxide alternatives in Table 2.1. Furthermore, the synthesis of MnO_2NPs can be tailored to produce different crystal phases, such as alpha, beta, and gamma, which can exhibit different properties and reactivity [67]. Additionally, the synthesis method can also influence the morphology and structure of the particles, such as the formation of hollow or porous structures, which can enhance their catalytic activity or drug delivery properties. The importance of the synthesis of manganese oxide nanoparticles lies in the ability to control and tailor their properties for various applications, which can lead to advancements in areas such as renewable energy, nanomedicine, and environmental science [38].

Table 2.1: The synthetic procedures used to produce MnO_2 with different geometries using different substrates are shown in the table.

Methods	Mn source	O_2 source	Temp(˚C)	Solvent	Product	Morphology	Ref
HT	$MnSO_4.H_2O$	$KMnO_4$	80	H_2O	α-MnO_2	nanorods	[68]
HT	$MnSO_4$	$KClO_3$	140-200	H_20	α-MnO_2	nanorods	[58]
HT	$KMnO_4$	-	140	CH_2COOH	α-MnO_2	nanowires	[56]
HT	$KMnO_4$	H_2SO_4	110	H_2O	α-MnO_2	nanorods	[64]
HT	$MnSO_4$	$NaMnO_4$	240	H_2O	β-MnO_2	nanobelts	[58]
HT	$MnCl_2.H_2O$	$KMnO_4$	450	NH_4OH	α-MnO_2	nanostructure	[62]
HT	$MnSO_4.H_2O$	$KMnO_4$	-	H_2O_2	MnO_2	nano powder	[25]
MWA	$MnSO_4.H_2O$	$K_2S_2O_8$	98	C_2H_6O	-	-	[48]
CP	$MnCl_2$	$KMnO_4$	80	H_2O	α-MnO_2	-	[69]
P	$MnCl_2$	NaOH	160	H_2O	-	-	[22]
HT	$KMnO_4$	-	200	HCl, H_2O	-	nanorods	[45]

HT, Hydrothermal, MWA, Microwave assisted method, CP, Chemical precipitation, P, precipitation method.

2.6.4 Modification of the Manganese oxide nanoparticle

Modification of manganese oxide nanoparticles involves changing the surface properties of the nanoparticles through chemical or physical methods. This change can affect the surface area of charge and group function, as well as increase their durability, dispersion, and responsiveness. Some common methods for modifying manganese oxide nanoparticles include surface functionalization with organic or inorganic molecules, surface coating with polymers or surfactants, and doping with other elements [69]. One example of modification is the synthesis of manganese oxide nanoparticles functionalized with amines, which can enhance their dispersibility in aqueous solutions and make them suitable for applications such as catalysis, biomedicine, and energy storage. Another example is the coating of manganese oxide nanoparticles with silica, which can improve their stability and reduce their toxicity in biological systems, making them useful for drug delivery and imaging applications. Overall, modification of manganese oxide nanoparticles can lead to a wide range of properties and applications, depending on the specific modification method and intended use [22].

2.7 Application of manganese oxide nanoparticle in sensors

Metal-oxide nanoparticles have gained significant attention in the development of sensors and biosensors due to their unique properties, such as high surface area, tunable morphology, and excellent chemical stability. These nanoparticles have found applications in various sensing platforms, contributing to advancements in areas such as environmental monitoring, healthcare, and food safety [57]. This results in improved sensitivity and selectivity of the sensor. Here are some examples of the application of manganese oxide in sensors namely chemical sensor, gas sensor and biosensors.

2.7.1 Chemical sensors

Chemical sensors are devices that detect and measure the concentration of chemical analytes in a sample. In sensing systems, there are typically two main components: the sensing material and the transducer [70]. The sensing material is responsible for detecting and responding to the target molecule or analyte of interest, while the transducer converts the resulting signal into a quantifiable output, typically an electronic signal. They are widely used in various fields such as environmental

monitoring, industrial process control, medical diagnosis, and food safety. Chemical sensors can be classified into different types based on their sensing mechanism, including optical sensors, electrochemical sensors, mass sensors, and thermal sensors [71]**.** Chemical sensors can be designed using different materials as the sensing element, including metals, metal oxides, polymers, and nanoparticles. Manganese oxide nanoparticles, for instance, have been extensively studied for their applications in chemical sensing due to their high sensitivity, selectivity, and stability toward a wide range of analytes. In summary, chemical sensors are versatile devices that are critical for a variety of applications in modern society. They can be based on different sensing mechanisms and materials, and the selection of the appropriate sensor depends on the specific application requirements [72]. Chemical sensors are becoming SnO_2, ZnO, Ga_2O_3, WO_2, and other compounds after recent major advancements in the detection and quantification of chemical species. Chemical sensors have been grouped here based on the kind of metal oxide that is employed to detect different target species. The most recent research on MON-based chemical sensors has been covered here, with Table 2.2 providing an overview. Tin oxide (SnO_2), incredibly sensitive and metal oxide that reacts quickly, has been extensively researched for the development of chemical detectors aiming multiple gases. Numerous geometries of nano-SnO_2 were utilized for specific or simultaneous chemical identification, such as NWs, hollow spheres, nanocrystals, and so on. Wang et al. demonstrated that the SnO_2 NW-based detector can identify hydrogen (H_2) concentrations ranging from 10 to 1000 ppm, which they ascribe to inadequately correlated molecules on the SnO_2 NWs edges [73]. In addition, Wang et al. suggested p-NiO/n-SnO_2 heterojunction nanofiber-based detectors with outstanding H_2 detecting features such as outstanding sensitivity and rapid response-recovery (3 s) behaviour with a threshold for detection of approximately 5 ppm H_2 at 320 °C, particularly for SnO_2 nanofibers with 4.11 mole% NiO [74]. Sensors for chemicals based on zinc oxide (ZnO) nanoscale have been attracting a lot of attention lately because of their distinct optical, electrical, and chemical sensing characteristics, as well as their ease of production. Generally speaking, numerous research groups have used ZnO NR or NW based sensors to detect a variety of substances [75]. Due to the material's chemical and thermal robustness, minimal hypersensitivity to moisture, moderate O_2 shortages, and imperfect crystallinity, For uses involving extreme temperature measuring, such as chemical, ecological, and explosion gas sensors, gallium oxide (Ga_2O_3) nanoscale is chosen [69,70].

Table 2.2: Comparison of performance of metal-oxide nanoparticle based chemical sensor.

Materials	**Target species**	**Detection of limit**	**Sensor response /temperature**	**Response / Recovery**	**Ref**
SnO_2 NW	H_2	10 ppm	20.4/ 300°C	N/A	[73]
SnO_2 nanocrystal	NO_2	100 ppb	–RT	–	[77]
NiO-SnO_2 nanofibers	Ethanol	100 ppm	25.5/ 300°C	1-3 s/1-3 min	[74]
ZnO NRs	Methanol	50 ppm	11.8/ 300°C	3 s/9 s	[75]
Ga_2O_3 NW	O_2/CO	1% O_2 / 20 ppm	1.02/20 4.75/400°C	N/A	[75]
NiO NTs	Ethanol	200 ppm	22.6/250	–	[78]
αFe_2O_3 hallow sphere	Ethanol	10 ppm	~/RT	–	[79]
WO_3 plates at nanoscale	Ethanol	10 ppm	~1.9/ / 300°C	–	[76]

2.7.2 Electrochemical sensor

Manganese oxide nanoparticles have also been extensively studied for their use in electrochemical sensing applications. Electrochemical sensors detect target analytes by measuring changes in electrical properties, such as voltage, current, or impedance, caused by the binding of the analyte to the sensing material. Manganese oxide nanoparticles can be used as the sensing material in electrochemical sensors due to their high surface area, excellent electrical conductivity, and redox activity [65]. The receptors that can be added to the nanoparticles to make them include enzymes, antibodies, and DNA strands that bind to target analytes only. In one study, manganese oxide nanoparticles were used as a sensing material for the detection of hydrogen peroxide (H_2O_2). The nanoparticles were functionalized with glucose oxidase, which catalyses the oxidation of glucose to produce H_2O_2. The H_2O_2 then reacted with the manganese oxide nanoparticles, altering the material's power characteristics. A common electrochemical method called cyclic voltammetry might be used to evaluate this change in power characteristics and connect it with the H_2O_2 concentration [38]. In another study, manganese oxide nanoparticles were used as a sensing material for the detection of dopamine, a neurotransmitter that plays an important role in the central nervous system. The nanoparticles were functionalized with aptamers, which are short single-stranded DNA or RNA molecules that specifically bind to target analytes. When dopamine bound to the aptamers on the surface of the nanoparticles, it caused a change in the electrical properties of the material, which could be measured using electrochemical impedance spectroscopy [54]. Overall, manganese oxide nanoparticles show great promise for use in electrochemical sensing applications due to their excellent electrical properties and ability to be functionalized with various receptors. Further research is needed to optimize their sensitivity and selectivity for different analytes and to develop more reliable and robust sensing devices [80]. The enhanced interaction and bigger contact area between MnOx and graphene were advantageous for the L-sensor for cysteine. MnOx/CNT/RGO nanohybrids-based exceptionally well electrodes for supercapacitor demonstrated this material's potential utility for modern energy-storage systems [81]. An excellent platform for measuring ferulic acid is provided by the f-MWCNT/MnO_2/GCE modified film. The combined impacts of CNTs and metal oxide nanocomposites may also increase electrode conductivity. A Pt/MnO_2/f-MWCNT/GCE modified electrode was created by electrochemically treating the f-MWCNT coated GCE to detect catechin [82]. This type of electrode offers a large linearity as well as a low sensitivity threshold. It detected melan in real-world samples of red wine, black tea, and green tea [83].

2.7.3 Gas sensor

Metal oxide semiconductors exhibit semiconducting behaviour due to deviations in stoichiometry, leading to the presence of defects. Cation vacancies act as acceptors, creating holes, while shallow states comprising oxygen vacancies act as n-type donors. The termination of the periodic structure at the free surface can lead to localized electronic states within the semiconductor bandgap [84]. A double layer of charge, known as a surface dipole, can form. Metal-semiconductor junctions at interfaces between layers and contacts are crucial for gas detection. The metal used for the contact can also act as a catalyst, enhancing gas detection capabilities. Contact resistance is more critical for single nanowires as it is in series with the semiconductor resistance. In bundles, contact resistance is connected to many resistances. Metal oxide gas sensors typically operate in air at temperatures between 500 and 800 K [82]. Conduction is electronic, and oxygen vacancies are doubly ionized and fixed. When the nanowire is fully depleted, carriers thermally activated from surface states contribute to conduction. Conduction in nanowire bundles is dominated by intercrystalline boundaries at nanowire connections The intergranular contact provides a significant portion of the sample resistance [84]. As shown in Figure 2.9, a metal oxide nanoparticle gas sensor typically it involves interconnecting electrodes to measure challenge, an insulation pad and wire to reach the right temperature for functioning, and a monitoring screen that changes opposition in response to contact. Conductometric gas sensors alter its electrical conductivity when confronted with a desired gas. The function of the receptor is determined by the interactions between gases and solids and can be altered while utilizing rare metals or combining several oxides, the transducer activity depends on the oxide's composition

[85]. Because absorption ions reduce surface resistivity while oxygen vacancies increase it, top equilibrium has a major impact on a metal oxide's barrier impedance. When molecules like O_2 or NO_2 attach themselves to the oxide's vacancy sites, the electrons leave the conduction band and conductivity drops. On the other hand, conductance increases and electrons are released when CO or H_2 from the O_2-rich environment combines the retained O_2 [86]. Most metal oxides have a solubility limit that typically ranges from 1 to 5%. When the sensing film's surface area is increased, the gas sensing performance rises as well, leading to the creation of porous nanostructures such nanotubes, nanospheres, nanowires, nanosheets, and so on that are rather loose in structure [87]. These hollow structures are typically created by hydrothermal, sol-gel, anodizing, or wet chemical procedures. Table 2.4 provides a summary of some instances of these structures, together with information on their shape, chemical makeup, and susceptibility to different gases [85]. Another way to modify electrical resistance and improve catalytic characteristics is doping, which can lead to the formation of p-n heterojunctions, smaller-sized doped metal oxides, increased activity through increased functional group density, or catalytic activity. The gap in energy is greatly reduced in the metal oxide when an insulating or not conductive nano oxide, a noble or transitional metal, or a particular impurity is added as the second component [87].

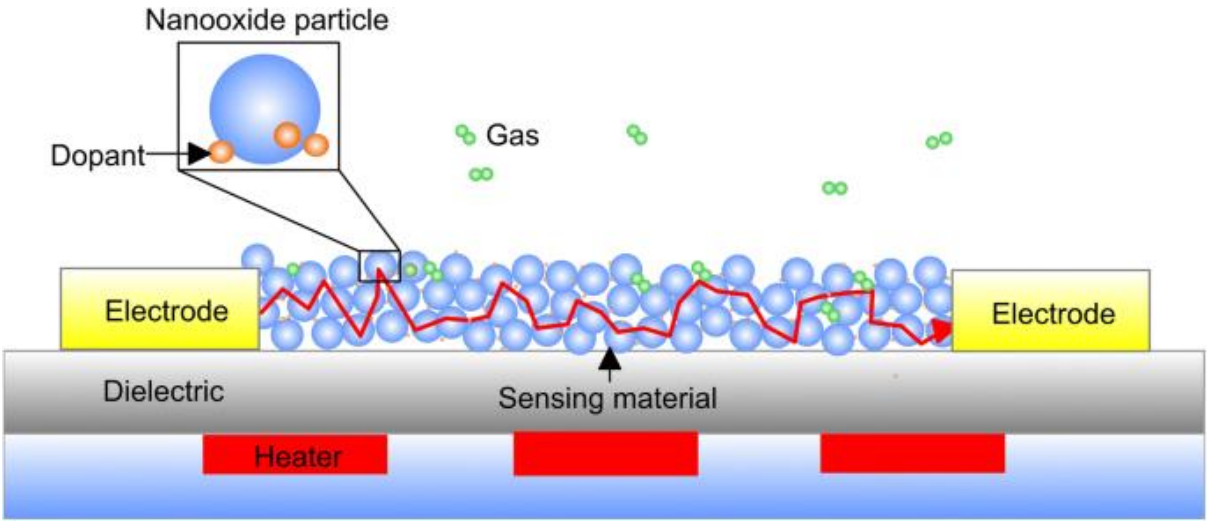

Figure 2.9: Diagrammatic representation of a conductometric gas sensor and its workings; an electrical signal is given when the metal oxide contacts with the environment, its sensor activity transfers the information to the electrode. Reprinted with permission [88].

Table 2.3: Gas sensing characteristics of diversely topological metal oxides.

Desired gas	metal oxide material	Morphology	Sensitivity	Optimal temperature (°C)	Ref
H_2	SnO_2	Nanorods	100 ppm	150	[84]
H_2S	ZnO	Dendrites	10 ppm	RT	[89]
NO_2	TeO_2	Nanowires	50 ppm	26	[86]
NH_3	WO_3	Nanowires	10 ppb	RT	[85]
CO	Au-doped In_2O_3	Nanowires	200 ppb–5 ppm	RT	[87]

Note: RT-Room Temperature

2.7.4 Optical sensor

Manganese oxide nanoparticles have also been explored for their potential application in optical sensors due to their unique optical properties. The optical properties of manganese oxide nanoparticles are dependent on their size, shape, and crystal structure. Manganese oxide nanoparticles exhibit interesting fluorescence, photoluminescence, and light absorption properties that make them suitable for use in optical sensors [64]. For instance, their fluorescence emission can be tuned by varying their size and shape, which makes them useful in fluorescent imaging and sensing applications. They are also good candidates for solar and photocatalytic uses due to their substantial absorbency in the visible spectrum. In one study, manganese oxide nanoparticles were used as fluorescence probes for the detection of mercury ions in water [22]. The nanoparticles were coated with a specific organic ligand that selectively bound to mercury ions, causing a change in their fluorescence intensity. This change in fluorescence intensity could then be detected and quantified, providing a highly sensitive and selective method for mercury ion detection. Furthermore, manganese oxide nanoparticles have also been used as SERS substrates for the detection of various analytes, including pharmaceuticals, pesticides, and heavy metals. The unique surface properties of manganese oxide nanoparticles make them suitable for enhancing the Raman signals of analytes, leading to highly sensitive and selective detection. Overall, the optical properties of manganese oxide nanoparticles make them promising candidates for various sensing applications, including in environmental monitoring, medical diagnosis, and food safety. A two-level reflecting visible sensor and dual-signal laser beam utilizing the structure of carbon dots (CD)/MnO_2 nano system developed for the detection of ascorbic acid (AA) was described by Tang et al. As demonstrated in Figure 2.10 below [64].

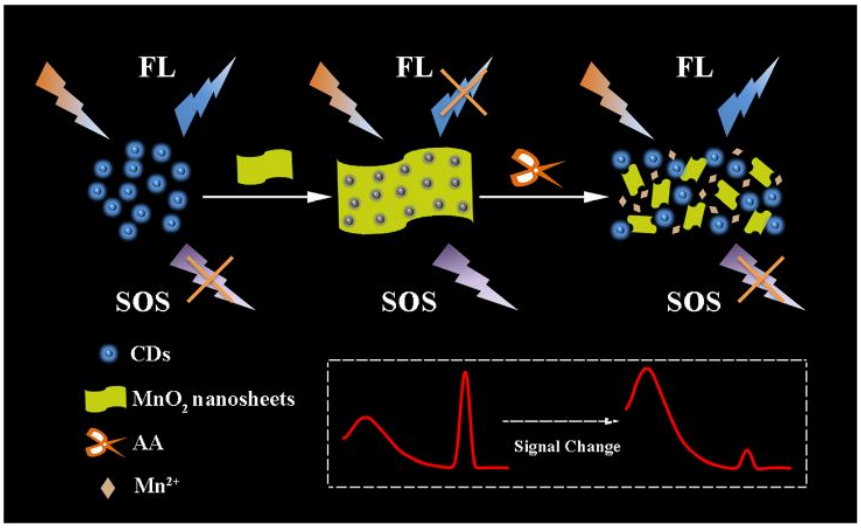

Figure 2.10: The detection of ascorbic acid (AA) using the principle of laser and MnO_2 with carbon dots as the foundation for second-degree dispersing (SOS). Reprinted with permission [64].

2.7.5 Thermal sensor

Manganese oxide nanoparticles have also been investigated for their potential use in thermal sensing applications. The unique thermal properties of manganese oxide nanoparticles make them suitable for use in temperature sensors and thermal energy conversion devices. One of the key thermal properties of manganese oxide nanoparticles is their high thermal conductivity. This property makes them efficient at conducting heat and transferring thermal energy, which is important for the accurate measurement and sensing of temperature [69]. Additionally, the high thermal stability of manganese oxide nanoparticles makes them resistant to thermal degradation, allowing them to maintain their thermal properties even at high temperatures. In one study, manganese oxide nanoparticles involve the creation of temperature detector on the thermoelectric effect. The nanoparticles functioned as a material that could produce electricity when they were added to a thermoelectric device. When the temperature of the device changed, a temperature gradient was generated across the nanoparticles, which caused a voltage to be produced, as demonstrated on Figure 2.11 [90]. This voltage could then be measured and correlated with the temperature, allowing for accurate temperature sensing. Moreover, manganese oxide nanoparticles have also been used in thermal energy conversion

devices, such as thermoelectric generators and thermoelectric coolers. These devices convert thermal energy into electrical energy or vice versa and rely on the thermoelectric properties of the material used. The high thermal conductivity and stability of manganese oxide nanoparticles make them promising candidates for use in such devices. Overall, the thermal properties of manganese oxide nanoparticles make them attractive materials for use in thermal sensing and energy conversion applications. Further research is needed to fully understand and optimize their thermal properties for these applications [57].

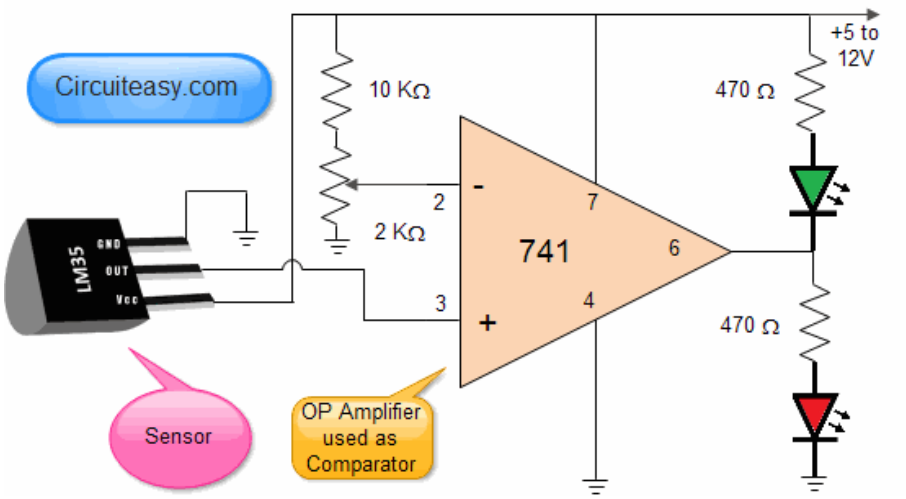

Figure 2.11: The temperature sensor as a type of a thermal sensor example. Reprinted with permission [91].

2.8 Other general application of manganese oxide nanoparticle

Manganese oxide nanoparticles have a wide range of applications in various fields due to their unique physical and chemical properties. Here are some of the applications of MnO_2 nanoparticles namely electrochemical material, energy storage, catalyst, adsorbents, biomedical applications, water treatment and environmental applications [22].

2.8.1 Electrochemical material

The electrochemical properties of manganese oxide make it a useful material for various applications, including as an oxygen reducing electrode in fuel cells. The oxygen reduction capacity of manganese oxide can be enhanced by modifying its defects or increasing its conductivity. Research has shown that manganese oxide nanoparticles prepared at lower temperatures with moderate defects and higher electrical conductivity have better oxygen reduction catalytic activity [92]. Additionally, the presence of a cationic dopant can increase the electron-donating ability of manganese oxide nanoparticles, resulting in higher oxygen reduction capacity. Studies have found that doped manganese oxide nanoparticles, such as Ni-α-MnO_2 and Cu-α-MnO_2, exhibit higher oxygen reduction capacity than undoped manganese dioxide. Moreover, the crystalline structure of manganese oxide nanoparticles also affects their oxygen reduction activity. According to Meng et al α-MnO_2 nanoparticles have been found to have higher oxygen reducing properties than other types of MnO_2 nanoparticles. Overall, manganese oxide nanoparticles show promise as efficient electrochemical materials with diverse applications, including in fuel cells for oxygen reduction reactions [56].

2.9 Chromatographic Methods for the detection of emerging pharmaceutical contaminants

2.9.1 Sulfamethoxazole

Sulfamethoxazole is a commonly used antibiotic, and chromatographic methods are frequently used for its detection in various samples [93]. One of the commonly used chromatographic methods for the detection of sulfamethoxazole is HPLC. Using this approach, an immobile phase-filled column is filled with a sample with sulfamethoxazole. After passing through the column with the mobile stage, which

is usually a blend of organic solvent and water, the components of the sample are separated according to how they interact with the stationary phase. The separated components are detected by a detector, usually a UV-Vis detector, and the amount of sulfamethoxazole in the sample can be determined based on its retention time and peak area [94]. Solid-phase extraction (SPE) is a common sample preparation technique used for the isolation and concentration of target analytes from complex matrices. SPE typically involves passing the sample through a sorbent material contained within a solid phase extraction cartridge, which selectively retains the target analytes while allowing interfering compounds to pass through The analytes can then be eluted from the cartridge, resulting in a concentrated and purified sample that is amenable to analysis through a chromatographic method, such as LC-MS or HPLC [95]. Many reported methods for the detection of sulfamethoxazole in wastewater have employed SPE for sample preparation, followed by HPLC or LC-MS for analyte determination. Table 2.4 lists the different chromatographic approach that determine sulfamethoxazole. using tandem mass spectrometry with LC-MS. According to Matongo et al [96] sulfamethoxazole was found at high amounts (59.28 µg/L) at the WWTP's influent with threshold detection of 0.370. For example, in research conducted in South Africa, sulfamethoxazole was detected in the influent of a WWTP at concentrations ranging from 23.7 to 64.2 ng/L, while in the effluent, concentrations ranged from below the detection limit to 35.6 ng/L. In surface water, in the investigation, sulfamethoxazole was found at values ranging from 10.7 to 61.5 ng/L. In another study conducted in Canada, sulfamethoxazole was detected in groundwater samples at concentrations ranging from 1.1 to 4.4 ng/L, while in sediments, concentrations ranged from below the detection limit to 71.5 ng/L.

Table 2.4: Chromatographic method used for the detection of sulfamethoxazole.

Technique	LOD (ng/L)	Matrix	Ref
LC-MS	37.2	Wastewater	[95]
LC-MS	35.6	Surface	[94]
LC-MS	0.370	Influent WWTP	[97]
LC-MS	35.6	Wastewater	[98]
LC-MS	71.5	Groundwater	[95]

2.9.2. Carbamazepine

Carbamazepine is an antiepileptic drug that has been detected in various water matrices as a contaminant. Chromatographic methods have been widely used for the determination of carbamazepine in water samples [99]. A popular sample preparation method for separating carbamazepine from aqueous matrices before analytical evaluation is solid-phase extraction (SPE). Carbamazepine has been determined using high-performance liquid chromatography (HPLC) in conjunction with an array of detection instruments, including fluorescence, UV-Vis, and mass spectrometry (MS). The very sensitive and selective technology of liquid chromatography-mass spectrometry (LC-MS) has become extensively used to determine the presence of carbamazepine in water samples. Several chromatographic methods have been reported for the determination of carbamazepine in water samples [97]. For example, Zeng et al. developed a sensitive and rapid HPLC method coupled with fluorescence detection for the determination of carbamazepine in wastewater samples. SPE extraction was used in the procedure, which produced an admissible limit of 0.01 µg/L. Shao et al. reported an LC-MS method for the determination of carbamazepine in river water samples. The method achieved a detection limit of 0.05 µg/L and was validated for accuracy and precision [98]. Table 2.5 lists the different approaches to chromatography that have been utilized in the past to determine carbamazepine. using tandem mass spectrometry with liquid chromatography (LC-MS). For example, in a study conducted in South Africa, carbamazepine was detected in the influent of a wastewater treatment plant (WWTP) at concentrations ranging from 8.1 to 85.4 ng/L, while in the effluent, concentrations ranged from below the detection limit to 24.2 ng/L. Carbamazepine was found in surface water in the research at values ranging from 8.9 to 70.9 ng/L. In another study conducted

in Italy, carbamazepine was detected in groundwater samples at concentrations ranging from 1.5 to 19.6 ng/L, while in sediments, concentrations ranged from below the detection limit to 54.6 ng/L. Olarinmoye et al reported the presence of two carbamazepine metabolites (carbamazepine-10, 11-epoxide and 10, 11-dihydroxy carbamazepine) in wastewater have been reported in concentrations of up to 0.052 ng/L. Overall, the concentrations of carbamazepine reported in Africa are somewhat similar to those reported in USA, Germany, and Portugal. For instance, the median concentrations of 1.9 and 0.47 ng/L have been reported in wastewater influent from Germany and Portugal, respectively [100].

Table 2.5: Chromatographic method used for the detection of carbamazepine.

Technique	LOD (ng/L)	Matrix	Ref
LC-MS	24.2	wastewater	[101]
LC-MS	27.2	Effluent WWTP	[102]
HPLC	54.6	River	[101]
LC-MS	52.0	Influent WWTP	[97]
LC-MS	57.0	wastewater	[95]

2.9.3 Ibuprofen

Ibuprofen is a nonsteroidal anti-inflammatory drug (NSAID) that is commonly used for pain relief, fever reduction, and inflammation reduction. The presence of ibuprofen in wastewater can have negative impacts on aquatic organisms and the environment [102]. Various chromatographic methods have been used for the detection and quantification of ibuprofen in wastewater samples. These include high-performance liquid chromatography (HPLC), gas chromatography-mass spectrometry (GC-MS), and liquid chromatography-mass spectrometry (LC-MS). In most cases, sample preparation involves solid-phase extraction (SPE) or liquid-liquid extraction (LLE) to isolate the analyte from the complex matrix of wastewater [96]. The reported concentrations of ibuprofen in wastewater vary widely depending on the location and the level of treatment of the wastewater. Studies have reported concentrations ranging from a few ng/L to several µg/L [94]. Table 2.6 lists the different approaches to chromatography that have been employed in the past to determine Ibuprofen. using tandem mass spectrometry with liquid chromatography (LC-MS/MS). According to Madikizela et al the ibuprofen is usually detected in higher concentrations in south African water resources. Wastewater influent for the Northern WWTP influent in Johannesburg, South Africa, an upper limit of 128 µg/L and a mean of 120 µg/L have been measured observed [103]. Wastewater effluent, the mean ibuprofen amount in the Northern WWTP effluent was 10 µg/L, but earlier reports of 12 µg/L were made [104]. Surface water: Ibuprofen was detected in surface water samples collected from different locations around the world, with concentrations ranging from <0.1 to 31.5 µg/L [105]. Groundwater: Ibuprofen was detected in groundwater samples collected from different locations with concentrations ranging from <0.01 to 0.66 µg/L [106]. Soil and sediments: Ibuprofen were detected in soil and sediment samples with concentrations ranging from 0.23 to 75.4 µg/L [107]. Biota: Ibuprofen was detected in various biota samples including fish, mussels, and algae with concentrations ranging from <0.1 to 238 µg/L [108].

Table 2.6: Chromatographic method used for the detection of ibuprofen.

Technique	LOD (ng/L)	Matrix	Ref
HPLC	1.00	Wastewater	[109]
LC-MS	0.70	Effluent WWTP	[102]
LC-MS	0.08	Surface water	[98]
LC-MS	1.00	Groundwater	[109]

LC-MS	0.535	Sediments	[96]

2.9.4 Metoprolol

Metoprolol is a beta-blocker medication that has been detected as a contaminant in water matrices, including wastewater and surface water [110]. Several chromatographic techniques have been employed to identify metoprolol, such as GC-MS, LC-MS, and HPLC. Sample preparation methods for metoprolol detection typically involve solid-phase extraction (SPE), where the analyte is extracted from the water matrix and concentrated onto a solid-phase sorbent. Other techniques such as solid phase microextraction (SPME) have also been used. Research has documented the discovery of metoprolol in surface water and wastewater, with levels varying from ng/L to µg/L. The use of LC-MS and SPE sample preparation has resulted in sensitive and selective methods for the detection of metoprolol in water matrices [95]. Using LC-MS/MS, many chromatographic approaches previously employed for metoprolol measurement are shown in Table 2.7. In surface water, metoprolol has been detected at concentrations ranging from <0.001 to 8.2 µg/L in different studies conducted around the world [111]. In wastewater, metoprolol has been found at concentrations ranging from <1 to 39,000 µg/L in influent and from <1 to 3,200 µg/L in effluent depending on the type of wastewater treatment plant [110]. In groundwater, metoprolol has been detected at concentrations ranging from <0.001 to 0.42 µg/L with the limit of detection 1.00 ng/L [102]. In sediment, metoprolol has been found at concentrations ranging from <0.1 to 4.4 µg/kg dry weight [97] The concentrations reported in the literature can vary depending on the sampling and analytical methods used, as well as the sensitivity of the equipment. Additionally, it is important to consider that the presence of metoprolol in the environment may have different implications depending on the matrix and the concentration, as well as the exposure routes and potential effects on biota and ecosystems [112].

Table 2.7: Chromatographic method used for the detection of metoprolol.

Technique	LOD (ng/L)	Matrix	Ref
LC-MS	0.081	Surface	[111]
LC-MS	1.02	Influent WWTP	[110]
LC-MS	1.00	Groundwater	[102]
LC-MS	0.48	Sediments	[97]
LC-MS	1.02	Wastewater	[101]

The chromatographic methods such as HPLC and LC-MS are highly sensitive and selective, they can also be expensive, time-consuming, and require trained personnel to operate and maintain the equipment. Additionally, sample preparation for chromatographic methods can also be laborious and require the use of hazardous chemicals [113]. The introduction of electrochemical sensing techniques offers a simpler and more cost-effective alternative for the detection of contaminants. Electrochemical sensors can be miniaturized, require less sample preparation, and have faster response times. They can also be used in the field and do not require extensive. However, one of the main challenges with electrochemical sensors is achieving high sensitivity and selectivity. One way to training to operate results this challenge is through the alteration of the electrode surface, which can enhance the sensor's ability to detect specific analytes. These modifications can include the use of nanomaterials, polymers, or enzymes to selectively bind to the target analyte and enhance the electrochemical response. Overall, the introduction of electrochemical sensing techniques and the modification of electrodes can offer a promising alternative for the detection of contaminants in water, with the potential for high sensitivity, selectivity, and cost-effectiveness [114].

2.10 Methods for detecting new drug contaminants using electrochemistry.

2.10.1 Sulfamethoxazole

There have been several studies on the electrochemical detection of sulfamethoxazole. One study used a screen-printed carbon electrode modified with multi-walled carbon nanotubes to enhance the sensitivity of the detection [93]. The electrochemical detection was performed using cyclic voltammetry, and the limit of detection was found to be 0.14 µM. Another study used a glassy carbon electrode modified with nickel oxide nanoparticles to detect sulfamethoxazole. The electrochemical detection was performed using differential pulse voltammetry, and the limit of detection was found to be 0.1 µM. The electrochemical techniques demonstrated good sensitivity and selectivity for sulfamethoxazole detection in both investigations [14]. As shown in Table 2.8, sulfamethoxazole has been detected using a variety of electrochemical techniques in urine, wastewater, prescription mixes and solutions containing electrolytes such BR, NaOH, and PBS. DPV is the main approach for identifying sulfamethoxazole. Thiago et al demonstrated the detection of sulfamethoxazole by using the modified rGNR/SPCE with the differential pulse voltammetry technique with the presence of electrolyte of phosphate buffer solution at the pH 6.0 within the linearity range of 1-10 µM obtained limit of detection of 0.09 µM while Abdollah et al used urine to detect the sulfamethoxazole using the same technique with the linearity range of 0.05-70 µM with a modified Ag/MWCNT/MPAC/GCE electrode to obtain the limit of detection of 0.01 [93]. The concentrations reported in the literature can vary depending on the sampling and analytical methods used, as well as the sensitivity of the equipment. Additionally, it is important to consider that the presence of sulfamethoxazole in the environment may have different implications depending on the matrix and the concentration, as well as the exposure routes and potential effects on biota and ecosystems [114].

Table 2.8: Analytically comparing electrodes for sulfamethoxazole detection.

Material	Method	Buffer/pH	LR (µM)	LOD (µM)	Matrix	Ref
rGNR/SPCE	DPV	PBS, pH 6.0	1-10	0.09	Tap water	[115]
GR-ZnO/GCE	DPV	PBS, pH 7.0	-	0.04	Urine Tap water Lake water	[116]
Ag/MWCNT/MTOAC/GCE	DPV	PBS, pH 6.0	0.05-70	0.01	Urine	[114]
SHL-GP/WP	DPV	BR buffer, pH 7.0	5.0-100	0.4	Tap water	[93]
MWCNT/PBnc/SPE	DPV		1.0-10.0	0.04		[116]
TFAB-COF@Pani/GCE	DPV	PBS, pH 6.5	1-450	0.107	Tap water	[115]
AuNP/TCBN/GCE	DPV	PBS	0.98-118	0.14	-	[93]

Mo_2O/GCE	SWV	PBS	10-100	0.144	-	[113]
GO/Zn/GCE	DPV	BR	0.1-1.5	0.028	-	[93]
BN-$Fe3O_4$-Pd/CPE	SWV	PBS	0.02-420	0.008	-	[114]

Note: *reduced graphene nanorode-screen printed carbon electrode (SPCE), graphene-zinc oxide-glassy carbon electrode (GCE), Silver-filled multiwalled carbon nanotube and methyltrioctyl ammonium chloride, Shellac graphite waterproof paper (WP), Multiwalled carbon nanotube decorated with Prussian blue nanocubes, Covalent organic frameworks (COF) polyaniline, gold nanoparticles, Graphene oxide-zinc, Molybdenum dimer oxide.*

2.10.2 Carbamazepine

Electrochemical methods have proven to be effective in the detection of Carbamazepine in various environmental samples. One such method is electrochemical sensing using carbon-based electrodes [117]. The electrochemical oxidation of Carbamazepine occurs at a potential of around 1.15 V vs. Ag/AgCl on a glassy carbon electrode, and this oxidation can be measured using cyclic voltammetry, square wave voltammetry, and differential pulse voltammetry. These techniques allow for the extremely accurate and specific measurement of carbamazepine in surroundings. Another electrochemical method for the detection of Carbamazepine is based on the use of molecularly imprinted polymers (MIPs) combined with electrochemical sensors. MIPs are synthetic materials that can selectively bind to specific target molecules, such as Carbamazepine, due to the presence of specific functional groups. The MIPs are then integrated into the electrode surface, and the binding of Carbamazepine to the MIP is detected by changes in the electrical properties of the electrode [13]. Overall, electrochemical methods are promising for the detection of Carbamazepine in environmental samples due to their high sensitivity, selectivity, and rapid response time. These methods have the potential to play an important role in monitoring the presence of Carbamazepine in the environment and ensuring the safety of our water resources. DPV, involves typically performed in solutions of PBS varying pH levels, is the primary method for detecting carbamazepine. Multiple electrochemical approaches have been utilized for determining the presence of carbamazepine in urine. sewage, pharmaceutical products, and different solutions of electrolytes, as illustrated in Table 2.9. [118].

Table 2.9: Analytically comparing electrodes for carbamazepine detection.

Working electrode	**Method**	**Buffer/pH**	**LR (µM)**	**LOD (µM)**	**Matrix**	**Ref**
Ce-ZnO/rGO/GCE	DPV	PBS	0.05-100	1.2	urine	[117]
Au/graphene-AuNPs/GCE	DPV	PBS	5-100	3.03	Lake water	[65]
MWCNT/GCE	LSV	PBS	0.13-1.60	0.040	Urine	[117]
Fullerene-C60/GCE	DPV	PBS	0.9-10	0.0016	Tap water	[117]
Fe-SnO_2NPS/SPCE	SWV	BRB	0.5-100	0.092	Pharmaceutical products	[119]

Graphite/GCE	DPV	BRB, pH 3	84.6-846	3.89	urine	[119]
NiO/ZnO/GCE	CV	BRB. PH 3	-	0.08	Pharmaceutical product	[119]
Gr-AuNPs/AuE/GCE	EIS	KCl		0.303	-	[119]
Ag/TiO_2/CPE	DPV	PBS, pH 5	-	0.86	-	[13]
ERG-SWCNT/GCE	Amperometry	-	50-3	29	Pharmaceutical samples	[117]

Note: *Multiwalled carbon nanotubes (MWCNTs), glassy carbon electrodes (GCEs), gold nanoparticles (AuNPs), and silver (Ag) Titanium dioxide, or TiO_2; (CPE) Carbon paste electrode; shell nanoparticles Au@AgPdNPs: AgPd with an Au center; Ce-Cerium; β-cyclodextrin-ionic liquid β-CD-IL-macrocyclic; (ZnO) Zinc oxide and (rGO) reduced graphene oxide.*

2.10.3 Ibuprofen

One effective method for identifying ibuprofen, a prevalent NSAID present in environmental samples, is electrochemical sensing. Electrochemical sensors can detect ibuprofen by measuring the electrochemical response of the molecule, allowing for its quantification in a sample [120]. Carbon-based electrodes, such as glassy carbon, carbon nanotubes, or graphene, are commonly used as the working electrode in electrochemical sensors for ibuprofen detection. Ibuprofen undergoes oxidation or reduction at particular potentials, which can be found using square wave voltammetry, differential pulse voltammetry, or cyclic voltammetry. Molecularly imprinted polymers (MIPs) can also be used in conjunction with electrochemical sensors for the detection of ibuprofen. MIPs are synthetic materials that are designed to selectively recognize a target molecule, such as ibuprofen, through specific binding sites. When ibuprofen molecules bind to the MIP, they can cause a change in the electrical properties of the electrode, which can be measured and used to determine the concentration of ibuprofen in the sample [109]. In addition to carbon-based electrodes and MIPs, other materials have been explored for the detection of ibuprofen, such as metal oxides, conducting polymers, and nanoparticles. These materials can also be integrated into electrochemical sensors for the detection of ibuprofen. Overall, electrochemical sensing is a highly sensitive and selective method for the detection of ibuprofen in environmental samples. Its potential applications include monitoring ibuprofen levels in wastewater treatment plants, surface water, and drinking water sources, as well as ensuring the safety of these resources for human and environmental health [120]. Ibuprofen identification is mainly concentrated on DPV, involves performed in solutions of PBS with varying pH readings. Multiple electrochemical approaches have been employed for determining the presence of Ibuprofen in urine, wastewater, pharmacological compositions, as well as different solutions of electrolytes, such as BR, NaOH, and PBS, as illustrated in Table 2.10. Using the modified GO/AgNPs/SPCE with the differential pulse voltammetry approach and an electrolyte of a PBS at pH 7.0, Hu et al. demonstrated the detection of Ibuprofen within the linearity range of 0.1–40 µM obtained limit of detection of 0.028 µM while Maleh et al used urine to detect the Ibuprofen using the same technique with the linearity range of 1–40 µM with a modified Ag/MWCNT/MPAC/GCE electrode to obtain the limit of detection of 0.4.

Table 2.10: Analytically comparing electrodes for Ibuprofen detection.

Material	Method	Buffer/pH	LR (µM)	LOD (µM)	Matrix	Ref
Apt/AuNPs/GCE	DPV	PBS	0.005-7	0.0005	Tap water	[120]
Apt/CdTeQD/GCE	CV	PBS	0.05-20.00	0.016	urine	[109]
GO/AgNPs/GCE	DPV	PBS, pH 7.0	0.1-40	0.028	Lake water	[120]
rGO/PdNPs/GCE	SWV	BR, pH 2.0	1-40	0.4	Urine	[120]
AuNPs/MWCNTs/GCE	CV	PBS, pH 7.0	1-100	0.55	wastewater	[120]
AuNPs@N-GQDs/GCE	DPV	-	10-200	0.033	-	[120]
MWCNT/GCE	FIA. AMP	-	10-1000	1.9	urine	[120]
Ag_2MWCNT/GCE	SWV	-	5-25	1.5	Pharmaceutical products	[120]

Note: *Aptasensor based gold nanoparticle-glassy carbon electrode (GCE), graphene oxide-silver nanoparticles (Ag) nanocomposite, reduced graphene oxide-lead nanoparticles nanocomposite, gold nanoparticles (AuNPs)-multiwalled carbon nanotubes (MWCNTs), Aptasensor based cadmium telluride quantum dots (CdTeQD), nitrogen doped graphene quantum dots (N-GQDs).*

2.10.4 Metoprolol

Electrochemical detection is a promising technique for the sensitive and selective detection of metoprolol in various environmental samples. For the electrochemical determination of metoprolol, carbon-based electrodes, such as glassy carbon or nanotubes of carbon, have been employed extensively [121]. The electrochemical oxidation of metoprolol occurs at a specific potential, typically around 0.7 V vs. Ag/AgCl, which can be detected using cyclic voltammetry, differential pulse voltammetry, or square wave voltammetry. As Table 2.11 illustrates, a range of electrochemical methods have been utilized to identify metoprolol in urine, wastewater, pharmaceutical formulations, and different electrolyte solutions such Britton Robinson buffer (BR), sodium hydroxide (NaOH), and phosphate buffer solutions (PBS). DPV, involves often performed in PBS solutions of varying pH levels, is the primary method used to detect metoprolol [122]. Berk et al demonstrated the detection of metoprolol by using the modified Ga_2-ZnO/BDDE electrode with the differential pulse voltammetry technique with the presence of electrolyte of phosphate buffer solution at the pH 7.0 within the linearity range of 9.99–3.38 µM obtained limit of detection of 7.53 µM while Zorluogh et al used urine to detect the metoprolol using the same technique with the linearity range of 0.95–9.45 µM with a modified HDME electrode to obtain the limit of detection of 0.29.

Table 2.11: Analytically comparing electrodes for metoprolol detection.

Material	Method	Buffer/pH	LR (µM)	LOD (µM)	Matrix	Ref
Ga_2-ZnO/BDDE	DPV	BR, pH 7	9.99-3.38	7.53	Pharmaceutical product	[122]
GRE/PtNPs/NFN	Ads DPV	BR, pH 7	0.0144-7.5	4.3	urine	[121]
GCE	DPV	PBS	0.06-1.08	0.02	urine	[122]
Nafion-CNT	DPV	PBS	0.07-90	35.1	-	[121]
BDD	LSV	BR	0.38-22.0	34	-	[112]
MIP/MWCNTs/PGE	SWV	PBS	0.06-490	2.9	-	[122]
HDME	DPV	BR	0.95-9.45	0.29	Urine	[122]
Lipid polymer film	SWV	PBS	20-1000	20	Urine	[121]
PVC-membrane-Graphite	SWV	-	0.2-800	0.126	Urine	[122]

Note: *Glassy carbon electrode (GCE), Carbon nanotube (CNT), multiwalled carbon nanotube (MWCNTs), gallium-zinc oxide boron doped diamond electrode (Ga_2-ZnO/BDDE), graphene/platinum nanoparticle nafion composite, hanging mercury drop electrode (HDME), molecularly imprinted polymer-pencil graphite electrode, SWV, square wave stripping voltammetry, LSV, Linear sweep voltammetry, DPV differential pulse voltammetry.*

References

[1] S. Marouzi, Z. Sabouri, and M. Darroudi, “Greener synthesis and medical applications of metal oxide nanoparticles,” *Ceram. Int.*, vol. 47, no. 14, pp. 19632–19650, 2021, doi: 10.1016/j.ceramint.2021.03.301.

[2] S. Sharma, Asha, Singh Anoop.Gupta, Vinay Sundramoorthy, Ashok K.Arya, “Involvement of metal organic frameworks in wearable electrochemical sensor for efficient performance,” *Trends Environ. Anal. Chem.*, vol. 38, no. September 2022, p. e00200, 2023, doi: 10.1016/j.teac.2023.e00200.

[3] D. S. Bilal, Muhammad, Bagheri, Ahmad Reza, Vilar, S. S. Aramesh, Nahal, Eguiluz, Katlin Ivon Barrios, Ferreira, Luiz Fernando Romanholo, Ashraf, and H. M. N. Iqbal, “Oxidoreductases as a versatile biocatalytic tool to tackle pollutants for clean environment – a review,” *J. Chem. Technol. Biotechnol.*, vol. 97, no. 2, pp. 420–435, 2022, doi: 10.1002/jctb.6743.

[4] M. Seo and H. R. Park, “Terahertz Biochemical Molecule-Specific Sensors,” *Adv. Opt. Mater.*, vol. 8, no. 3, pp. 1–14, 2020, doi: 10.1002/adom.201900662.

[5] T. Ozer, B. J. Geiss, and C. S. Henry, “Review—Chemical and Biological Sensors for Viral Detection,” *J. Electrochem. Soc.*, vol. 167, no. 3, p. 037523, 2020, doi: 10.1149/2.0232003jes.

[6] Y. Sohrabi, Hessamaddin. Dezhakam, Ehsan.Khataee, Alireza. Nozohouri, Ehsan Majidi, Mir Reza.Mohseni, Nazanin.Trofimov, Evgeny Yoon, “Recent trends in layered double hydroxides based electrochemical and optical (bio)sensors for screening of emerging pharmaceutical compounds,” *Environ. Res.*, vol. 211, no. March, p. 113068, 2022, doi: 10.1016/j.envres.2022.113068.

[7] L. Lu, Zhiwei.Zhao, Wenyuan. Wu and J. He, Jie. Dai, Wanlin Zhou, Cailong Du, Haijun. Ye, “Tunable electrochemical of electrosynthesized layer-by-layer multilayer films based on multi-

walled carbon nanotubes and metal-organic framework as high-performance electrochemical sensor for simultaneous determination cadmium and lead," *Sensors Actuators, B Chem.*, vol. 326, no. September 2020, p. 128957, 2021, doi: 10.1016/j.snb.2020.128957.

[8] C. Negut Cioates, "Review—Electrochemical Sensors Used in the Determination of Riboflavin," *J. Electrochem. Soc.*, vol. 167, no. 3, p. 037558, 2020, doi: 10.1149/1945-7111/ab6e5e.

[9] M. B. Antuña-Jiménez, Daniel. González-García and P. Hernández-Santos, David.Fanjul-Bolado, "Screen-printed electrodes modified with metal nanoparticles for small molecule sensing," *Biosensors*, vol. 10, no. 2, pp. 1–22, 2020, doi: 10.3390/bios10020009.

[10] A. L. Araújo, Diele A.G.Camargo, Jéssica R.Pradela-Filho, Lauro A.Lima, Ana P.Muñoz, Rodrigo A.A.Takeuchi, Regina M. Janegitz, Bruno C. Santos, "A lab-made screen-printed electrode as a platform to study the effect of the size and functionalization of carbon nanotubes on the voltammetric determination of caffeic acid," *Microchem. J.*, vol. 158, no. July, p. 105297, 2020, doi: 10.1016/j.microc.2020.105297.

[11] G. Fu, Li. Yu, Aimin Lai, "Conductive Hydrogel-Based Electrochemical Sensor: A Soft Platform for Capturing Analyte," *Chemosensors*, vol. 9, pp. 2–18, 2021.

[12] R. Mincu, Nicolae Bogdan. Lazar, Veronica. Stan, Dana. Mihailescu, Carmen Marinela. Iosub and A. L. Mateescu, "Screen-Printed Electrodes (SPE) for in vitro diagnostic purpose," *Diagnostics*, vol. 10, no. 8, pp. 1–21, 2020, doi: 10.3390/diagnostics10080517.

[13] C. Chen, Y. Wang, S. Ding, C. Hong, and Z. Wang, "A novel sensitive and selective electrochemical sensor based on integration of molecularly imprinted with hollow silver nanospheres for determination of carbamazepine," *Microchem. J.*, vol. 147, no. February, pp. 191–197, 2019, doi: 10.1016/j.microc.2019.03.024.

[14] R. Sivaranjanee, P. Senthil Kumar, R. Saravanan, and M. Govarthanan, "Electrochemical sensing system for the analysis of emerging contaminants in aquatic environment: A review," *Chemosphere*, vol. 294, no. December 2021, p. 133779, 2022, doi: 10.1016/j.chemosphere.2022.133779.

[15] X. Luo, A. Morrin, A. J. Killard, and M. R. Smyth, "Application of nanoparticles in electrochemical sensors and biosensors," *Electroanalysis*, vol. 18, no. 4, pp. 319–326, 2006, doi: 10.1002/elan.200503415.

[16] M. Nasrollahzadeh, S. Mahmoudi-Gom Yek, N. Motahharifar, and M. Ghafori Gorab, "Recent Developments in the Plant-Mediated Green Synthesis of Ag-Based Nanoparticles for Environmental and Catalytic Applications," *Chem. Rec.*, vol. 19, no. 12, pp. 2436–2479, 2019, doi: 10.1002/tcr.201800202.

[17] A. Kumar, A. Choudhary, H. Kaur, S. Mehta, and A. Husen, "Metal-based nanoparticles, sensors, and their multifaceted application in food packaging," *J. Nanobiotechnology*, vol. 19, no. 1, 2021, doi: 10.1186/s12951-021-00996-0.

[18] M. O. Parveen, Nazish.Ansari, Sajid Ali. Ansari, Mohd Zahid. Ansari, "Manganese oxide as an effective electrode material for energy storage: a review," *Environ. Chem. Lett.*, vol. 20, no. 1, pp. 283–309, 2022, doi: 10.1007/s10311-021-01316-6.

[19] W. Wei, X. Cui, W. Chen, and D. G. Ivey, "Manganese oxide-based materials as electrochemical supercapacitor electrodes," *Chem. Soc. Rev.*, vol. 40, no. 3, pp. 1697–1721, 2011, doi: 10.1039/c0cs00127a.

[20] T. N. BEISWENGER, "CHARACTERIZATION AND IDENTIFICATION OF ACTINIDE BEARING MINERALS AND SOILS USING," no. December, 2020.

[21] N. Dawadi, Sonika. Gupta, Aakash. Khatri, Manita. Budhathoki, Biplab. Lamichhane, Ganesh. Parajuli, "Manganese dioxide nanoparticles: synthesis, application and challenges," *Bull. Mater. Sci.*, vol. 43, no. 1, pp. 1–10, 2020, doi: 10.1007/s12034-020-02247-8.

[22] H. Shoba, A. Kavitha, B. Aswathaman and N. Ganesan, H. Senthil Kumar, "Synthesis, characterization and electrochemical sensors application of MnO2nanoparticles," *Mater. Today*

Proc., vol. 48, pp. 521–526, 2019, doi: 10.1016/j.matpr.2021.05.476.

[23] B. R. Cuenya, “Synthesis and catalytic properties of metal nanoparticles: Size, shape, support, composition, and oxidation state effects,” *Thin Solid Films*, vol. 518, no. 12, pp. 3127–3150, 2010, doi: 10.1016/j.tsf.2010.01.018.

[24] H. G. Liao, K. Niu, and H. Zheng, “Observation of growth of metal nanoparticles,” *Chem. Commun.*, vol. 49, no. 100, pp. 11720–11727, 2013, doi: 10.1039/c3cc47473a.

[25] Y. Wang, Wei. Kan, Yongchun. Yu, Bin Pan. Ying. Liew, K. M.Song, Lei.Hu, “Synthesis of MnO2 nanoparticles with different morphologies and application for improving the fire safety of epoxy,” *Compos. Part A Appl. Sci. Manuf.*, vol. 95, pp. 173–182, 2017, doi: 10.1016/j.compositesa.2017.01.009.

[26] D. Ghiuță, I. Cristea, D. Munteanu, “Synthesis Methods of Metallic Nanoparticles-an Overview,” *Bull. Transilv. Univ. Braşov*, vol. 10, no. 2, pp. 133–140, 2017, [Online]. Available: http://webbut.unitbv.ro/bulletin/Series I/2017/BULETIN I/Ghiuta_I.pdf

[27] S. Zhu, H. Zhou, M. Hibino, I. Honma, and M. Ichihara, “Synthesis of MnO2 nanoparticles confined in ordered mesoporous carbon using a sonochemical method,” *Adv. Funct. Mater.*, vol. 15, no. 3, pp. 381–386, 2005, doi: 10.1002/adfm.200400222.

[28] J. Huang, Anqi.He, Yangzhuo.Zhou, Yuzhou Zhou, Yaoyu Yang, Yuan. Zhang, Jiachao Luo, Lin.Mao, Qiming. Hou, Dongmei Yang, “A review of recent applications of porous metals and metal oxide in energy storage, sensing and catalysis,” *J. Mater. Sci.*, vol. 54, no. 2, pp. 949–973, 2019, doi: 10.1007/s10853-018-2961-5.

[29] J. Klębowski, Bartosz. Depciuch and J. Parlińska-Wojtan, Magdalena. Baran, “Applications of noble metal-based nanoparticles in medicine,” *Int. J. Mol. Sci.*, vol. 19, no. 12, 2018, doi: 10.3390/ijms19124031.

[30] V. K. Parashar, Mritunjaya. Shukla and R. Singh, “Metal oxides nanoparticles via sol–gel method: a review on synthesis, characterization and applications,” *J. Mater. Sci. Mater. Electron.*, vol. 31, no. 5, pp. 3729–3749, 2020, doi: 10.1007/s10854-020-02994-8.

[31] M. Patel, S. Mishra, R. Verma, and D. Shikha, “Synthesis of ZnO and CuO nanoparticles via Sol gel method and its characterization by using various technique,” *Discov. Mater.*, vol. 2, no. 1, 2022, doi: 10.1007/s43939-022-00022-6.

[32] T. Chitradevi, A. Jestin Lenus, and N. Victor Jaya, “Structure, morphology and luminescence properties of sol-gel method synthesized pure and Ag-doped ZnO nanoparticles,” *Mater. Res. Express*, vol. 7, no. 1, 2019, doi: 10.1088/2053-1591/ab5c53.

[33] S. Bach, J. P. Pereira-Ramos, and N. Baffier, “Electrochemical sodium insertion into the sol-gel birnessite manganese dioxide,” *Electrochim. Acta*, vol. 38, no. 13, pp. 1695–1698, 1993, doi: 10.1016/0013-4686(93)85063-5.

[34] Y. Wang and J. Wang, “Multicore-shell MnO 2 @ Ppy @ N-doped porous carbon nanofiber ternary composites as electrode materials for high- performance supercapacitors,” 2023.

[35] M. Aliofkhazraei, *Handbook of nanoparticles*. 2015. doi: 10.1007/978-3-319-15338-4.

[36] A. Moulahi and F. Sediri, “ZnO nanoswords and nanopills: Hydrothermal synthesis, characterization and optical properties,” *Ceram. Int.*, vol. 40, no. 1 PART A, pp. 943–950, 2014, doi: 10.1016/j.ceramint.2013.06.090.

[37] W. C. Kwak, No Woo.Jeong, Seung Jin Seo, Han Gil. Lee, Siwon. Kim, Yeon Ju. Kim, Jun Kyu. Byeon, Pilgyu. Chung, Sung Yoon Jung, “In situ synthesis of supported metal nanocatalysts through heterogeneous doping,” *Nat. Commun.*, vol. 9, no. 1, pp. 1–8, 2018, doi: 10.1038/s41467-018-07050-y.

[38] W. Wei, Weifeng. Cui, Xinwei. Chen and D. G. Ivey, “Manganese oxide-based materials as electrochemical supercapacitor electrodes,” *Chem. Soc. Rev.*, vol. 40, no. 3, pp. 1697–1721, 2011, doi: 10.1039/c0cs00127a.

[39] C. Bai, Xianlin. Tong, Xinglin Gao, Yanli. Zhu, Wanqing Fu and H. Ma, Jingyao Tan, Tianci Wang, Chunlei Luo, Yongsong Sun, “Electrochimica Acta Hierarchical multidimensional MnO 2 via hydrothermal synthesis for high performance supercapacitors,” *Electrochim. Acta*, vol. 281, pp. 525–533, 2018, doi: 10.1016/j.electacta.2018.06.003.

[40] S. Saravanan, A..Kumar, P. Senthil. Karishma, S. Vo, Dai Viet N.. Jeevanantham and C. S. Yaashikaa, P. R.George, “A review on biosynthesis of metal nanoparticles and its environmental applications,” *Chemosphere*, vol. 264, p. 128580, 2021, doi: 10.1016/j.chemosphere.2020.128580.

[41] P. G. Jamkhande, N. W. Ghule, A. H. Bamer, and M. G. Kalaskar, “Metal nanoparticles synthesis: An overview on methods of preparation, advantages and disadvantages, and applications,” *J. Drug Deliv. Sci. Technol.*, vol. 53, no. July, p. 101174, 2019, doi: 10.1016/j.jddst.2019.101174.

[42] V. Chandrakala, V. Aruna, and G. Angajala, “Review on metal nanoparticles as nanocarriers: current challenges and perspectives in drug delivery systems,” *Emergent Mater.*, vol. 5, no. 6, pp. 1593–1615, 2022, doi: 10.1007/s42247-021-00335-x.

[43] M. S. Aguilar, R. Esparza, and G. Rosas, “Synthesis of Cu nanoparticles by chemical reduction method,” *Trans. Nonferrous Met. Soc. China*, vol. 29, no. 7, pp. 1510–1515, 2019, doi: 10.1016/S1003-6326(19)65058-2.

[44] N. Zare, A. Zabardasti, A. Mohammadi, F. Azarbani, and A. Kakanejadifard, “Sonochemical synthesis, characterization, biological applications, and DFT study of new nano-sized manganese complex of azomethine derivative of diaminomaleonitrile,” *J. Iran. Chem. Soc.*, vol. 16, no. 7, pp. 1501–1516, 2019, doi: 10.1007/s13738-019-01626-1.

[45] A. Abulizi, G. H. Yang, K. Okitsu, and J. J. Zhu, “Synthesis of MnO2 nanoparticles from sonochemical reduction of MnO4O in water under different pH conditions,” *Ultrason. Sonochem.*, vol. 21, no. 5, pp. 1629–1634, 2014, doi: 10.1016/j.ultsonch.2014.03.030.

[46] T. Kamal, I. Ahmad, S. B. Khan, M. Ul-Islam, and A. M. Asiri, “Microwave Assisted Synthesis and Carboxymethyl Cellulose Stabilized Copper Nanoparticles on Bacterial Cellulose Nanofibers Support for Pollutants Degradation,” *J. Polym. Environ.*, vol. 27, no. 12, pp. 2867–2877, 2019, doi: 10.1007/s10924-019-01565-1.

[47] M. Bello, A..Fashedemi, O. O..Fabiane and N. Lekitima, J. N..Ozoemena, K. I..Manyala, “Microwave assisted synthesis of MnO2 on nickel foam-graphene for electrochemical capacitor,” *Electrochim. Acta*, vol. 114, pp. 48–53, 2013, doi: 10.1016/j.electacta.2013.09.134.

[48] X. Zhang, X. Sun, H. Zhang, D. Zhang, and Y. Ma, “Microwave-assisted reflux rapid synthesis of MnO2 nanostructures and their application in supercapacitors,” *Electrochim. Acta*, vol. 87, pp. 637–644, 2013, doi: 10.1016/j.electacta.2012.10.022.

[49] D. Zhang, X. L. Ma, Y. Gu, H. Huang, and G. W. Zhang, “Green Synthesis of Metallic Nanoparticles and Their Potential Applications to Treat Cancer,” *Front. Chem.*, vol. 8, no. October, 2020, doi: 10.3389/fchem.2020.00799.

[50] M. S. AGUILAR, R. ESPARZA, and G. ROSAS, “Synthesis of Cu nanoparticles by chemical reduction method,” *Trans. Nonferrous Met. Soc. China (English Ed.*, vol. 29, no. 7, pp. 1510–1515, 2019, doi: 10.1016/S1003-6326(19)65058-2.

[51] T. C. Bharat, Shubham, S. Mondal, H. S. Gupta, P. K. Singh, and A. K. Das, “Synthesis of doped zinc oxide nanoparticles: A review,” *Mater. Today Proc.*, vol. 11, pp. 767–775, 2019, doi: 10.1016/j.matpr.2019.03.041.

[52] I. Izquierdo-Lorenzo, S. Sanchez-Cortes, and J. V. Garcia-Ramos, “Adsorption of beta-adrenergic agonists used in sport doping on metal nanoparticles: A detection study based on surface-enhanced Raman scattering,” *Langmuir*, vol. 26, no. 18, pp. 14663–14670, 2010, doi: 10.1021/la102590f.

[53] K. E. Toghill and R. G. Compton, “Metal nanoparticle modified boron doped diamond electrodes

for use in electroanalysis," *Electroanalysis*, vol. 22, no. 17–18, pp. 1947–1956, 2010, doi: 10.1002/elan.201000072.

[54] T. Shafiq, M. Uzair, M. J. Iqbal, M. Zafar, S. J. Hussain, and S. A. A. Shah, "Green synthesis of metallic nanoparticles and their potential in bio-medical applications," *Nano Biomed. Eng.*, vol. 13, no. 2, pp. 191–206, 2021, doi: 10.5101/NBE.V13I2.P191-206.

[55] N. T. K. Thanh and L. A. W. Green, "Functionalisation of nanoparticles for biomedical applications," *Nano Today*, vol. 5, no. 3, pp. 213–230, 2010, doi: 10.1016/j.nantod.2010.05.003.

[56] L. Baral, Ayonbala. Satish and M. K. Zhang, Guoying. Ju, Shaohua Ghosh, "A Review of Recent Progress on Nano MnO2: Synthesis, Surface Modification and Applications," *J. Inorg. Organomet. Polym. Mater.*, vol. 31, no. 3, pp. 899–922, 2021, doi: 10.1007/s10904-020-01823-z.

[57] B. Ding, P. Zheng, P. Ma, and J. Lin, "Manganese Oxide Nanomaterials: Synthesis, Properties, and Theranostic Applications," *Adv. Mater.*, vol. 32, no. 10, pp. 1–35, 2020, doi: 10.1002/adma.201905823.

[58] T. Mounika, S. L. Belagali, and K. T. Vadiraj, "Manganese oxide nanoparticles synthesis route, characterization and optical properties," *Mater. Today Proc.*, vol. 75, pp. 72–76, 2023, doi: 10.1016/j.matpr.2022.11.017.

[59] Z. Sobańska, J. Roszak, K. Kowalczyk, and M. Stępnik, "Applications and biological activity of nanoparticles of manganese and manganese oxides in in vitro and in vivo models," *Nanomaterials*, vol. 11, no. 5, 2021, doi: 10.3390/nano11051084.

[60] A. U. Ubale, M. A. Waghmare, K. S. Iqbal, and H. M. Pathan, "Manganese oxides: promising electrode materials for Li-ion batteries and supercapacitors," *J. Mater. Sci. Mater. Electron.*, vol. 31, no. 17, pp. 14003–14021, 2020, doi: 10.1007/s10854-020-04033-y.

[61] X. Liu, C. Chen, Y. Zhao, and B. Jia, "A review on the synthesis of manganese oxide nanomaterials and their applications on lithium-ion batteries," *J. Nanomater.*, vol. 2013, 2013, doi: 10.1155/2013/736375.

[62] T. N. J. I. Edison, R. Atchudan, N. Karthik, D. Xiong, and Y. R. Lee, "Direct electro-synthesis of MnO 2 nanoparticles over nickel foam from spent alkaline battery cathode and its supercapacitor performance," *J. Taiwan Inst. Chem. Eng.*, vol. 97, pp. 414–423, 2019, doi: 10.1016/j.jtice.2019.01.019.

[63] B. Huang, X. Zhang, J. Cai, W. Liu, and S. Lin, "A novel MnO2/rGO composite prepared by electrodeposition as a non-noble metal electrocatalyst for ORR," *J. Appl. Electrochem.*, vol. 49, no. 8, pp. 767–777, 2019, doi: 10.1007/s10800-019-01325-y.

[64] L. Tang, Qian. Fan, Yu Zhu. Han and H. Q. Yang, Yu Zhu. Li, Nian Bing. Luo, "Redox induced dual-signal optical sensor of carbon dots/MnO2 nanosheets based on fluorescence and second-order scattering for the detection of ascorbic acid," *Microchim. Acta*, vol. 187, no. 8, 2020, doi: 10.1007/s00604-020-04459-5.

[65] R. Yang, Ruijie. Fan, Yingying. Ye, Z. Tang, Yuxin. Cao, Xiehong. Yin, and Z. Zeng, "MnO2-Based Materials for Environmental Applications," *Adv. Mater.*, vol. 33, no. 9, pp. 1–53, 2021, doi: 10.1002/adma.202004862.

[66] G. C. Robinson, David M.Go, Yong Bok Mui, Michelle. Gardner, Graeme Zhang, Zhijuan.Mastrogiovanni, Daniel Garfunkel, Eric.Li, Jing. Greenblatt, Martha Dismukes, "Photochemical water oxidation by crystalline polymorphs of manganese oxides: Structural requirements for catalysis," *J. Am. Chem. Soc.*, vol. 135, no. 9, pp. 3494–3501, 2013, doi: 10.1021/ja310286h.

[67] C. M. Julien and A. Mauger, "Nanostructured MnO2 as electrode materials for energy storage," *Nanomaterials*, vol. 7, no. 11, 2017, doi: 10.3390/nano7110396.

[68] G. Cao, L. Su, X. Zhang, and H. Li, "Hydrothermal synthesis and catalytic properties of α- and β-MnO2 nanorods," *Mater. Res. Bull.*, vol. 45, no. 4, pp. 425–428, 2010, doi:

10.1016/j.materresbull.2009.12.016.

[69] S. Sivakumar and L. Nelson Prabu, “Synthesis and Characterization of a-MnO2nanoparticles for Supercapacitor application,” *Mater. Today Proc.*, vol. 47, pp. 52–55, 2021, doi: 10.1016/j.matpr.2021.03.528.

[70] M. Aghazadeh, M. G. Maragheh, M. R. Ganjali, P. Norouzi, and F. Faridbod, “Electrochemical preparation of MnO 2 nanobelts through pulse base-electrogeneration and evaluation of their electrochemical performance,” *Appl. Surf. Sci.*, vol. 364, pp. 141–147, 2016, doi: 10.1016/j.apsusc.2015.12.146.

[71] Y. Zhao, Xiaoyu.Hou and Z. Wang, Yanfei Yang, Libin Zhu, Liang Cao, Ruge Sha, “Prepared MnO2 with different crystal forms as electrode materials for supercapacitors: Experimental research from hydrothermal crystallization process to electrochemical performances,” *RSC Adv.*, vol. 7, no. 64, pp. 40286–40294, 2017, doi: 10.1039/c7ra06369e.

[72] B. Cheng, Gao Yu, Lin Lan, Bang Sun, Ming Lin, Ting Fu, Zhiwei Su, Xiaohui Qiu, Minqiao Guo, Canhui Xu, “Controlled synthesis of α-MnO2 nanowires and their catalytic performance for toluene combustion,” *Mater. Res. Bull.*, vol. 75, pp. 17–24, 2016, doi: 10.1016/j.materresbull.2015.11.017.

[73] Z. Q. Wang, Bing Zheng and H. Y. Zhu, Lian Feng Yang, Yu Hua Wu, “Self-assembled and Pd decorated Zn2SnO4/ZnO wire-sheet shape nano-heterostructures networks hydrogen gas sensors,” *Sensors Actuators, B Chem.*, vol. 195, pp. 549–561, 2014, doi: 10.1016/j.snb.2014.01.073.

[74] J. Liu, Xianghong, Zhang, S. Guo, Xianzhi, Wu, and S. Wang, “Enhanced sensor response of Ni-doped SnO2 hollow spheres,” *Sensors Actuators, B Chem.*, vol. 152, no. 2, pp. 162–167, 2011, doi: 10.1016/j.snb.2010.12.001.

[75] D. Cao, Yali, Hu, Pengfei Pan, Weiyu, Huang, Yudai, Jia, “Methanal and xylene sensors based on ZnO nanoparticles and nanorods prepared by room-temperature solid-state chemical reaction,” *Sensors Actuators, B Chem.*, vol. 134, no. 2, pp. 462–466, 2008, doi: 10.1016/j.snb.2008.05.026.

[76] Y. S. Kim, I. S. Hwang, S. J. Kim, C. Y. Lee, and J. H. Lee, “CuO nanowire gas sensors for air quality control in automotive cabin,” *Sensors Actuators, B Chem.*, vol. 135, no. 1, pp. 298–303, 2008, doi: 10.1016/j.snb.2008.08.026.

[77] M. Epifani, Mauro, Prades, Joan Daniel Comini, Elisabetta Pellicer, Eva Avella, G. Siciliano, Pietro, Faglia, and J. R. Cirera, A, S, R Morazzoni, F M, “The role of surface oxygen vacancies in the NO2 sensing properties of SnO2 nanocrystals,” *J. Phys. Chem. C*, vol. 112, no. 49, pp. 19540–19546, 2008, doi: 10.1021/jp804916g.

[78] X. Song, L. Gao, and S. Mathur, “Synthesis, characterization, and gas sensing properties of porous nickel oxide nanotubes,” *J. Phys. Chem. C*, vol. 115, no. 44, pp. 21730–21735, 2011, doi: 10.1021/jp208093s.

[79] K. Wu, Zhengcui, Yu, S. Zhangand, and Y. Xie, “Hematite hollow spheres with a mesoporous shell: Controlled synthesis and applications in gas sensor and lithium ion batteries,” *J. Phys. Chem. C*, vol. 112, no. 30, pp. 11307–11313, 2008, doi: 10.1021/jp803582d.

[80] Y. Meng, W. Song, H. Huang, Z. Ren, S. Y. Chen, and S. L. Suib, “Structure-property relationship of bifunctional MnO2 nanostructures: Highly efficient, ultra-stable electrochemical water oxidation and oxygen reduction reaction catalysts identified in alkaline media,” *J. Am. Chem. Soc.*, vol. 136, no. 32, pp. 11452–11464, 2014, doi: 10.1021/ja505186m.

[81] F. Farid, Mohammad Masoudi Goudini, Leila Piri and F. Zamani, Abbasali, Saadati, “Molecular imprinting method for fabricating novel glucose sensor: Polyvinyl acetate electrode reinforced by MnO2/CuO loaded on graphene oxide nanoparticles,” *Food Chem.*, vol. 194, pp. 61–67, 2016, doi: 10.1016/j.foodchem.2015.07.128.

[82] A. T. E. Vilian and S. M. Chen, “Preparation of carbon nanotubes decorated with manganese

dioxide nanoparticles for electrochemical determination of ferulic acid," *Microchim. Acta*, vol. 182, no. 5–6, pp. 1103–1111, 2015, doi: 10.1007/s00604-014-1431-2.

[83] Y. Gan, Tian, Shi, Zhaoxia, Wang, Kaili Sun, Junyong Lv, Zhen Liu, *Rifampicin determination in human serum and urine based on a disposable carbon paste microelectrode modified with a hollow manganese oxide@mesoporous silica oxide core-shell nanohybrid*, vol. 93, no. 10. 2015. doi: 10.1139/cjc-2015-0017.

[84] L. Kuang, Qin, Lao, Changshi Zhong, Lin Wang Xie, Zhaoxiong Zheng, "High-sensitivity humidity sensor based on a single SnO2 nanowire," *J. Am. Chem. Soc.*, vol. 129, no. 19, pp. 6070–6071, 2007, doi: 10.1021/ja070788m.

[85] Y. M. Zhao and Y. Q. Zhu, "Room temperature ammonia sensing properties of W18O49 nanowires," *Sensors Actuators, B Chem.*, vol. 137, no. 1, pp. 27–31, 2009, doi: 10.1016/j.snb.2009.01.004.

[86] T. Liu, Zhifu Yamazaki, Toshinai Shen, Yanbai Kikuta and T. Nakatani, Noriyuki Kawabata, "Room temperature gas sensing of p -type Te O2 nanowires," *Appl. Phys. Lett.*, vol. 90, no. 17, pp. 2–5, 2007, doi: 10.1063/1.2732818.

[87] P. S. Singh, Nandan, Gupta, Raju Kumar Lee, "Gold-nanoparticle-functionalized In2O3 nanowires as CO Gas sensors with a significant enhancement in response," *ACS Appl. Mater. Interfaces*, vol. 3, no. 7, pp. 2246–2252, 2011, doi: 10.1021/am101259t.

[88] M. P. Chavali, Murthy S. Nikolova, "Metal oxide nanoparticles and their applications in nanotechnology," *SN Appl. Sci.*, vol. 1, no. 6, pp. 1–30, 2019, doi: 10.1007/s42452-019-0592-3.

[89] Z. Q. Zhang, N., Yu, Ke, Li, Q. Zhu and Q. Wan, "Room-temperature high-sensitivity H2 S gas sensor based on dendritic ZnO nanostructures with macroscale in appearance," *J. Appl. Phys.*, vol. 103, no. 10, 2008, doi: 10.1063/1.2924430.

[90] E. Moazzen, E. V. Timofeeva, and C. U. Segre, "Controlled synthesis of MnO2 nanoparticles for aqueous battery cathodes: polymorphism–capacity correlation," *J. Mater. Sci.*, vol. 52, no. 13, pp. 8107–8118, 2017, doi: 10.1007/s10853-017-1018-5.

[91] A. Wang, Guijie. Heidary, "Smart temperature sensors and temperature sensor systems," no. November, 2018, doi: 10.1016/B978-0-08-102055-5.00003-6.

[92] I. Djerdj, D. Arčon, Z. Jagličič, and M. Niederberger, "Nonaqueous synthesis of manganese oxide nanoparticles, structural characterization, and magnetic properties," *J. Phys. Chem. C*, vol. 111, no. 9, pp. 3614–3623, 2007, doi: 10.1021/jp067302t.

[93] T. S. Martins, J. L. Bott-Neto, O. N. Oliveira, and S. A. S. Machado, "Paper-based electrochemical sensors with reduced graphene nanoribbons for simultaneous detection of sulfamethoxazole and trimethoprim in water samples," *J. Electroanal. Chem.*, vol. 882, 2021, doi: 10.1016/j.jelechem.2021.114985.

[94] L. S. Andrade, M. C. de Moraes, R. C. Rocha-Filho, O. Fatibello-Filho, and Q. B. Cass, "A multidimensional high performance liquid chromatography method coupled with amperometric detection using a boron-doped diamond electrode for the simultaneous determination of sulfamethoxazole and trimethoprim in bovine milk," *Anal. Chim. Acta*, vol. 654, no. 2, pp. 127–132, 2009, doi: 10.1016/j.aca.2009.09.035.

[95] A. V. Pereira and Q. B. Cass, "High-performance liquid chromatography method for the simultaneous determination of sulfamethoxazole and trimethoprim in bovine milk using an on-line clean-up column," *J. Chromatogr. B Anal. Technol. Biomed. Life Sci.*, vol. 826, no. 1–2, pp. 139–146, 2005, doi: 10.1016/j.jchromb.2005.08.006.

[96] S. Matongo, G. Birungi, B. Moodley, and P. Ndungu, "Pharmaceutical residues in water and sediment of Msunduzi River, KwaZulu-Natal, South Africa," *Chemosphere*, vol. 134, pp. 133–140, 2015, doi: 10.1016/j.chemosphere.2015.03.093.

[97] L. M. Madikizela, N. T. Tavengwa, and L. Chimuka, "Status of pharmaceuticals in African water

bodies: Occurrence, removal and analytical methods," *J. Environ. Manage.*, vol. 193, pp. 211–220, 2017, doi: 10.1016/j.jenvman.2017.02.022.

[98] L. M. Madikizela, S. Ncube, and L. Chimuka, "Uptake of pharmaceuticals by plants grown under hydroponic conditions and natural occurring plant species: A review," *Sci. Total Environ.*, vol. 636, pp. 477–486, 2018, doi: 10.1016/j.scitotenv.2018.04.297.

[99] S. T. Alrashood, "Carbamazepine," *Profiles Drug Subst. Excipients Relat. Methodol.*, vol. 41, pp. 133–321, 2016, doi: 10.1016/bs.podrm.2015.11.001.

[100] W. Bahlmann, Arnold, Brack and M. Schneider, Rudolf J, Krauss, "Carbamazepine and its metabolites in wastewater: Analytical pitfalls and occurrence in Germany and Portugal," *Water Res.*, vol. 57, no. September 2018, pp. 104–114, 2014, doi: 10.1016/j.watres.2014.03.022.

[101] L. M. Madikizela and L. Chimuka, "Occurrence of naproxen, ibuprofen, and diclofenac residues in wastewater and river water of KwaZulu-Natal Province in South Africa," *Environ. Monit. Assess.*, vol. 189, no. 7, 2017, doi: 10.1007/s10661-017-6069-1.

[102] H. Khazri, S. Ben Hassine, I. Ghorbel–Abid, R. Kalfat, and M. Trabelsi-Ayadi, "Presence of carbamazepine, naproxen, and ibuprofen in wastewater from northern Tunisia," *Environ. Forensics*, vol. 20, no. 2, pp. 121–128, 2019, doi: 10.1080/15275922.2019.1597779.

[103] L. Amdany, Robert. Chimuka and E. Cukrowska, "Determination of naproxen, ibuprofen and triclosan in wastewater using the polar organic chemical integrative sampler (POCIS): A laboratory calibration and field application," *Water SA*, vol. 40, no. 3, pp. 407–414, 2014, doi: 10.4314/wsa.v40i3.3.

[104] G. Matongo, Solomon, Birungi and P. Moodley, Brenda Ndungu, "Occurrence of selected pharmaceuticals in water and sediment of Umgeni River, KwaZulu-Natal, South Africa," *Environ. Sci. Pollut. Res.*, vol. 22, no. 13, pp. 10298–10308, 2015, doi: 10.1007/s11356-015-4217-0.

[105] R. A. Trenholm, B. J. Vanderford, and S. A. Snyder, "On-line solid phase extraction LC-MS/MS analysis of pharmaceutical indicators in water: A green alternative to conventional methods," *Talanta*, vol. 79, no. 5, pp. 1425–1432, 2009, doi: 10.1016/j.talanta.2009.06.006.

[106] A. Jelic, Aleksandra.Gros, Meritxell. Ginebreda, R. Cespedes-Sánchez, and D. Ventura, Francesc.Petrovic, Mira Barcelo, *Occurrence, partition and removal of pharmaceuticals in sewage water and sludge during wastewater treatment*, vol. 45, no. 3. Elsevier Ltd, 2011. doi: 10.1016/j.watres.2010.11.010.

[107] D. J. Peng, G.Meier, W. N. Scott and M. H. Savoie, "A long-term and reproducible passive microwave sea ice concentration data record for climate studies and monitoring," *Earth Syst. Sci. Data*, vol. 5, no. 2, pp. 311–318, 2013, doi: 10.5194/essd-5-311-2013.

[108] P. Verlicchi, M. Al Aukidy, and E. Zambello, "Occurrence of pharmaceutical compounds in urban wastewater: Removal, mass load and environmental risk after a secondary treatment-A review," *Sci. Total Environ.*, vol. 429, pp. 123–155, 2012, doi: 10.1016/j.scitotenv.2012.04.028.

[109] A. Ouarda, Yassine.Bouchard, Florence.Azaïs, S. Vaudreuil, Marc Antoine Drogui, Patrick.Dayal Tyagi, Rajeshwhar. Sauvé, and R. Buelna, Gerardo. Dubé, "Electrochemical treatment of real hospital wastewaters and monitoring of pharmaceutical residues by using surrogate models," *J. Environ. Chem. Eng.*, vol. 7, no. 5, p. 103332, 2019, doi: 10.1016/j.jece.2019.103332.

[110] M. Aqil, A. Ali, A. Ahad, Y. Sultana, A. K. Najmi, and N. Saha, "A validated HPLC method for estimation of metoprolol in human plasma," *Acta Chromatogr.*, no. 19, pp. 130–140, 2007.

[111] S. S. Panda, S. Dutta, R. K. V. V. Bera, and S. Jammula, "Analytical eco-scale and quality by design-oriented liquid chromatography method for simultaneous quantification of metoprolol succinate, telmisartan, and cilnidipine in their fixed-dose combination," *Sep. Sci. Plus*, vol. 4, no. 3, pp. 128–136, 2021, doi: 10.1002/sscp.202000115.

[112] A. Chokshi, R. Prajapati, P. Desai, and M. Patel, "Development of a quick reverse phase liquid

chromatographic method with photodiode-array detection for quantitative determination of chlorthalidone, metoprolol succinate and telmisartan in tablet formulation," *J. Chem. Metrol.*, vol. 15, no. 2, pp. 163–171, 2021, doi: 10.25135/JCM.6012106.2098.

[113] G. Padmalaya, K. Krishna Kumar, P. Senthil Kumar, B. S. Sreeja, and S. Bose, "A recent advancement on nanomaterials for electrochemical sensing of sulfamethaoxole and its futuristic approach," *Chemosphere*, vol. 290, no. December 2021, p. 133115, 2022, doi: 10.1016/j.chemosphere.2021.133115.

[114] P. Balasubramanian, R. Settu, S. M. Chen, and T. W. Chen, "Voltammetric sensing of sulfamethoxazole using a glassy carbon electrode modified with a graphitic carbon nitride and zinc oxide nanocomposite," *Microchim. Acta*, vol. 185, no. 8, 2018, doi: 10.1007/s00604-018-2934-z.

[115] J. Melo Henrique, J. Rocha Camargo, G. Gabriel de Oliveira, J. Santos Stefano, and B. Campos Janegitz, "Disposable electrochemical sensor based on shellac and graphite for sulfamethoxazole detection," *Microchem. J.*, vol. 170, no. May, 2021, doi: 10.1016/j.microc.2021.106701.

[116] X. Yue, Z. Li, and S. Zhao, "A new electrochemical sensor for simultaneous detection of sulfamethoxazole and trimethoprim antibiotics based on graphene and ZnO nanorods modified glassy carbon electrode," *Microchem. J.*, vol. 159, no. April, p. 105440, 2020, doi: 10.1016/j.microc.2020.105440.

[117] G. Lavanya, N. Sekar, C. Ficarra, S. Tellone, E. Bonavita, A. Leonardi, S. G. Neri, "A novel disposable electrochemical sensor for determination of carbamazepine based on Fe doped SnO2 nanoparticles modified screen-printed carbon electrode," *Mater. Sci. Eng. C*, vol. 62, pp. 53–60, 2016, doi: 10.1016/j.msec.2016.01.027.

[118] A. Hammoud, D. Chhin, D. K. Nguyen, and M. Sawan, "A new molecular imprinted PEDOT glassy carbon electrode for carbamazepine detection," *Biosens. Bioelectron.*, vol. 180, no. February 2020, 2021, doi: 10.1016/j.bios.2021.113089.

[119] N. H. Qambrani, Nadeem Buledi, Jamil A. Khand and F. Solangi, Amber R. Ameen, Sidra Jalbani, Nida S. Khatoon, Amna Taher, Mohammad Ali Moghadam, F. H.Shojaei, Moein Karimi, "Facile Synthesis of NiO/ZnO nanocomposite as an effective platform for electrochemical determination of carbamazepine," *Chemosphere*, vol. 303, no. P3, p. 135270, 2022, doi: 10.1016/j.chemosphere.2022.135270.

[120] A. S. Nair and M. P. Sooraj, "Molecular imprinted polymer-wrapped AgNPs-decorated acid-functionalized graphene oxide as a potent electrochemical sensor for ibuprofen," *J. Mater. Sci.*, vol. 55, no. 8, pp. 3700–3711, 2020, doi: 10.1007/s10853-019-04258-1.

[121] M. Mehmandoust, S. Çakar, M. Özacar, and N. Erk, "The Determination of Timolol Maleate Using Silver/Tannic Acid/Titanium Oxide Nanocomposite as an Electrochemical Sensor in Real Samples," *Electroanalysis*, vol. 34, no. 7, pp. 1150–1162, 2022, doi: 10.1002/elan.202100363.

[122] B. Koçak, Y. Ipek, and A. Keçeci, "Diamond & Related Materials A novel electrochemical sensor for metoprolol analysis based on glutardialdehyde – zinc oxide modified boron doped diamond electrode," vol. 131, no. November 2022, 2023, doi: 10.1016/j.diamond.2022.109558.

Chapter 3: Methodology

Summary

This chapter describes all the chemical reagents that were utilized to generate the MnO_2 NPs materials as well as the characterization methods that were used to investigate the materials' properties. The hydrothermal method approach was chosen for this research because it provides the ability to regulate the nanoparticles' shape and dimensions by modifying a few synthesis parameters, including substrate quantity, temperature of the reaction, and response time. This control over the synthesis conditions allows the production of nanoparticles with uniform size distribution and specific morphologies, which is crucial for many uses. Due of their tiny size and particular forms, the synthesis process also results in the creation of nanoparticles with vast surface area. Describes the characterization approach employed to study the properties of MnO_2NPs which comprises FTIR, Raman spectroscopy for functional group analysis, SEM for surface morphology, X-ray diffraction for crystallinity research, and vibrational features, UV/vis spectrometry for optical properties, and SAXS spectroscopy. Outlines the use of synthesized MnO_2NPs for the electro-oxidation of analytes (Carbamazepine, sulfamethoxazole, Ibuprofen, and Metoprolol). Specify the electrochemical approach employed, including CV, DPV, and EIS. Mentions the use of MnO_2NPs as a modified electrode for electrochemical studies. Discusses interference studies to evaluate the electrochemical sensors' reliability. Highlights the importance of stability studies to assess the over time performance, reliability, and durability of the electrochemical sensor under various environmental conditions. Describes the use of the proposed sensors for determining concentrations of CBZ, SMX, IBU, and MP utilizing actual wastewater samples, proving the created sensor's usefulness.

3.1 Characterisations Technique

3.1.1 Spectroscopic Technique

Spectroscopic techniques are a set of scientific methods used to study the interaction between matter and electromagnetic radiation. These techniques provide valuable details regarding the atomic and molecular setup, arrangement, and characteristics of materials [1]. Spectroscopic techniques can be highly sensitive, and able to recognize and measure even small amounts of substances in a sample [2]. The versatility of spectroscopic techniques enables the analysis of diverse types of samples and provides access to different types of information, such as molecular structure, chemical composition, and elemental examination [3].

3.1.1.1 FTIR

For researching molecular interactions, FTIR is a useful and potent instrument. It offers details regarding the existence of particular functional groups within a compound [4]**.** Because of its versatility, FTIR may involve analysing both organically and inorganically compounds. The range of the FTIR spectra measured is 400 cm^{-1} to 4000 cm^{-1} [2]. The FTIR instrument used in this study is specified as the PerkinElmer FTIR spectrometer Frontier (South Africa). The approach KBr pellet was used for FTIR studies. Samples were mixed with potassium bromide (KBr). Overnight, the blend was dry at 60 °C in an enclosed oven. For evaluation, the dehydrated dust was crushed and formed into an extremely thin pellet.

3.1.1.2 Raman spectroscopy

An effective analytical method for characterising and analysing materials is Raman spectroscopy. [5]. It provides data about the vibrational modes of atoms, allowing for the identification of chemical compounds, structural analysis, and investigation of molecular interactions [6]. The synthetic nanoparticles were subjected to Raman spectroscopy using a 100× magnification on a WiTec Raman spectrometer (Alpha 300, TS 150) with an excitation wavelength of 532 nm (Germany). Glass slides were used for sample analysis.

3.1.1.3 Ultraviolet-Visible Spectroscopy

A prominent analytical approach for examining how compounds absorb ultraviolet and visible light is UV-vis spectroscopy [7]. It is a non-destructive and quantitative approach that provides valuable data

about the electronic structure of compounds [8]. The device measures the absorbance by comparing the intensity of the transmitted radiation (denoted as I) with the intensity of the incident radiation (known as incident radiation, denoted as I0). The following formula is then used to determine how much light the sample absorbs at a specific wavelength [7]:

$$Absorbane\ (A) = \log_{10} \frac{I0}{I}$$

The absorbance (A) is a dimensionless quantity representing the extent of light absorbed by the sample. It is associated with the path length of the absorbing medium and the amount present of the absorbing species, which is typically a solute in a solvent [9]. This relationship is described by Beer Lambert's law:

$$A = \varepsilon \times c \times l$$

Where:

A is the absorbance, ε (epsilon) is the molar absorptivity or molar extinction coefficient, a constant specific to the absorbing species and the wavelength of light, c is the concentration of the absorbing species in the solution, where l is the length of the specimen (in centimetres). [7].

UV-vis spectroscopy was employed in the existence study to examine the optical characteristics of the synthesised MnO_2 nanoparticle. On the PerkinElmer UV-vis spectrometer Lambada 6505 (South Africa), UV-vis studies were examined in the wavelength range of 250–800 nm. This typically involves grinding the material into a fine powder and possibly mixing it with a transparent matrix to form a thin film or pellet. Before measuring the sample, establish a baseline using a blank reference (e.g., the matrix without manganese oxide). This helps correct for any absorption or scattering that might occur due to the matrix itself. A standard of 100% reflectivity was employed as a reference, and a pinch of the MnO_2 nanoparticle sample was applied directly to the sample holder for reflectance measurements [10].

3.1.1.4 X-ray diffraction (XRD)

XRD is an approach that measures how scattering of X-rays affects an object's crystal form [11]. It offers important details regarding how atoms or molecules are arranged within crystal form. Bragg's Law, which asserts that when X-rays are impacted on a crystal lattice at a particular angle, is the foundation of XRD, the X-rays will undergo effective interference occurs in the event that the dispersed pulses' route variation is a multiple of integers of the wavelength of the radiation [12]. This interference produces a diffraction pattern that can be detected and analysed. The Bragg's Law equation (3.3) forms a diffraction pattern.

$n\lambda = 2d \sin\theta$ (3.1)

Grain size is determined by the peak broadening principle, which states that decreasing crystalline or grain size causes an increase in diffraction width [13]. Therefore, the widening of an XRD peak indicates that there aren't enough feasible planes in a tiny crystallite to provide total destructive interference. The Scherrer equation below involve predicting particle size:

$d = K\lambda / \beta \cos\theta$ (3.2)

Where d is the crystallite size, K its form factor, the X-ray wavelength, the full-width half-maximum (FWHM), and the angle of reflection are represented by the values of β, β, and θ [12]. In this research, the crystallinity of MnO_2NPs using a Bruker AXS D8 advanced diffractometer (Japan). The MATCH and Diamond software was used for analysis. Powder X-ray diffraction patterns of the samples were recorded with CuKα radiation (λ = 1.5406 Å) in the range of 20 – 80 °C.

3.1.1.5 Small angle X-ray scattering

SAXS instruments are versatile tools involve a wide range of materials and biological macromolecules [14]. They provide valuable information about nanoparticle size distributions, pore sizes, macromolecule shapes, and distances between structural elements in materials [15]. The resulting

scattering curve, obtained after background subtraction, is then subjected to data analysis. Two software tools used for this are SAXStreat and SAXSquant [14]. SAXSquant is used for additional data processing and evaluation following data reduction in SAXStreat [15]. The scattering data is Fourier transformed using the GIFT (Generalized Indirect Fourier Transformation) program [14]. The PDDF provides information about the distribution of distances between scattering centers in the sample, while the size distribution curve gives insight into the particles composition or structures in the sample [16]. The structure and size of the generated MnO_2 nanoparticle were examined involving the SAX Space instrument (Anton Paar, GmbH, North Ryde, Australia) and a solid sample in a quartz sample holder with a diameter of 1 mm. A temperature of 20 °C was maintained, and for each measurement, five frames were taken at a 60-second exposure time and averaged.

3.1.2 Microscopic techniques

Microscopic techniques reveal the overall morphology and structure of the material. This includes features such as shape, size, surface topography, and internal structure. By examining the material's physical characteristics [17].

3.1.2.1 Scanning electron microscopy (SEM)

SEM uses an imaging approach that concentrates a beam of electrons to look at a specimen's surface [18]. It provides excellent quality, three-dimensional pictures and allows for the characterization of the sample's topography, morphology, and composition [19]. SEM-ready glass slides were used to prepare the samples. Agar Turbo gold coaters were used to coat known volumes of the sample (10 µL) that had been put to arid at RT. Images were taken with a JEOL JSM-IT300 (United States of America) series SEM. MnO_2NPs were characterized involve a JEOL JSM-7800FLV field emission SEM.

3.2 Electrochemical Techniques

Environmental monitoring, industrial operations, medical diagnosis, scientific research, and other sectors have all seen a substantial increase in the use of electrochemical sensors [20,21]. These approach, involves CV, DPV, and EIS, provide useful data about the electrochemical behaviour, kinetics, and stability of the sensor materials and their interactions with analytes [20]. As seen in the diagram below Figure 3.1, SPCE constitutes involve intriguing designs that integrate a working (made of carbon-based material), reference, and counter electrode in a single-printed substrate [21].

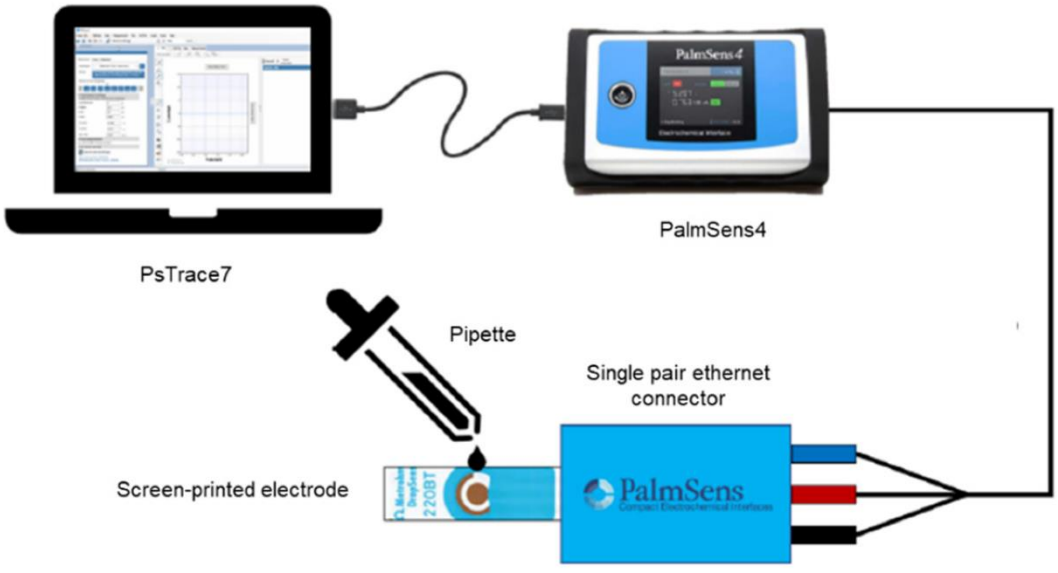

Figure 3.1: A schematic diagram for Screen printed electrode electrochemical sensor [21].

3.2.1 CV and EIS

CV involves electrochemical approach used to investigate the redox behaviour of electroactive species in a solution. It useful data about the electrochemical reactivity, kinetics, and stability of substances, as well as their concentration and diffusion coefficients [22]. EIS involves electrochemical techniques used to study the impedance behaviour of electrochemical systems. It provides valuable information about the electrical properties and approach occurring at the electrode-electrolyte interface [23]. The electrochemical measurements were performed using the Emstat Blue 400 potentiostat, which is a type of instrument used for controlling the voltage of an electrochemical cell. Metrohm 110 Drop Sens SPCE involve the working, reference, and counter electrodes. SPCE are a type of electrode where carbon ink is screen-printed onto a substrate, providing a convenient and versatile platform for electrochemical studies [24]. Both the altered and raw screen-printed carbon electrodes were subjected to electrochemical analysis. The Metrohm Autolab Potentiostat (South Africa) was specifically used for conducting CV and EIS.

3.2.2 DPV

DPV involve the electrochemical approach involve study the redox behaviour of a solution containing electroactive species [25]. DPV resides in the evaluation of the working electrode's current output surface during each pulse. The current is measured differentially, meaning it is the difference in current between the beginning and the end of each pulse. This helps to eliminate the background charging current and other capacitive contributions, making it easier to isolate and analyse the redox reactions of interest [26]. It is a useful tool for many electrochemical research and sensor development because, in comparison to other voltammetric techniques, it can deliver better ratios of signal to noise and reduced thresholds for detection [27]. DPV method analysing electrocatalytic activity toward different concentrations of carbamazepine, sulfamethoxazole, Ibuprofen, and metoprolol. This technique was used to observe and calculate the electroactive species in solution.

3.3 Materials and Methods

3.3.1 Chemical reagents

Manganese sulphate monohydrate ($MnSO_4 \bullet H_2O$, 98%), Potassium permanganate ($KMnO_4$, $\geq$ 99.0%), ethanol (C_2H_5OH, 95.0%), Sodium hydroxide (NaOH, 97%), ($Na_2HPO_4 \bullet 2H_2O$, $\geq$ 99.5%) disodium hydrogen phosphate dibasic, Methanol (CH_3OH, $\geq$ 99.8%), Carbamazepine (CBZ, 50 mg), Sulfamethoxazole (SMX, 50mg), ($H_2NaPO_4 \bullet 2H_2O$, $\geq$ 99%) Sodium phosphate monobasic dehydrate, Ibuprofen (IBU, 50mg), and Metoprolol (MP, 50mg), hydrochloric acid (HCl, 37%) were bought from Sigma-Aldrich, South Africa. Laboratory standard reagents were all employed, and no additional purification was necessary. The 0.1 M PBS at pH 7.0. The pH of the buffer solution was adjusted using either 0.1 M HCl to decrease the pH or 0.1 M NaOH to increase the pH. A stock solution of CBZ, SMX, and IBU (20 mM) was prepared in methanol while the metoprolol (20 mM) dissolved best in distilled water. The 10 mM working solution of CBZ, SMX, IBU, and MP were prepared by pipetting 900 µL in 0.1 M PBS. The chemicals were stored at four degrees Celsius in a freezer.

3.3.2 Preparation of standards solution

Appropriate amounts of CBZ, SMX, IBU and MP were weighed on the separate vials to prepare a 10 mM solution. Thereafter, the analyte solutions were dissolved in a double-distilled water to reach the required concentrations. 0.1 M PBS solution was prepared by dissolving the appropriate amount of PBS powder in double-distilled water. For each drug/analyte (CBZ, SMX, IBU, and MP), 900 µL of the 10 mM stock solution was transferred into a clean vial. A volume of 100 µL, 0.1 M PBS solution was then added to the vial, making the final volume 1000 µL. This dilution step resulted in a working solution concentration that was appropriate for electrochemical analysis.

3.4 Synthesis of manganese oxide nanoparticle

1.26 g of potassium permanganate ($KMnO_4$) and 0.5 g of manganese sulfate ($MnSO_4$) were mixed with 35 mL of deionized water in a beaker. The mixture was stirred thoroughly until both $KMnO_4$ and $MnSO_4$ were completely dissolved, resulting in a homogeneous solution. The resultant was transferred into a Teflon-lined stainless-steel autoclave. The sealed autoclave was then placed in an oven and heated at 180°C and maintained the temperature for 30 minutes. This step facilitated the formation of MnO_2 nanorods. The resulted residue was collected and washed thoroughly with a

solution of ethanol and water to remove any residual reactants and impurities. MnO_2 nanorods were filtered and dried in an oven at 80°C. As seen in Figure 3.2, continued drying until the MnO_2 nanorods was completely dry and a fine powder was obtained [28]. Eq 3.3 presents the suggested equation for the reaction.

(3.3)

$$2MnSO_{4\,(s)} + 2KMnO_{4\,(s)} + 2H_2O_{(l)} \longrightarrow K_2SO_{4\,(aq)} + 2H_2SO_{4\,(aq)} + 5MnO_{2\,(s)}$$

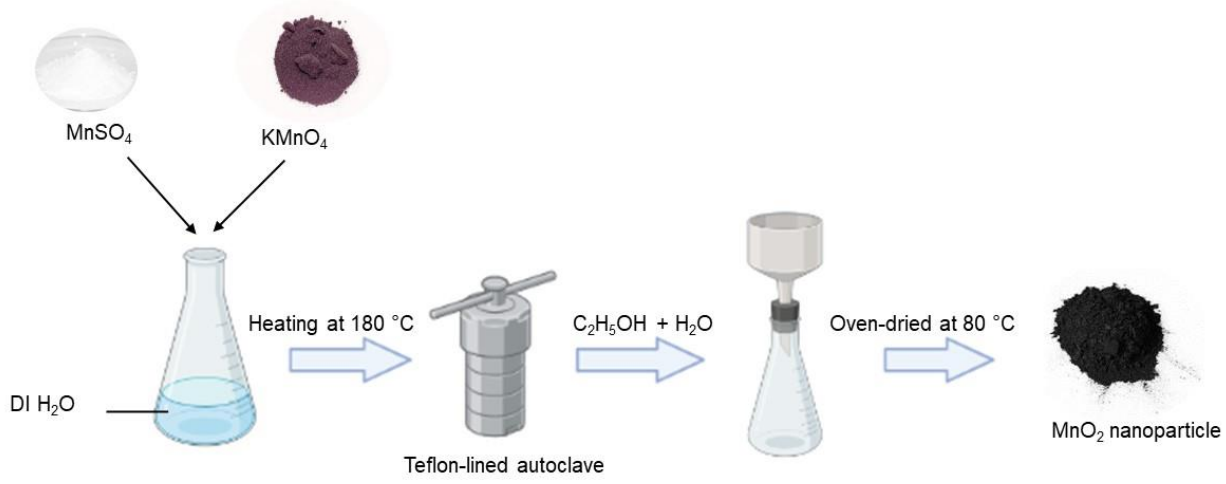

Figure 3.2: *Diagram showing the steps involved in created the MnO_2 nanoparticle*.

3.5 Electrochemical Characterisation

3.5.1 Fabrication of the manganese oxide nanoparticle on SPCE

5 mg of MnO_2 powder was weighed and transferred into a small vial. 1 mL of double-distilled water was added into the container with the MnO_2 powder. The solution was sonicated for 15 minutes to create a homogeneous suspension. Using a pipette, 8 µL of the prepared MnO_2 suspension was dropped onto the surface of the SPCE. The MnO_2 modified SPCE was allowed to dry at room temperature for 1 hour. This step ensured that the MnO_2 nanoparticles adhered to the electrode surface properly. After the drying period, the modified SPCE was ready for use in electrochemical experiments [29]. Figure 3.3 showed a schematic representation that visually communicated the steps involved in the modification process for carbamazepine and sulfamethoxazole.

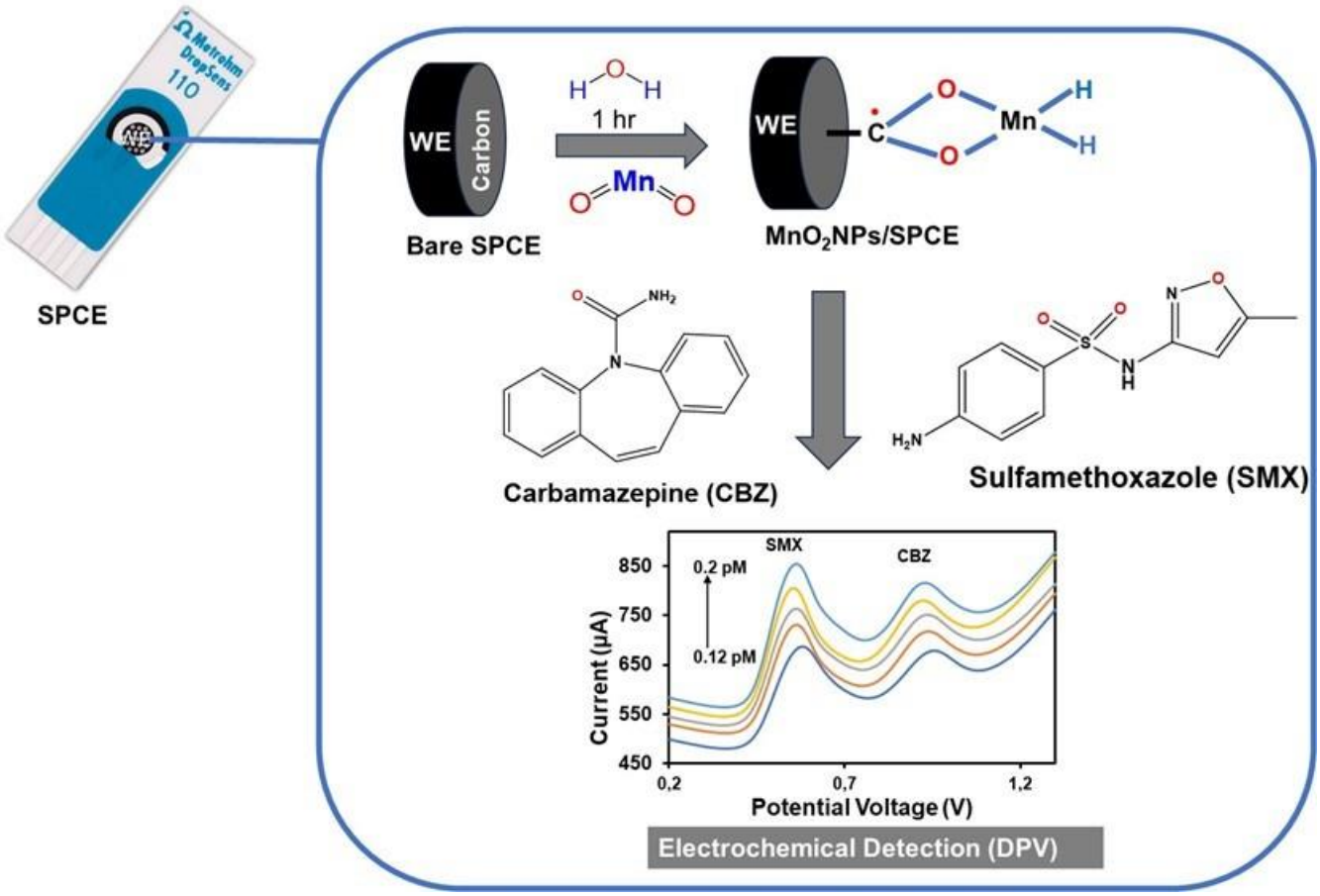

Figure 3.3: Diagrammatic representation of the electrochemical sensor's modification approach.

3.5.2 Sample preparation of real water

After the samples were collected, they were carefully handled and preserved to ensure their integrity for accurate analysis. The wastewater effluent was filtered through a 0.45 µm filter to remove any particulate matter. The filtered water was collected in a clean container. Standard solutions of the desired analytes (ibuprofen, metoprolol, carbamazepine and sulfamethoxazole) were prepared at known concentrations. The filtered water sample was fortified by adding known amounts of the analytes to achieve the desired concentration. A precise volume of each standard solution was added to the filtered water to obtain a target concentration. 100 µL of the fortified water sample was pipetted into a small vial. 1000 µL of the supporting electrolyte solution was added to the vial containing the 100 µL aliquot of the fortified water sample. This step ensured proper ionic strength and conductivity for the electrochemical measurements. The solution was mixed thoroughly using a vortex mixer or by gentle shaking to ensure homogeneity. The SPE was placed into the electrochemical workstation's cell. The prepared sample solution (1000 µL of electrolyte solution + 100 µL of fortified water sample) was introduced onto the SPE. The electrochemical measurements were then performed. [28].

3.6 Sampling site

Sampling of wastewater was conducted at the Northern WWTP located in the Diepsloot suburb, close to the N14 highway in Gauteng Province, South Africa. The plant treated 400 ML/d of residential wastewater from areas including Alexandra, Randburg, Sandton, and parts of Midrand and Roodeplaat. The sampling sites were depicted in Figure 3.4.

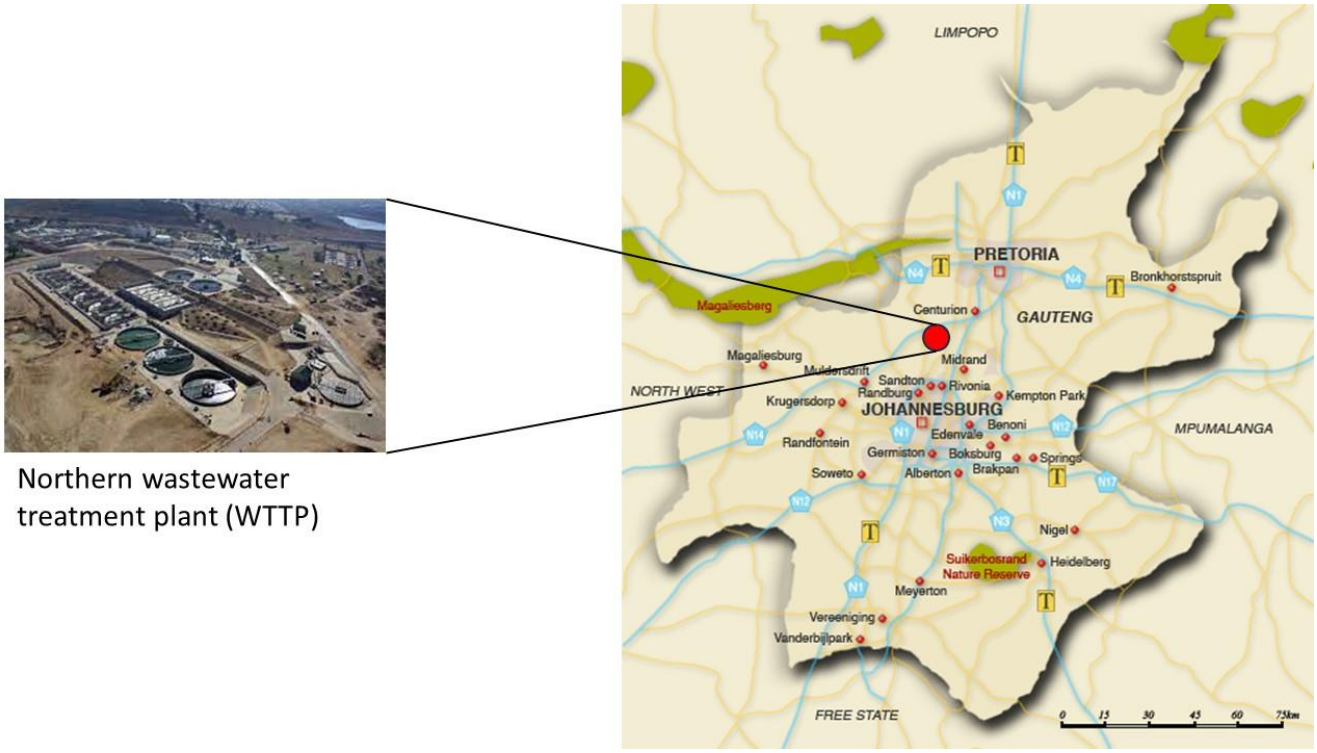

Figure 3.4: Map for the sampling site from the Northern WWTP in Gauteng province.

References

[1] D. I. Cătălina Vasilachi, Ionela A, Dana Mihaela Fertu and M. Gavrilescu, "Occurrence and Fate of Emerging Pollutants in Water Environment and Options for Their Removal," 2021, doi: 10.3390/w13020181.

[2] G. Laborda, Francisco.Bolea, Eduardo. Cepriá and J. R. Gómez, María T. Jiménez, María S. Pérez-Arantegui, Josefina Castillo, "Detection, characterization and quantification of inorganic engineered nanomaterials: A review of techniques and methodological approaches for the analysis of complex samples," *Anal. Chim. Acta*, vol. 904, pp. 10–32, 2016, doi: 10.1016/j.aca.2015.11.008.

[3] R. S. Das and Y. K. Agrawal, "Raman spectroscopy: Recent advancements, techniques and applications," *Vib. Spectrosc.*, vol. 57, no. 2, pp. 163–176, 2011, doi: 10.1016/j.vibspec.2011.08.003.

[4] G. Qu, Shaohua, Wu, D. Fang, Jianwu, Zang, and H. Xing, Hui, Wang, Liuding, Wu, *Dielectric and Magnetic Loss Behavior of Nanooxides*, vol. 2, no. December. 2017. doi: 10.1016/B978-0-323-46140-5.00011-X.

[5] W. Zhang, J. Ma, and D. W. Sun, "Raman spectroscopic techniques for detecting structure and quality of frozen foods: principles and applications," *Crit. Rev. Food Sci. Nutr.*, vol. 61, no. 16, pp. 2623–2639, 2021, doi: 10.1080/10408398.2020.1828814.

[6] H. Schulz and M. Baranska, "Identification and quantification of valuable plant substances by IR and Raman spectroscopy," *Vib. Spectrosc.*, vol. 43, no. 1, pp. 13–25, 2007, doi: 10.1016/j.vibspec.2006.06.001.

[7] S. L. Upstone, "Ultraviolet/Visible Light Absorption Spectrophotometry and Fluorescence Spectroscopy in Clinical Chemistry," *Encycl. Anal. Chem.*, pp. 1–25, 2022, doi: 10.1002/9780470027318.a0547.pub3.

[8] A. B. D. Nandiyanto, R. Ragadhita, and M. Aziz, "How to calculate and measure solution concentration using uv-vis spectrum analysis: Supporting measurement in the chemical decomposition, photocatalysis, phytoremediation, and adsorption process," *Indones. J. Sci. Technol.*, vol. 8, no. 2, pp. 345–362, 2023, doi: 10.17509/ijost.v8i2.57783.

[9] R. Ríos-Reina and S. M. Azcarate, “How Chemometrics Revives the UV-Vis Spectroscopy Applications as an Analytical Sensor for Spectralprint (Nontargeted) Analysis,” *Chemosensors*, vol. 11, no. 1, 2023, doi: 10.3390/chemosensors11010008.

[10] T. N. Beiswenger, “Characterization and identification of actinide bearing minerals and soils using,” no. December, 2020.

[11] D. P. Sharma, Ravi. Bisen and B. G. Shukla, Usha. Sharma, “X-ray diffraction: a powerful method of characterizing nanomaterials,” *Recent Res. Sci. Technol.*, vol. 4, no. 8, pp. 77–79, 2012, [Online]. Available: http://recent-science.com/

[12] A. A. Bunaciu, E. gabriela Udriştioiu, and H. Y. Aboul-Enein, “X-Ray Diffraction: Instrumentation and Applications,” *Crit. Rev. Anal. Chem.*, vol. 45, no. 4, pp. 289–299, 2015, doi: 10.1080/10408347.2014.949616.

[13] A. S. Khan, Hayat.Yerramilli and G. S. D’Oliveira, Adrien. Alford, Terry L. Boffito, Daria C. Patience, “Experimental methods in chemical engineering: X-ray diffraction spectroscopy—XRD,” *Can. J. Chem. Eng.*, vol. 98, no. 6, pp. 1255–1266, 2020, doi: 10.1002/cjce.23747.

[14] C. E. Blanchet and D. I. Svergun, “Small-angle X-ray scattering on biological macromolecules and nanocomposites in solution,” *Annu. Rev. Phys. Chem.*, vol. 64, pp. 37–54, 2013, doi: 10.1146/annurev-physchem-040412-110132.

[15] T. W. Gräwert and D. I. Svergun, “Structural Modeling Using Solution Small-Angle X-ray Scattering (SAXS),” *J. Mol. Biol.*, vol. 432, no. 9, pp. 3078–3092, 2020, doi: 10.1016/j.jmb.2020.01.030.

[16] P. Bernadó and D. I. Svergun, “Structural analysis of intrinsically disordered proteins by small-angle X-ray scattering,” *Mol. Biosyst.*, vol. 8, no. 1, pp. 151–167, 2012, doi: 10.1039/c1mb05275f.

[17] M. M. Modena, B. Rühle, T. P. Burg, and S. Wuttke, “Nanoparticle Characterization: What to Measure?,” *Adv. Mater.*, vol. 31, no. 32, pp. 1–26, 2019, doi: 10.1002/adma.201901556.

[18] A. M. Akhtar, Kalsoom. Khan, Shahid Ali. Khan, Sher Bahadar. Asiri, *Scanning electron microscopy: Principle and applications in nanomaterials characterization*. 2018. doi: 10.1007/978-3-319-92955-2_4.

[19] S. Eberle, A. L. Mikula, J. Schalek, R. Lichtman, and D. Knothe Tate, M. L. Zeidler, “High-resolution, high-throughput imaging with a multibeam scanning electron microscope,” *J. Microsc.*, vol. 259, no. 2, pp. 114–120, 2015, doi: 10.1111/jmi.12224.

[20] G. Zhu, Chengzhou.Yang and Y. Li, He.Du, Dan. Lin, “Electrochemical sensors and biosensors based on nanomaterials and nanostructures,” *Anal. Chem.*, vol. 87, no. 1, pp. 230–249, 2015, doi: 10.1021/ac5039863.

[21] D. W. Kimmel and D. E. Leblanc, Gabriel.Meschievitz, Mika E. Cliffel, “Electrochemical sensors and biosensors,” *Anal. Chem.*, vol. 84, no. 2, pp. 685–707, 2012, doi: 10.1021/ac202878q.

[22] P. T. Kissinger and W. R. Heineman, “Cyclic voltammetry,” *J. Chem. Educ.*, vol. 60, no. 9, pp. 702–706, 1983, doi: 10.1021/ed060p702.

[23] O. Wang, Shangshang. Zhang, Jianbo.Gharbi and M. E. Vivier, Vincent.Orazem, “Electrochemical impedance spectroscopy To cite this version :,” 2021.

[24] R. R. Suresh, M. Lakshmanakumar, and J. B. B. A. Jayalatha, “Fabrication of screen-printed electrodes : opportunities and challenges,” *J. Mater. Sci.*, vol. 56, no. 15, pp. 8951–9006, 2021, doi: 10.1007/s10853-020-05499-1.

[25] E. Mendoza, Sandra.Bustos and L. A. Manríquez, Juan. Godínez, “Voltammetric Techniques,” *Agric. Food Electroanal.*, pp. 21–48, 2015, doi: 10.1002/9781118684030.ch2.

[26] D. Zhuang, Xuming.Chen, H. Wang, Shengnan.Liu, and L. Chen, “Manganese dioxide nanosheet-decorated ionic liquid-functionalized graphene for electrochemical theophylline

biosensing," *Sensors Actuators, B Chem.*, vol. 251, pp. 185–191, 2017, doi: 10.1016/j.snb.2017.05.049.

[27] M. F. Thomaz, Douglas Vieira.Leite, Karla Carneiro de Siqueira.Moreno, Emily.Kussmaul Gonçalves.Garcia, Luane Ferreira Alecrim, Morgana Fernandes.Macêdo, Isaac Yves Lopes. Caetano, Marcos Pereira.de Carvalho and E. de S. Machado, Fabio Bahls.Gil, "Electrochemical study of commercial black tea samples," *Int. J. Electrochem. Sci.*, vol. 13, no. 6, pp. 5433–5439, 2018, doi: 10.20964/2018.06.55.

[28] A. O. Idris, P. J. Mafa, E. O. Oseghe, T. A. M. Msagati, U. Feleni, and B. B. Mamba, "A facile approach for the preparation of NiONPs@MnO2NRs nanocomposite material and its photocatalytic activity," *J. Nanoparticle Res.*, vol. 23, no. 7, 2021, doi: 10.1007/s11051-021-05257-7.

[29] P. M. Jahani and S. A. Ahmadi, "MnO2 nanorods modified screen-printed electrode for the electrochemical determination of Sudan dye in food sample," *J. Electrochem. Sci. Eng.*, vol. 12, no. 6, pp. 1121–1131, 2022, doi: 10.5599/jese.1415.

Chapter 4

Manganese oxide-based electrochemical sensor for signaling carbamazepine and sulfamethoxazole in wastewater samples

Summary

Carbamazepine and sulfamethoxazole are two commonly used pharmaceutical compounds with various therapeutic applications. The accurate determination of these compounds is of great importance in pharmaceutical analysis and environmental monitoring. In this research, we created an electrochemical sensor system for figuring out carbamazepine and sulfamethoxazole involve a manganese oxide nanoparticle modified on a SPCE. MnO_2 offers several advantages, including its electrochemical activity, extremely surface area, and catalytic properties, which improve the efficiency of screen-printed electrodes. The characterisation of MnO_2 nanoparticles (NPs) modifier was investigated via FTIR, XRD, SEM, and Raman spectroscopy approaches. The electrochemical behavior of the MnO_2NPs was researched involving DPV and CV techniques The impact of pH and scan speed on the CV outputs were examined to determine the ideal experimental settings. The outcome observed for carbamazepine and sulfamethoxazole have an irreversible behavior at the potential of 1.0 V and 0.73 V correspondingly, and their current increases. The use of the MnO_2NPs/SPCE electrode with the DPV approach displayed a limit of detection of 0.0005 μM and 0.002 μM in the concentrations range of 0.97- 5.82 pM (linear range) for the carbamazepine and sulfamethoxazole in a 0.1 M PBS. In addition, interference and stability investigations were examined to assess the effectiveness of the MnO_2NPs/SPCE detector under optimal conditions, which resulted in an excellent performance. The suggested sensor worked effectively to determine carbamazepine and sulfamethoxazole in real-world water samples.

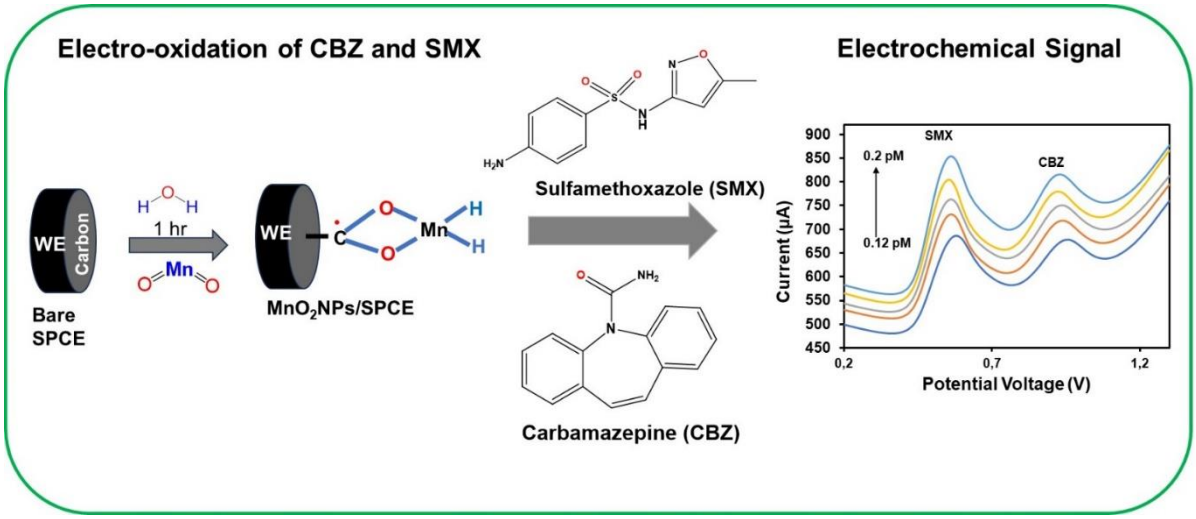

4.1 Introduction

Pharmaceuticals (Pharm) are important for maintaining human and animal health [1]. However, their extensive use and high consumption patterns have led to their release into the aquatic environment [2]. Pharm are present in the aquatic environment through treated sewage effluent discharge, landfill leaching, and direct discharge from pharmaceutical manufacturing plants [3]. Many Pharm are highly soluble in water, and their high chemical stability and low biodegradability contribute to their persistence in the surrounding [4]. The range of Pharm found in the aquatic surrounding is broad and

includes a variety of compounds involve antibiotics, antipyretics, analgesics, anti-inflammatories, antimicrobials, and hormones [5]. These contaminants might be destructive to people's health as well as aquatic surrounding [6]. Among the Pharm, antibiotics are known to encourage the emergence of antibiotic-resistant bacteria, while hormones can impede with the body's natural production of hormones and cause infertility and developmental problems in aquatic organisms and potentially in humans [7]. These pollutants are detected in the aquatic environment at low concentrations, about in the range of µg/L to ng/L [6].

Traditional wastewater treatment techniques do not adequately eliminate these pollutants, which may remain in the environment over time [8]. Sulfamethoxazole and carbamazepine as shown in Figure 4.1 are problematic in the aquatic surrounding due to their significant persistence and ubiquitous presence [9]. Carbamazepine is an anticonvulsant drug that is used to treat various medical conditions such as epilepsy, bipolar disorder, and neuropathic pain while sulfamethoxazole is an antibiotic that involve the treat bacterial infections [10]. Both medications are not entirely broken down by the body, and a large amount of them are eliminated unaltered in the urine [2]. The existence of these drugs in the surrounding is an issue since they may negatively impact marine life. For example, they affect the behavior, reproduction, and development of some fish and invertebrate species [11]. Various quantitative analytical strategies involve identification of carbamazepine and sulfamethoxazole in environmental samples [12]. These approach include spectrofluorimetry, GC [13], spectrophotometry [14], planar chromatography [15], electrokinetic chromatography [14], LC-MS tandem, and HPLC [13]. However, many of these approach require expensive instruments, high costs, and the use of environmentally unfriendly and toxic solvents [16]. The establishment of innovative, economical, and ecologically friendly techniques for identifying and measuring pharmaceutical contaminants in the surrounding has garnered more attention in the last decade [14]. Electrochemical sensor sensors have become a viable substitute for traditional approach of pollutant identification, including pharmaceuticals, in the environment [17].

Electrochemical sensors are low-cost, portable, and relatively simple to use, creating them an attractive choice for monitoring use in both laboratory and field settings [11]. A precise differential pulse voltammetric technique for identifying CBZ was introduced by Dhanalakshmi et al. utilizing a GCE altering with Ce-ZnO/rGO [18]. A threshold of measurement for 0.0012 µM was attained. In separate research by Qambrani et al., a successful method of analysis to identify CBZ was demonstrated involve a NiO-ZnO/GCE as the base electrode [19]. A threshold of measuring 0.08 µM was reported by them. Several investigations conducted in the last decade indicate that the effectiveness of electrochemical sensors to identify varied pharmaceuticals, involves sulfamethoxazole and carbamazepine [8]. However, further research and development are needed to optimize the sensitivity, selectivity, and accuracy of these sensors, as well as to improve their performance under different environmental conditions [17]. One strategy that shows promise for enhancing electrochemical sensors' ability to identify pharmaceutical contaminants in the environment is their modification [16]. One approach to modifying electrochemical sensors is to incorporate novel materials or altering the surface of the sensor to boost the detector's strength, specificity, and responsiveness [20].

Manganese oxide nanoparticles have been explored as a potential modification for electrochemical detector for the identification of pharmaceutical contaminants in the surrounding [21]. MnO_2 nanoparticles have several desirable properties for use in electrochemical sensors, including significant area of surface, chemical resistance, and excellent conductivity [20]. In this work, the aim is to develop a sensor that can detect two different compounds, carbamazepine, and sulfamethoxazole, in wastewater samples. The sensor is intended to be simple, portable, low-cost, and reliable. To achieve this goal, the plan is to modify a screen-printed carbon electrode using manganese dioxide (MnO_2) nanoparticles. The modified electrode will then be used as the sensing component of the device. Overall, the purpose of this work is to create a detector that can provide a quick and accurate way to detect the presence of these two compounds in wastewater samples, which can ultimately contribute to better management and treatment of wastewater.

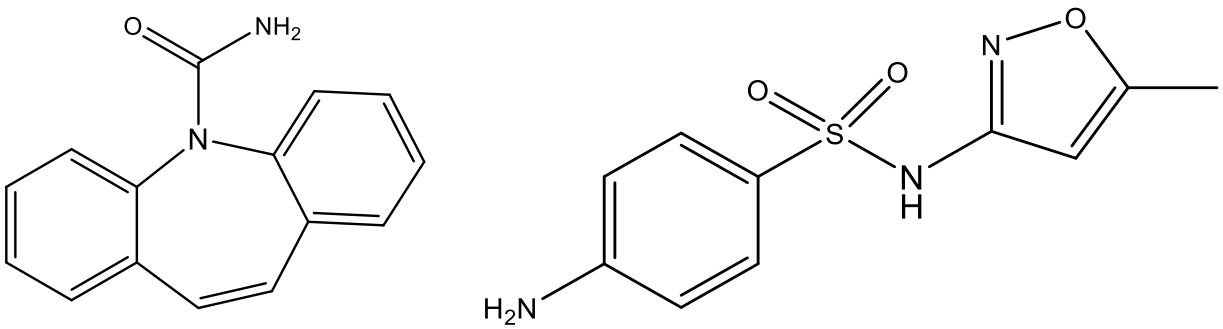

Carbamazepine **Sulfamethoxazole**

Figure 4.1: The structure of carbamazepine and sulfamethoxazole

4.2 Results and Discussions

4.2.1 FTIR results

The FTIR analysis of the synthesized nanoparticle, specifically MnO_2, was performed to investigate its functional groups and molecular vibrations. The obtained FTIR spectrum, shown in Figure 4.2, covered a range of wavenumbers from 400 cm^{-1} to 4500 cm^{-1}. In the spectrum, a broad band centered around 3440 cm^{-1} was observed, this represents the oscillation of hydroxyl (-OH) and hydrogen-bonded surface molecules of H_2O. This implies that the nanoparticles of MnO_2 possess surface water molecules and hydroxyl groups that are involved in hydrogen bonding interactions [22]. The presence of these hydrated properties in MnO_2 can enhance the diffusion of cations, thereby increasing the capacitance of the material. Two distinct vibrational bands were seen at 1651 cm^{-1} and 1387 cm^{-1}. These bands correspond to the residual -OH groups, demonstrating that the outermost layer of the MnO_2 nanoparticles had absorbed molecules of water. The stretching vibrations of these adsorbed water molecules contribute to these vibrational bands [23]. Additionally, a broad band around 590 cm^{-1} and 517 cm^{-1} was obtained in the spectrum. This band can be form to the band of the Mn-O bonds within the MnO_6 octahedra present in the α-MnO_2 nanoparticles. These octahedra are structural units within the MnO_2 crystal lattice [15,12,14]. From the spectra, the vibrational band at 1027 and 2062 cm^{-1} was obtained, which is the band of C-O and C-H bonds respectively. The occurrence of ethanol from the hydrothermal synthesis process indicated the occurrence of C-H and C-O vibrations in manganese oxide FTIR spectra [26,27].

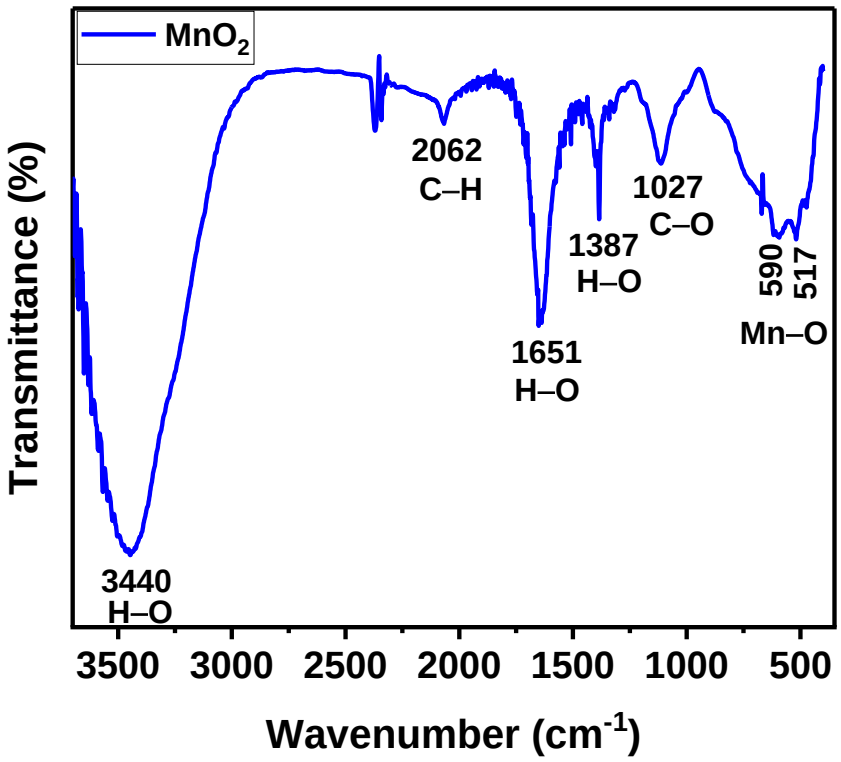

Figure 4.2: The FTIR spectrum of the MnO_2 nanoparticle.

4.2.2 Raman spectroscopy

Raman spectroscopies involve validate the functional form of the manufactured MnO_2 nanoparticles. The Raman spectra, displayed in Figure 4.3, supplied further details regarding the vibrational modes and structural characteristics of the nanoparticles. A prominent peak was observed at a high-intensity region of 637 cm^{-1} in the Raman spectrum. This peak indicates the presence of well-developed tetragonal structures, specifically 22 tunnels, 11 tunnels, and interstitials [28]. These features are indicative of the strong presence of α-MnO_2 in the synthesized nanoparticles. The peak at 637 cm^{-1} c equivalent to a specific vibrational mode associated with the structural arrangement of α-MnO_2. Another significant Raman peak was seen at 115 cm^{-1}. This peak can be offered to an external vibration caused by the translational motion of the MnO within the crystal lattice. The presence of this peak further supports the conclusion that the nanoparticles exhibit a strong presence of α-MnO_2 [29]. Additionally, a peak at 344 cm^{-1} was seen in the Raman spectrum. This peak can be ascribed to the layered structure of the δ-MnO_2 phase. The presence of this peak agrees with previous literature findings and provides further evidence of the specific crystal structure of the MnO_2 nanoparticles [25].

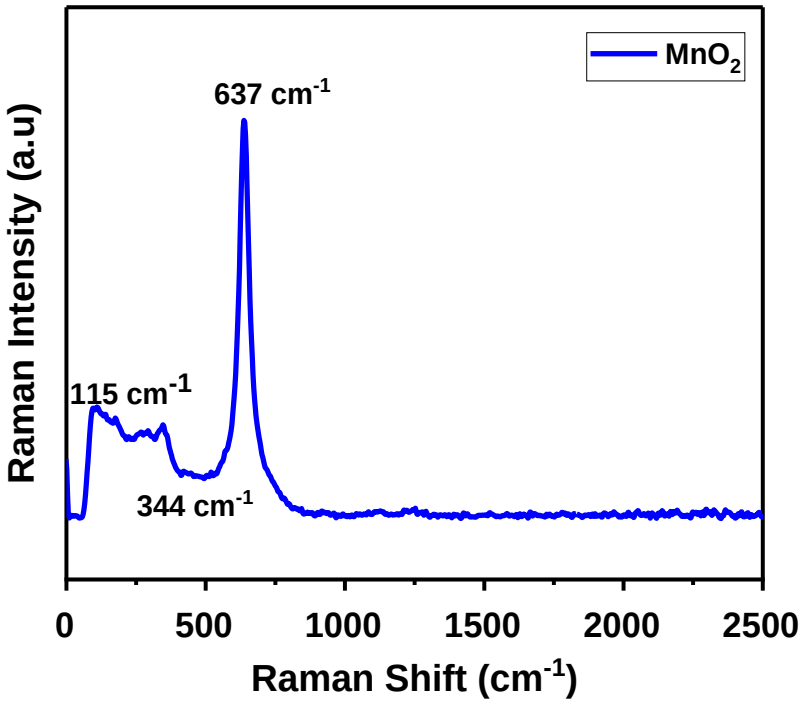

Figure 4.3: The MnO_2 nanoparticle's Raman spectroscopy.

4.2.3 X-Ray Diffraction

The crystalline form of the MnO_2 nanoparticles was investigated using XRD. The obtained XRD pattern, as depicted in Figure 4.4, showed sharp diffraction peaks at specific 2θ angles. These peaks were identified and indexed to corresponding crystal facets. The observed diffraction peaks at 2θ angles of 12.9°, 18.3°, 28.7°, 37.7°, 42.1°, 49.9°, and 60.3° could be successfully indexed to specific crystal facets, namely (110), (200), (310), (211), (301), (411), and (521) respectively. These indices represent the crystallographic planes of tetragonal α-MnO_2 form. The XRD pattern for MnO_2 nanoparticles was found to be in excellent concur with the XRD standard card (JSPDF 44-0141) [28,29]. This indicates that the diffraction peaks seen in the experimental XRD spectra correspond well to the expected positions based on the known crystallographic information for α-MnO_2 [30]. Furthermore, the absence of any visible peaks related to impurities in the XRD spectrum indicates a high purity of the α-MnO_2 nanoparticles [31]. This suggests that the synthesized MnO_2 nanoparticles predominantly exhibit the desired tetragonal crystalline structure without significant impurities [14,12,16]. The crystallite size of 175.1 Å (17.51 nm) indicates that the manganese oxide material exhibited in the nanoscale range. This suggests that the material has a significant surface area to volume ratio, which can enhance its chemical reactivity and catalytic properties.

Using the Scherrer equation, to calculate the crystallite size:

$$D = \frac{K\lambda}{\beta Cos\,\theta}$$

Where, D is the crystallite size

K is the shape factor, typically about 0.9

λ is the wavelength of the X-ray in the 1.5406 A

β is the full width at half maximum of the peak, in (0.01 radians)

θ is the Bragg angle 37.7 ℃

Convert θ from degree to radians

$$\theta = 37.7 \times \frac{\pi}{180}$$

$$= 0.657\ radians$$

$$\mathrm{D} = \frac{0.9 \times 1.5406}{0.01 \times \mathrm{Cos}\,(0.657)}$$

$$= \frac{1.38654}{0.00792}$$

$$= 175.1\ \text{Å}$$

Therefore, the crystallite size D is 175.1 Å

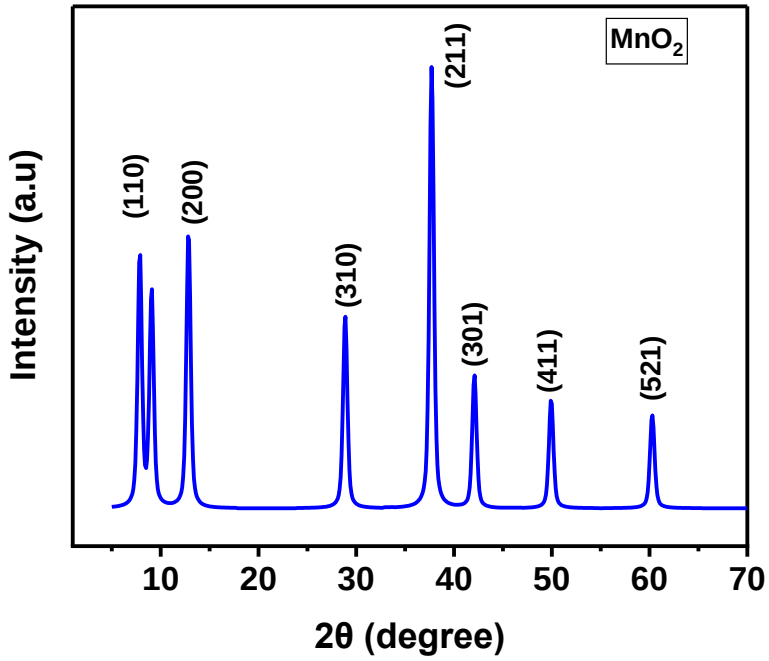

Figure 4.4: XRD pattern of the MnO_2 nanoparticle

4.2.4 SEM results

The surface form of the MnO_2 nanoparticle involve SEM at the diameter of 5 and 10 µm. The SEM images of the MnO_2 nanoparticles are presented in Figure 4.5. The surface form of nanomaterials is known to have a noteworthy effect on their output. Upon inspection of the SEM images, the grains of the MnO_2 nanoparticles are uniformly distributed. The SEM images of the MnO_2 nanoparticles indicate that the grains are uniformly distributed. This suggests that the MnO_2 nanoparticles are evenly dispersed throughout the sample [32]. This uniform distribution implies that the particles are well-mixed or homogeneously dispersed, rather than clumped or localized in specific regions [33]. It indicates that the synthesis process resulted in a relatively uniform dispersion of the nanoparticles. This arrangement of nanorods contributes to the overall morphology of the MnO_2 nanoparticles. The observed surface characteristics of the synthesized MnO_2 nanoparticles Particle dispersion and the creation, such as the porous structure, of flower-like structures, are noteworthy [34]. These features can serve a vital part in considering the MnO_2 nanoparticles as suitable electrode promoters for electrochemical sensing applications. The porous structure provides a extremely surface area, which can enhance the electrochemical reactivity and increase the effectiveness of the electrode [35]. The

presence of nanorods and the assembly of flower-like structures can further contribute to the unique properties and performance of the MnO_2 nanoparticles in electrochemical sensing applications [25].

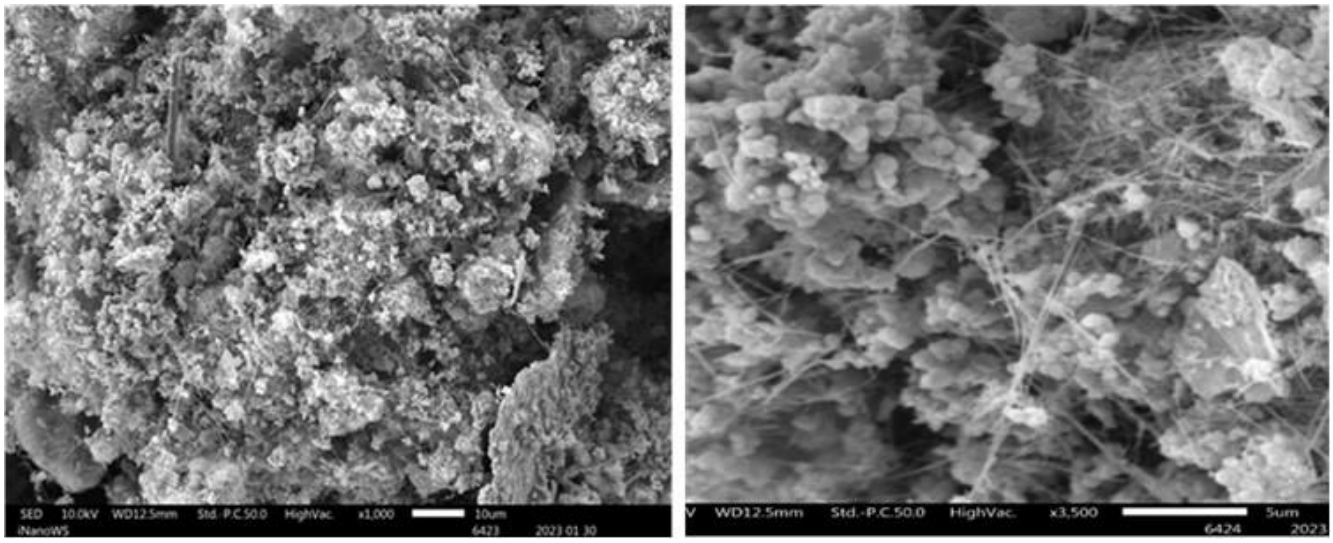

Figure 4.5: SEM image of MnO_2 nanoparticle

4.2.5 Cyclic Voltammetry Studies on MnO_2NPs/SPCE

At a scanning speed of 50 mV/s, CV was examined to evaluate the bare and MnO_2NPs/SPCE in 1.0 mM $[Fe(CN)_6]^{4-}$ solution, as illustrated in Figure 4.6A. The peak potential separation was calculated using equation $\Delta Ep = (Epc - Epa)$ [36]. The CV curve revealed a reversible electrochemical reaction of reach their highest potential division for bare SPCE at 0.249 V while the peak potential separation for MnO_2NPs/SPCE was 0.269 V, indicating that the movement of electrons on the MnO_2NPs/SPCE was fast due to the small peak potential separation, implying a rapid and efficient reaction at the electrode surface as opposed to a bare electrode, which indicated slower electron transfer. The electrochemical response on a bare, at a peak potential of 180 mV, an output with a modest oxidation current of 22.14 µA was seen. On the other hand, MnO_2NPs/SPCE demonstrated a much decreased over potential Ep = 199 mV along with an elevated abrupt anodic peak current (ipa = 88.79 µA). From the observation, the MnO_2NPs/SPCE has a higher peak current, which indicates faster electron transfer rates due to efficient charge exchange taking place between the electroactive substance and the conductor of electricity. This outcome demonstrated that by raising peak current, the MnO_2NPs/SPCE increased the modified electrode's responsiveness. The nano-flower-like form is visible in the highest point from the MnO_2NPs/SPCE. In addition to decreasing the reactive peak's potential separation, the increased current suggests that the effective surface area could be increased, potentially promoting the movement of electrons at the electrode-solution contact.

The capability of electron transfers of bare SPCE and MnO_2NPs SPCE was examined by EIS, seen in Figure 4.6B. The Nyquist plots are seen with the real part (Z') on the X-axis and the imaginary part (−Z'') on the Y-axis [37,39]. The bare and MnO_2NPs SPCE was investigated in 1 mM $[Fe(CN)_6]^{4-}$ solution as shown in Figure 4.6B. The spectra show that the modified MnO_2NPs/SPCE exhibits improved conductivity compared to the bare SPCE. This conclusion is drawn based on the observation that the spectra of the bare SPCE show a semi-circular region, whereas the modified MnO_2NPs/SPCE exhibits a different behaviour. The presence of a semi-circular region in the spectra of the bare SPCE suggests higher charge transfer resistance, indicating less efficient electron transfer compared to the MnO_2NPs/SPCE. The modified MnO_2NPs/SPCE, on the other hand, exhibits low charge transfer resistance, indicating more efficient electron transfer and better conductivity. To further support this finding, fitted a circuit to obtain the charge transfer resistance values. The barrier that hinders charge transference of the MnO_2NPs/SPCE was determined to be 86.9 Ω, while the bare SPCE had a higher charge transfer resistance of 3.95 kΩ. This comparison further confirms the enhanced conductivity and improved electron transfer efficiency of the MnO_2NPs/SPCE compared to the bare SPCE.

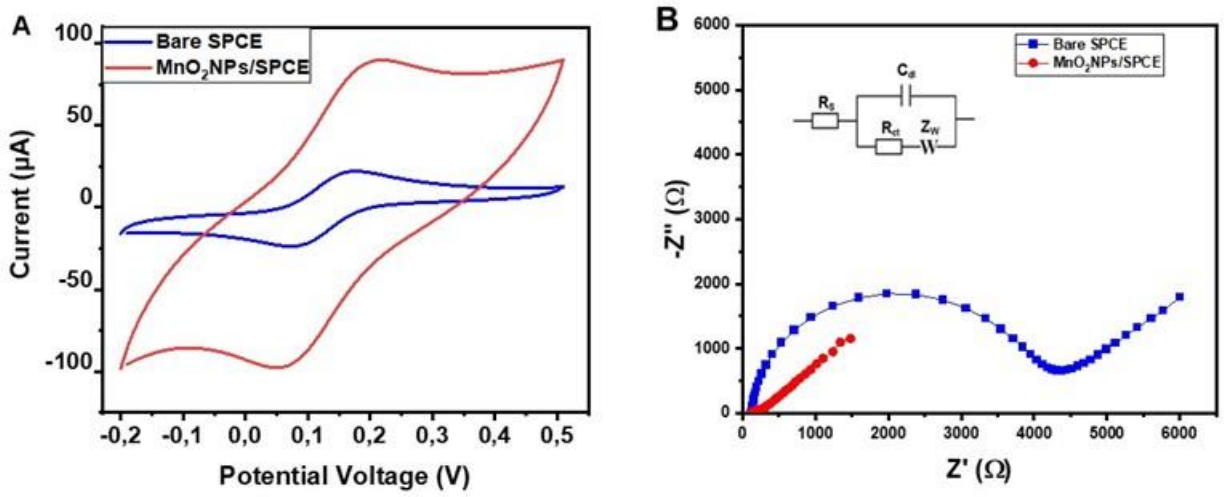

Figure 4.6: CV of bare SPCE and Modified MnO_2NPs/SPCE in a 1.0 mM $[Fe(CN)_6]^{4-}$ solution at a scan speed of 50 mV/s (A) CV (B) EIS.

4.2.7 Optimization studies: Scan rate

Peak current (ip) and peak potential (Ep) of CBZ at the MnO_2NPs/SPCE altered electrode have been examined in relation to scan rate using CV in the setting of 100 µM CBZ (pH 7.0). As the scan rate was raised, Figure 4.8A demonstrates that the anodic peak current (Ipa) of CBZ rose within the 5–50 mV s^{-1} range. Diffusion control is used in the electrochemical of CBZ on MnO_2NPs/SPCE [19]. Furthermore, the irreversible nature of the redox reaction on CBZ at the modified electrode's surface is indicated by the oxidation peak potential's rise as the scan accelerates. The CBZ oxidation peak displayed a maximum peak at a scan speed of 50 mV/s, indicating the increase of the MnO_2NPs/SPCE. Utilizing the Randles-Sevcik Equation, the active surface area of the electrode.

$$i_p = 2.69 \times 10^5 (n^{3/2}) (A) (C) (D^{1/2}) (V^{1/2}) \quad (4.1)$$

Where n is the number of electron transfers (2), A is the electrode's active surface, D is the electrolyte's electroactive species' diffusion coefficient (3.64×10^{-6} cm^2/s), C is the CBZ concentration, and v is the scan speed [17]. The MnO_2NPs/SPCE modified electrode exhibited a greater active surface area in comparison to the naked SPCE surface area.

As shown in Figure 4.8C, in PBS pH 7.0, the impact of various scanning speeds on the electrochemical oxidation behaviour of SMX were examined at various scanning speed between 5 and 50 mV/s. The oxidation current grows in tandem with the scanning speed, causing a steady shift in the oxidation potential in a positive direction. Figure 4.8D shows that, with a correlation coefficient of 0.9768, the anodic peak current is proportional to the square root of the scan rates. This dependency suggests that the oxidation of SMX is often diffusion regulated, which is in keeping with other research.

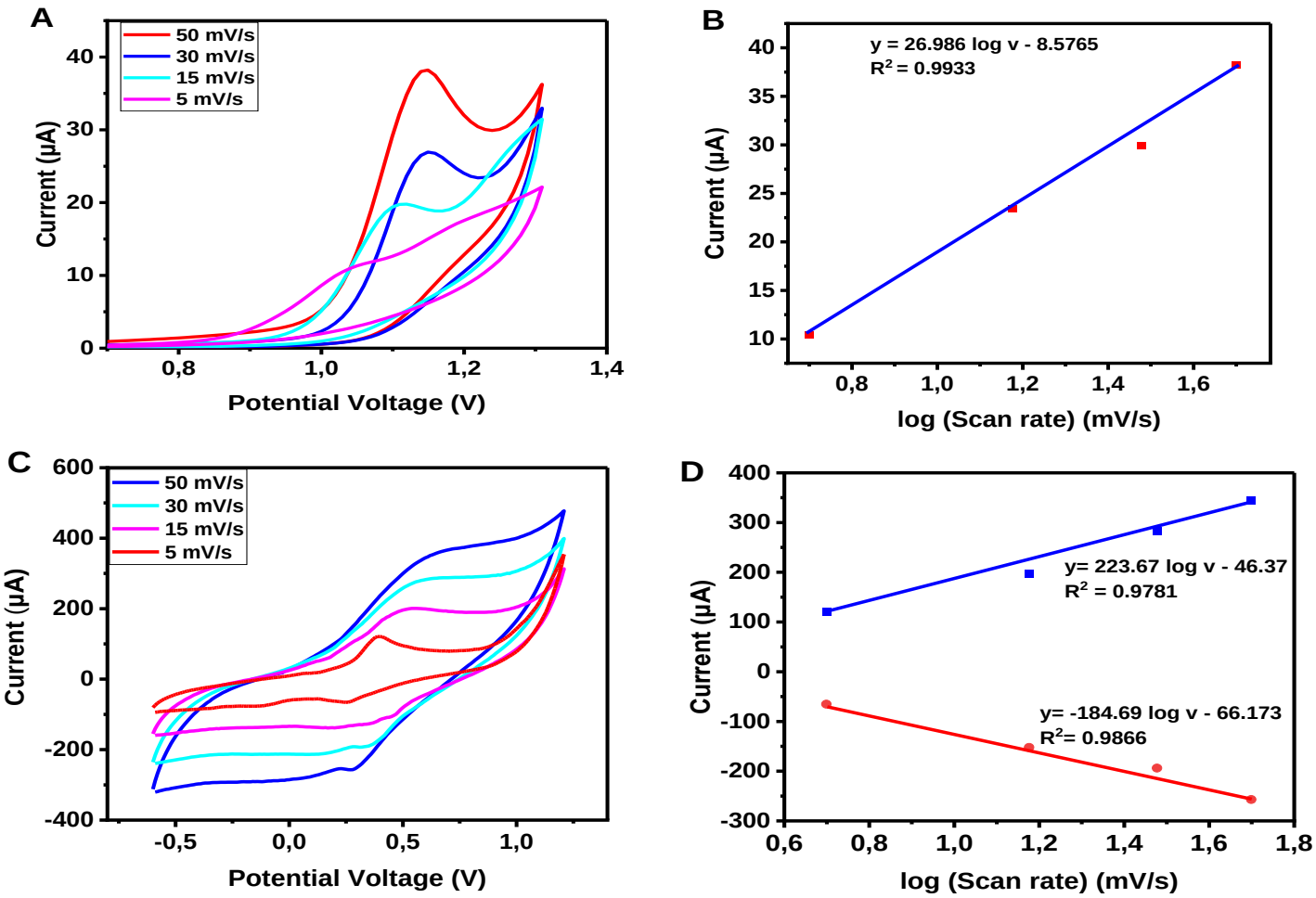

Figure 4.7: CV of the MnO_2NPs/SPCE at varied scan rate range 5-50 mV/s and linear plot relationship (A-B) carbamazepine (C-D) sulfamethoxazole.

4.2.8 Electrochemical behaviour of CBZ on MnO_2NPs/SPCE

The DPV involve the electrochemical behaviour of CBZ on bare and MnO_2NPs/SPCE under the optimum conditions. By reducing the background current input, the DPV approach provides the required resolving power and produces well-differentiated heights even with incredibly little amounts [12]. Figure 4.9C shows the measurement of CBZ at various levels involving MnO_2NPs/SPCE under ideal experimental circumstances. With the updated electrode calibration curves, as CBZ concentration rises, so does its oxidation peak current in the linearity of 0.97 to 5.82 pM. The correlation coefficients detected from the plot were $i_p/\mu A = 33.243$ [CBZ] + 409.12 ($R^2 = 0.9635$), as shown in Figure 4.9D. The MnO_2NPs/SPCE display a stable, sharp, and well-defined anodic peak at 1.0 V. The observation of the oxidation approach of CBZ molecules display a great reaction of MnO_2NPs/SPCE as compared to the bare SPCE. Better features and better sensitivity for analytic use are two areas where the DPV excels above other electroanalytical approaches [13]. Using DPV, an accurate measurement of CBZ at the MnO_2NPs/SPCE under the previously mentioned ideal circumstances was accomplished. The oxidation peak current had a linear association with the CBZ level in the 0.97–5.82 pM range, as shown in Figure 4.9C, using a calibration equation of:

$i_p = 33.243$ [CBZ] + 409.12 ($R^2 = 0.9635$)

The mechanism for the electro-oxidation of carbamazepine onto the surface of MnO_2NPs/SPCE is shown in Figure 4.10. Carbamazepine molecules in the solution adsorb onto the manganese oxide-modified electrode surface. The adsorption occurs due to interactions of the carbamazepine

molecules and the active sites on the manganese oxide. Once adsorbed, the carbamazepine molecules undergo electrochemical oxidation at the manganese oxide's areas of activity. The existence of manganese oxide enhances the oxidation process by facilitating electron transfer. When carbamazepine molecules and the electrode are transferring electrons, manganese oxide may serve as a mediator. [39]. The manganese oxide accepts electrons from the carbamazepine molecules and transfers them to the electrode. The electro-oxidation of carbamazepine on the manganese oxide-modified electrode leads to the creation of oxidation products [40].

Comparing the performance of sensors involve common practice to assess their capabilities and determine their suitability for specific applications. When evaluating a sensor, two important parameters that are often considered are the linearity and the threshold of detection (LOD). To compare the LOD of different sensors, you typically subject each sensor to progressively lower concentrations or smaller magnitudes of the target parameter until the sensor's response becomes indistinguishable from the noise level. The sensor with the lowest concentration or smallest magnitude at which it can still reliably detect and differentiate the signal from the noise is considered to have a lower limit of detection. In Table 4.1, the intensely electroactive MnO_2NPs/SPCE electrode demonstrated a low detection threshold (0.0005 μM) throughout a wider linearity (0.010–0.006 μM) when compared to other altered electrodes for CBZ identification.

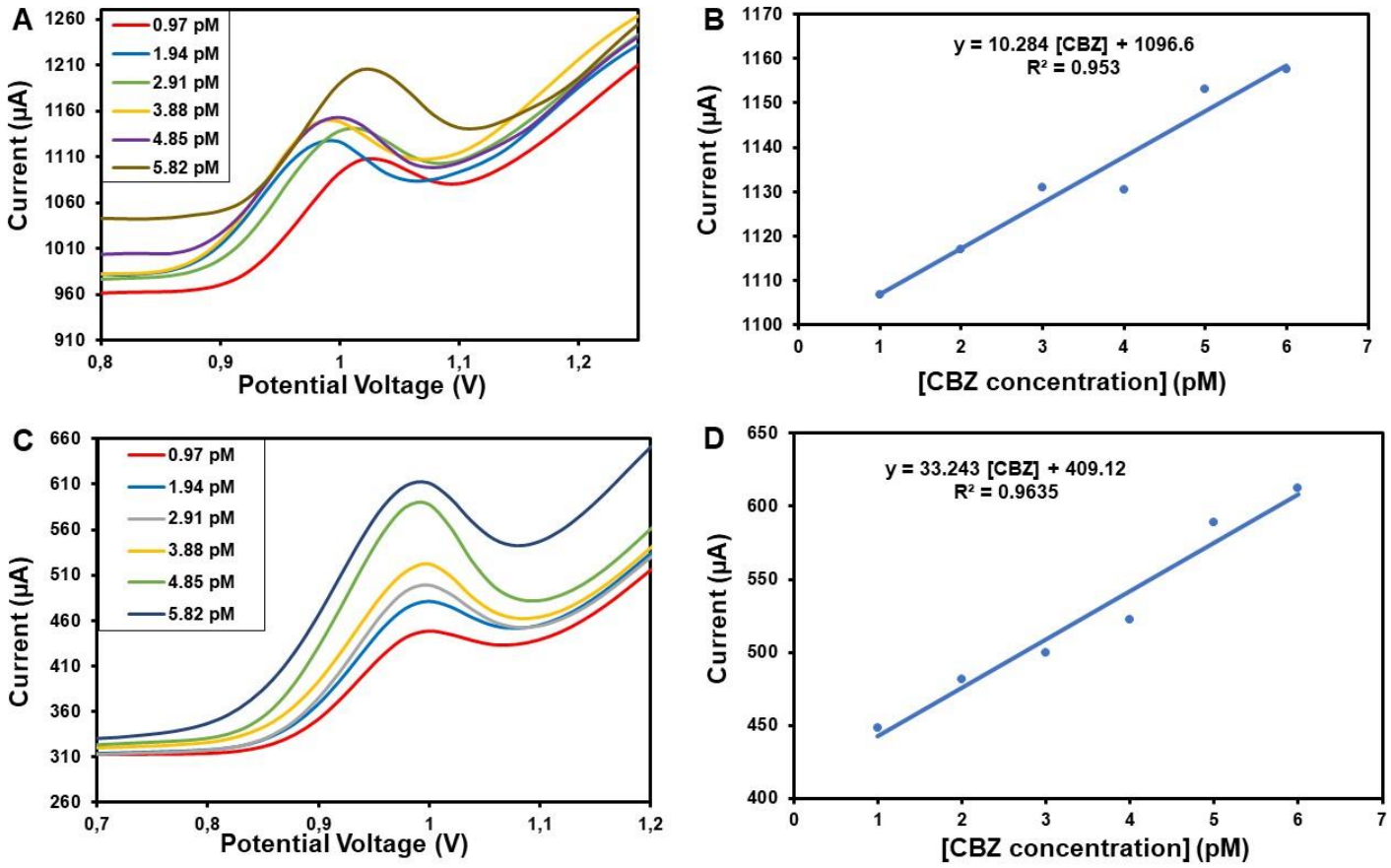

Figure 4.8: DPV signals of (A) Bare SPCE to calculate CBZ in 0.1 M PB solution (pH 7) between 0.97 and 5.82 pM. (B) The CBZ concentration vs. anodic peak current calibration curve. (C) adjusted MnO_2NPs/ SPCE to measure CBZ in 0.1 M PBS solution (pH 7) between 0.97 and 5.82 pM, and (D) the simple plot of CBZ concentrations against anodic peak currents.

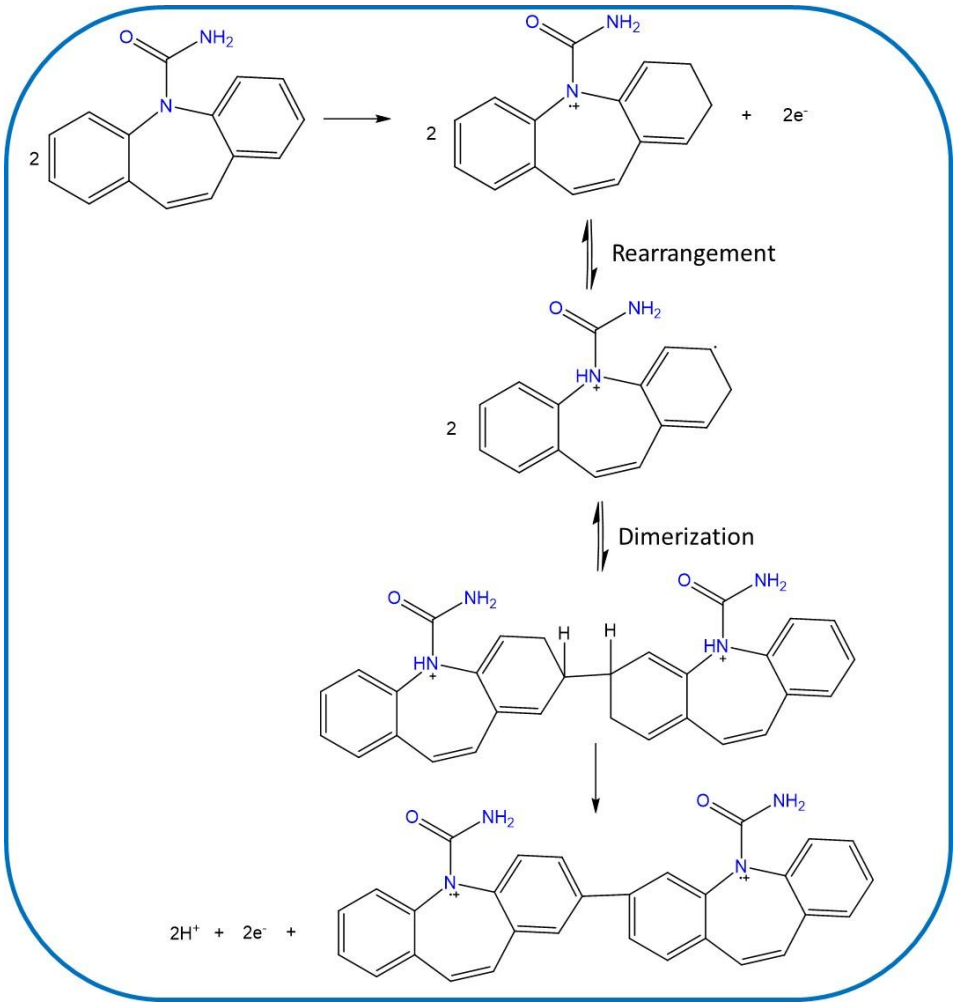

Figure 4.9: The oxidation mechanism of the CBZ on the electrode.

Table 4.1: Qualities of similar techniques for CBZ determination.

Material	Technique	Linearity (µM)	LOD (µM)	Ref
MWCNT/GCE	LSV	0.1 –1.60	0.040	[41]
Au/graphene-AuNPs/GCE	DPV	5.0 – 100	3.03	[11]
Fullerene-C60/GCE	DPV	0.9 – 10	0.016	[42]
Au@AgPdNPs-β-CD-IL/GCE	SWV	0.5 – 9.0	0.089	[18]
Ag/TiO_2/CPE	DPV	2.5 – 100	0.86	[43]
Ce-ZnO/rGO/GCE	DPV	0.0 – 100	0.001	[18]
MnO_2NPs/SPCE	DPV	0.010– 0.006	0.0005	This work

Note: *Multiwalled carbon nanotubes (MWCNTs), glassy carbon electrodes (GCEs), gold nanoparticles (AuNPs), and silver (Ag) Titanium dioxide, or TiO_2; (CPE) Carbon paste electrode; shell nanoparticles Au@AgPdNPs: AgPd with an Au center; Ce-Cerium; β-cyclodextrin-ionic liquid β-CD-IL-macrocyclic; (ZnO) Zinc oxide and (rGO) reduced graphene oxide. These values were converted to µM.*

4.2.9 Application of CBZ in real water samples

The identification of CBZ in wastewater effluent samples was carried out to show the upgraded detector's capability. Table 4.2 offers an overview of the recovery results from the real sample observation at the MnO_2NPs/SPCE detector. The effective CBZ recoveries were achieved at between 95% and 11%, indicating that the MnO_2NPs/SPCE sensor had strong potential to enable applications in environmental monitoring. The %RSD value was found to be 0.151 which indicates less variability and higher precision. A low %RSD suggests that the sensor provides consistent and reproducible results, increasing confidence in its accuracy and precision.

Table 4.2: Identification of CBZ in wastewater.

Samples	[added] (pM)	[Found] (pM)	% Recovery
1	0.21 ± 0.10	0.20 ± 0.13	95%
2	0.29 ± 0.10	0.31 ± 0.13	107%
3	0.40 ± 0.10	0.45 ± 0.13	113%

% Recovery Formula = $\frac{|[\boldsymbol{spiked}]-[\boldsymbol{unspiked}]|}{[\boldsymbol{added}]} \times \mathbf{100}$

4.2.10 Electrochemical behaviour of SMX on MnO_2NPs/SPCE

The electrochemical behaviour of sulfamethoxazole on MnO_2NPs/SPCE involve 0.1 M PBS under optimal conditions. DPV involve the evaluation of the electrochemical reaction of SMX using the MnO_2NPs/SPCE at the potential window between 0.35-1.11 V. SMX was detected at varied levels ranging from 0.97 to 5.82 pM. In Figure 4.10C, the observations of both the bare electrode and the MnO_2NPs/SPCE were depicted. As the concentration of SMX increases, there is a corresponding increase in the measured current. This indicates a direct proportional relationship. The observation of an increase in current with increasing concentration suggests that the MnO_2NPs/SPCE sensor exhibits sensitivity towards SMX. By acting as an active interface for the oxidation reaction involved in the detection process, the MnO_2NPs modification on the outermost layer of the electrode most likely improves the electrochemical detection of SMX. The coefficients of correlation obtained from the graph are presented in the calibration graph as: $i_p/\mu A = 34.465$ [SMX]+ 1309.2 ($R^2 = 0.9885$) as displayed in Figure 4.10D. The MnO_2NPs/SPCE shows a sharp, and well-defined anodic peak at 0.75 V. The scientific literature has proven that two protons and two electrons react in the electrochemical oxidation of SMX. [44]. The equivalent amino benzoquinone is created by first one-electron oxidation within the -NH_2 group, which forms the cation radical at the nitrogen. Next, a fast disappearance of the second electron occurs, as shown in Figure 4.11, producing an oxidation peak that is noticed in voltammetric measurements. Table 4.3 examines the sensing qualities of MnO_2NPs/SPCE with the other electrodes described in the current publications for SMX identification. The sensor used in the present research possesses outstanding accuracy, but other than that, its properties are similar to those of the electrodes that have been published.

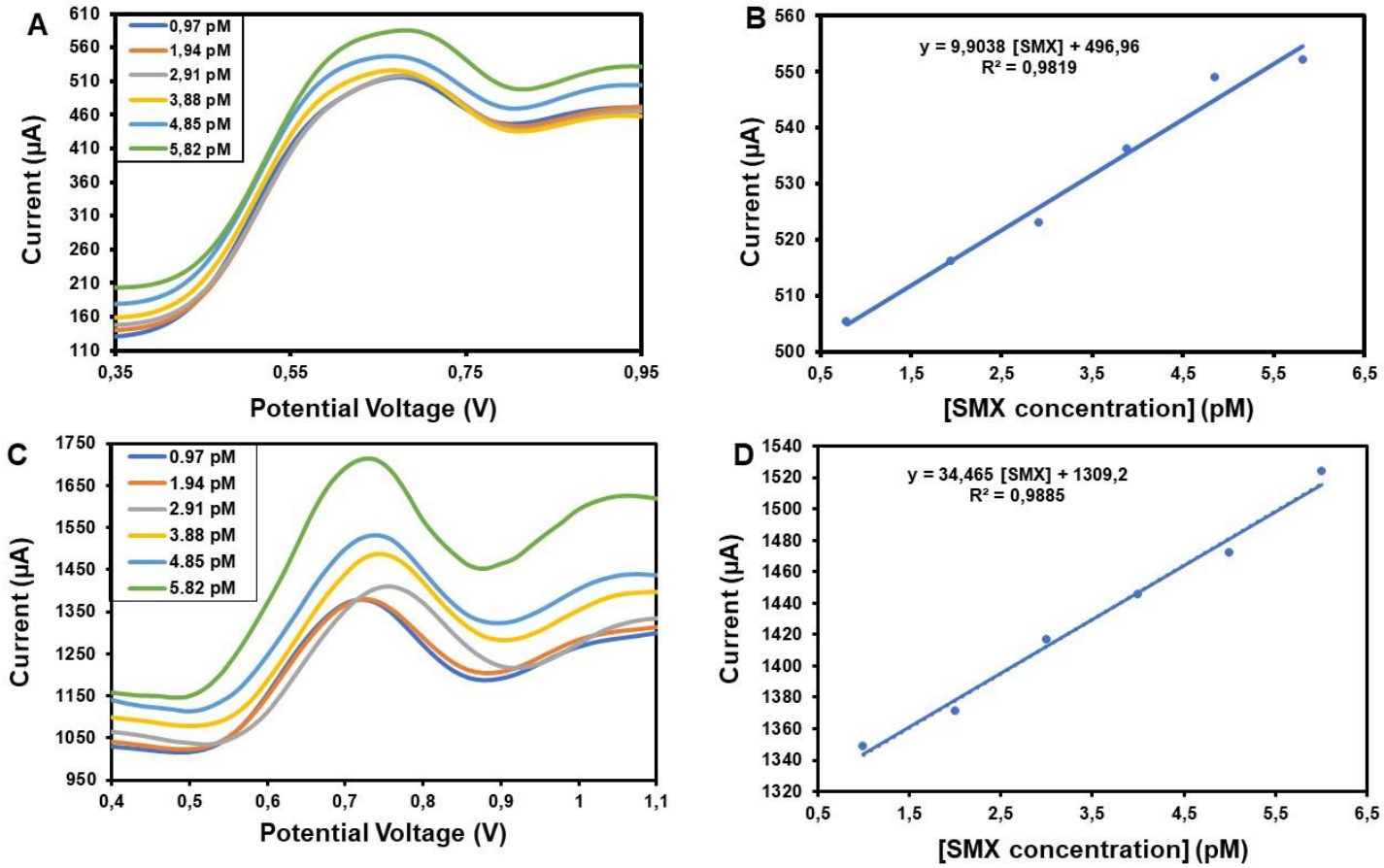

Figure 4.10: Using 0.1 M PBS (pH 7) and DPV signals of (A) Bare SPCE to determine SMX from 0.97 to 5.82 pM. (B) anodic peak currents of SMX vs the concentrations in simple plot. (D) Concentrations vs. anodic peak currents of SMX in simple plot and (C) modified MnO_2NPs/SPCE to determine SMX from 0.97-5.82 pM in 0.1 M PBS (pH 7).

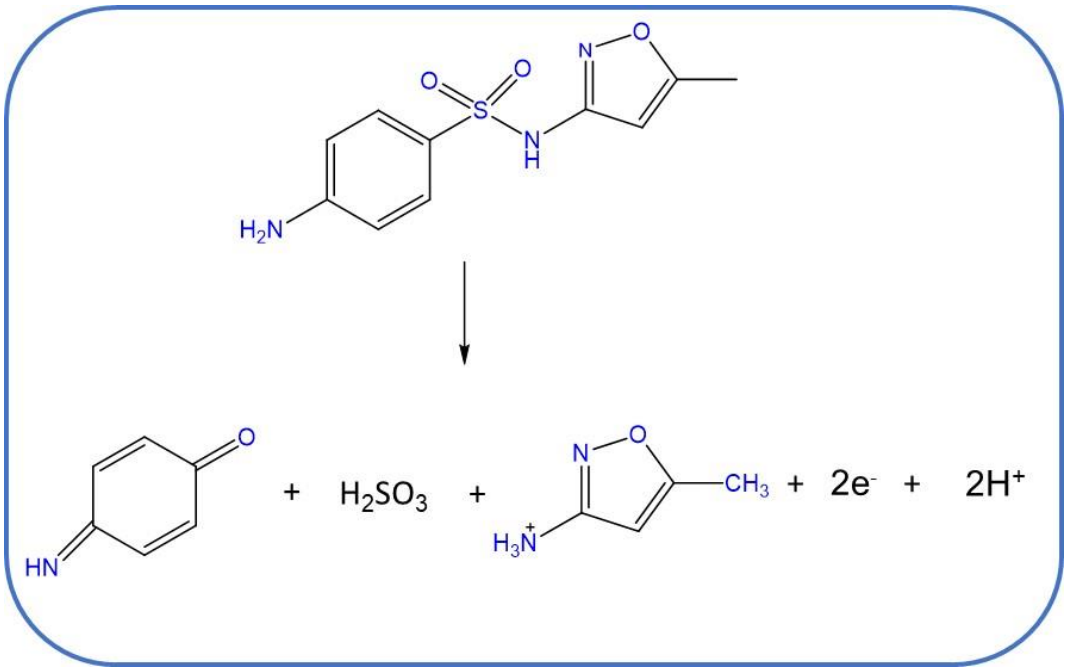

Figure 4.11: The oxidation mechanism of the SMX on the electrode

Table 4.3: Attributes of similar techniques for figuring out SMX.

Material	Technique	Linearity (μM)	LOD (μM)	Ref
MWCNT-SbNP	DPV	0.1 – 0.70	0.02	[45]
SHL-GP/WP	DPV	5.0 – 100	0.40	[9]
MWCNT/PBnc/SPE	DPV	1.0 – 10.0	0.04	[46]
AArGO-modified electrode	DPV	0.5 – 50.0	0.04	[47]
MnO_2NPs/SPCE	DPV	0.010–0.006	0.0002	This work

Note: *These values were converted to μM. reduced graphene nanorode-screen printed carbon electrode (SPCE), graphene-zinc oxide-glassy carbon electrode (GCE), Silver-filled multiwalled carbon nanotube and methyltrioctyl ammonium chloride, Shellac graphite waterproof paper (WP), Multiwalled carbon nanotube decorated with Prussian blue nanocubes, Covalent organic frameworks (COF) polyaniline, gold nanoparticles, Graphene oxide-zinc, Molybdenum dimer oxide.*

4.2.11 Application of SMX in Wastewater

The suggested sensor's usefulness and dependability were evaluated in addition to its ability to identify SMX in wastewater effluent samples. A typical addition approach was utilized to estimate the recovery values, and Table 4.4 presents a summary of the findings. With recovery rates ranging from 90 to 105%, the suggested electrochemical sensor has the precise, effective, and dependable capacity to estimate the quantities of SMX in wastewater samples. It was discovered that the %RSD was 0.290, indicating greater precision and reduced variability.

Table 4.4: SMX measurement in wastewater.

Effluent	[added] (pM)	[Found] (pM)	% Recovery
1	0.10 ± 0.15	0.19 ± 0.12	90%
2	0.29 ± 0.15	0.30 ± 0.12	103%
3	0.40 ± 0.15	0.42 ± 0.12	105%

4.2.12 Interference studies

Interference studies of MnO_2NPs/SPCE sensors involve investigating the potential effects of interfering substances on the sensor's performance and accuracy [48]. These studies are crucial for understanding the sensor's selectivity, reliability, and robustness in real-world applications in the existence of CBZ and SMX. In addition, the MnO_2NPs/SPCE altered electrode's suppression of interference capability was tested for the detection of CBZ and SMX in the form of two widely used drugs that may interfere with signalling: metoprolol (MP) and ibuprofen (IBU). Organic substances that are utilized as pharmaceuticals include metoprolol, ibuprofen, sulfamethoxazole, and carbamazepine. While they have distinct chemical structures and belong to different drug classes, they do share some chemical similarities. Carbamazepine is an anticonvulsant and mood stabilizer, sulfamethoxazole is an antibiotic, ibuprofen involve NSAID, and metoprolol is a beta-blocker involve the cardiovascular conditions [17,50]. The electrochemical reaction of MnO_2NPs/SPCE of the detector did not show an enough alteration in the peak current within the potential window of 0.7 V to 1.2 V, even in the presence of interfering species (not shown). In Figure 4.12A, the interfering species were oxidized at different potentials, indicating that their oxidation did not overlap with the potential range used for the detection of the CBZ. This non-overlapping oxidation behaviour suggests that the interfering species did not

interfere with the electrochemical detection of CBZ. However, despite the absence of direct interference, an interaction between the species was observed because of the existence of similar functional groups such as aromatic rings and heteroatoms. This interaction may lead to some changes in the electrochemical behaviour of the detector. The presence of aromatic rings, which provide stability and specific chemical properties to the molecules, is noted as a shared characteristic among the compounds, including CBZ and the interfering species. Additionally, the presence of nitrogen atoms (N) in all four compounds is highlighted. As a result of this interaction, a decrease in the observed response is mentioned when the interfering species were added, compared to the detection of CBZ alone. The same trend is observed in Figure 4.12B in the existence of sulfamethoxazole (SMX), where a slight decrease in the response compared to the CBZ detection. These findings show that while the interfering species may not directly interfere with the electrochemical detection of CBZ, their presence and shared chemical characteristics can still result in some interaction and a decrease in the observed response.

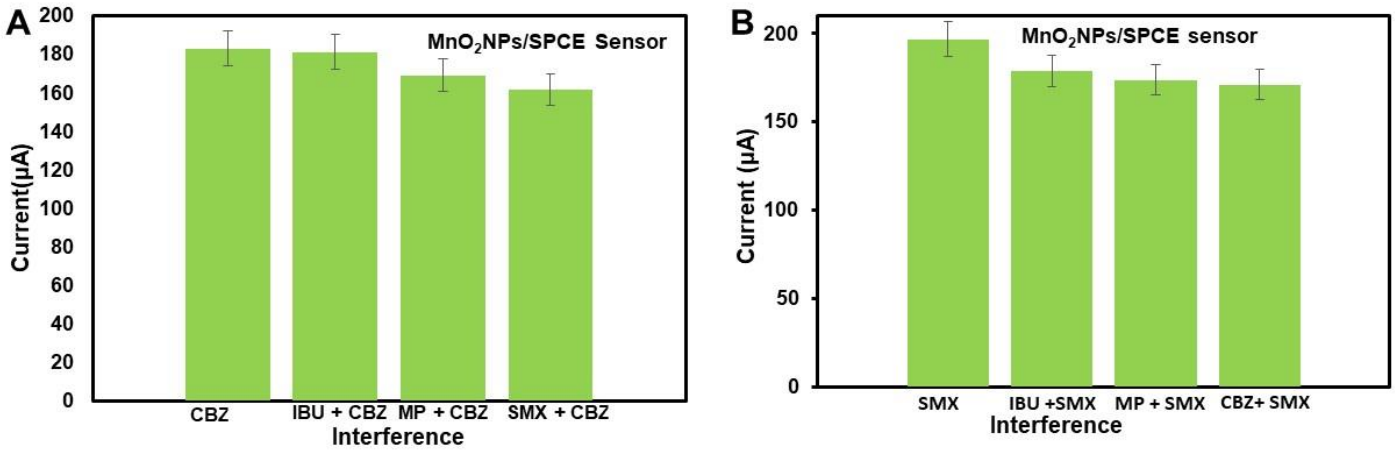

Figure 4.12: Peak current responses of (A) 20 pM CBZ in the presence of interfering species (20 pM SMX, 20 pM IBU, and 20 pM MP), (B) 20 µM SMX in the presence of interfering species (20 pM CBZ, 20 pM IBU and 20 pM MP).

4.2.13 Analysis of stability

The preserved stability of the MnO_2NPs/SPCE sensor was demonstrated by DPV in 0.1 M PBS having 20 µM CBZ and SMX. Two preservation settings were examined: the sensor was kept at ambient temperature for 9 days, as well as in the refrigerator at 4 °C. Two conditions of storage were examined. after the first experiment, the sensor was preserved at RT after 9 days, and the findings shown in Figure 4.13 A-C demonstrate that the current observed of the detector reduced to 68% of the original reaction. Surprisingly, the detector kept 85% of its original reaction after 9 days in another reaction of the preserved in the refrigerator within 4°C, as demonstrated in Figure 4.13B-D. As a result, the detector was placed within 4°C is favoured due to retain the detector's quality. According to these findings, the sensor was reliable for carbamazepine and sulfamethoxazole detection. Tito et al investigated the long-term reliability of the 3-MPA-$NiSe_2$QD/L-cyst/Au detector for NVP measurement at room temperature and 4 °C. The outcome seen that storing the sensor at 4 °C is appropriate [50]. The stability involves AchE/PEDOT-f-MWCNTs detector for the identification of organophosphates such as Chlorpyrifos-methyl was examined by Kaur et al. The detector was preserved at 4 °C for one month. After 5 days, the shift in present response was assessed. The AChE molecule retained 89% of its functioning after one month of preservation, indicating the sensor's excellent durability because of the beneficial microclimate involve PEDOT-f-MWCNTs film of the molecule of AChE. [51]. Previous research has shown that storing the sensor at 4 °C is appropriate, which is consistent with our findings.

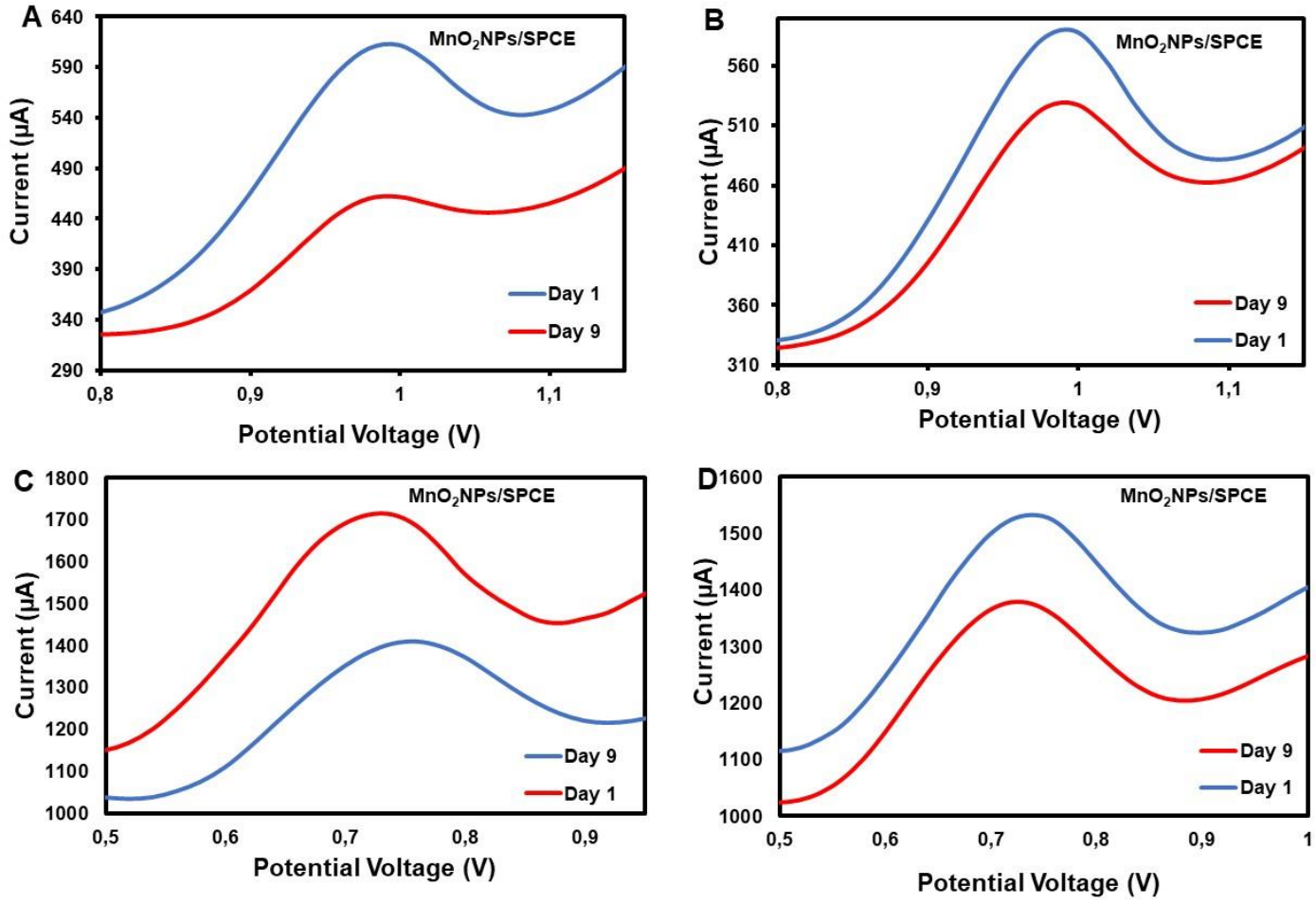

Figure 4.13: Pulse differential Voltammetry responses of MnO_2NPs/SPCE to 20 M carbamazepine (CBZ) and sulfamethoxazole (SMX) on day 1 and 9 following storage (A-C) at ambient temperature and (B-D) at 4°C, respectively.

4.2.14 Simultaneously detection of CBZ and SMX on MnO_2NPs/SPCE sensor

The performance of MnO_2NPs/SPCE, further evaluation was performed for the concurrent identification of CBZ and SMX in 0.1 M PBS (pH 7.0). The DPV oxidation peak currents of CBZ and SMX grew proportional to their amounts when their amounts rose concurrently, as Figure 4.14 illustrates. The simultaneous detection of carbamazepine and sulfamethoxazole using MnO_2NPs/SPCE exhibits a slight shift to the negative potential compared to individual detection. The shift to the negative potential suggests that both CBZ and SMX undergo reduction processes rather than oxidation processes when detected simultaneously. The reduction potentials for SMX and CBZ are obtained at 0.59 V and 0.98 V, respectively. This behaviour indicates that both compounds are being reduced at the electrode surface, possibly because of the existence of reactive species or electrochemical interactions occurring between the analytes and the electrode material (MnO_2NPs/SPCE). The reduction processes might involve the gain of electrons and the formation of reduced species.

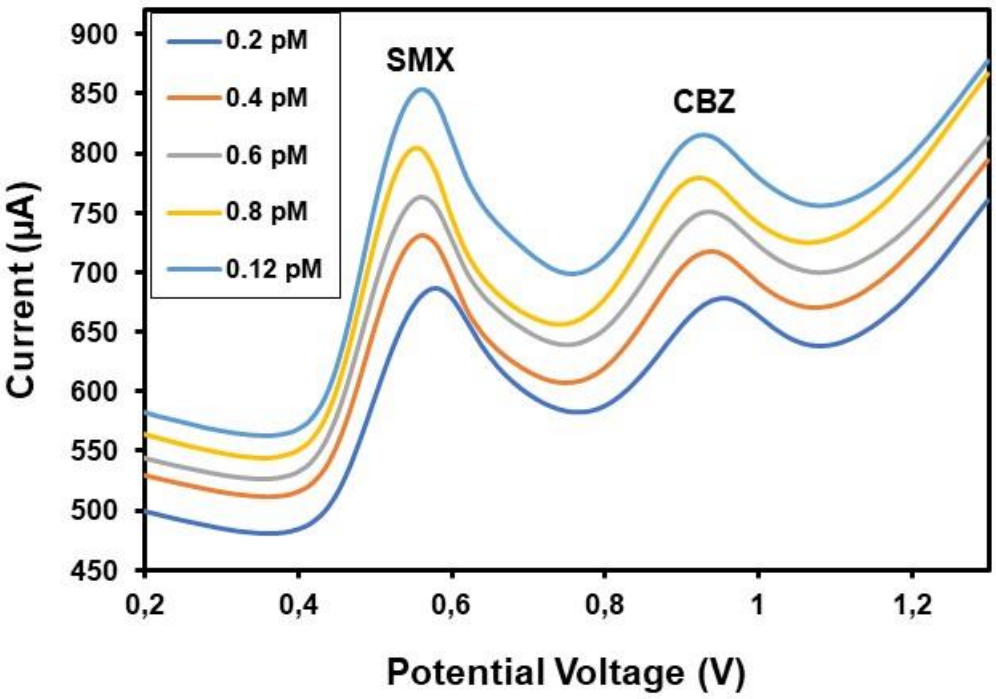

Figure 4.14: Using optimized settings in pH 7 (0.1 M PBS) for the simultaneous detection of SMX and CBZ, DPV voltammograms for the MnO_2NPs/SPCE.

4.3 Conclusion

This work reports on the use of MnO_2NPs/SPCE in the specific, exceptionally sensitive, and precise catalytic voltammetric detection of CBZ and SMX. When the electrochemical responses of MnO_2NPs/SPCE and bare were examined, MnO_2NPs/SPCE was discovered to have the best response. Comparing the developed electrochemical sensor to the other voltammetric techniques utilized for the detection of SMX and CBZ, respectively, the best LOD values are 0.0005 and 0.0002 µM. The MnO_2NPs/SPCE altered electrode has outstanding activity to the oxidation process of CBZ and SMX, as shown by electrochemical studies, which also show an exceptional amplification of peak currents with an adverse change in the oxidation peak potentials. It is argued that the enhanced electron transfer rate by MnO_2NPs electro-catalysis and the rise in the active surface sites of the electrode are the outcomes of the modified electrode's superior electrochemical performance. Furthermore, it is commonly recognized that SPCE is easier to modify and less expensive than the other electrodes utilized in the fabrication process. Consequently, compared to the other electrodes, the created electrochemical is easier, faster, and less expensive. Excellent selectivity, reproducibility, stability, and repeatability were demonstrated by the modified electrochemical sensor. Consequently, MnO_2NPs/SPCE presents itself as a viable option for the identification of CBZ and SMX in wastewater samples.

Reference

[1] B. Kasprzyk-Hordern, “Pharmacologically active compounds in the environment and their chirality,” *Chem. Soc. Rev.*, vol. 39, no. 11, pp. 4466–4503, 2010, doi: 10.1039/c000408c.

[2] A. Yu-Chen Lin, S. C. Panchangam, and H. Y. Chen, “Implications of human pharmaceutical occurrence in the Sindian river of Taiwan: A strategic study of risk assessment,” *J. Environ. Monit.*, vol. 12, no. 1, pp. 261–270, 2010, doi: 10.1039/b903880a.

[3] S. Khan, Nadeem A. Khan, Saif Ullah Ahmed and F. Farooqi, Izharul Haq Yousefi, MahmoodMohammadi, Ali Akbar Changani, “Recent trends in disposal and treatment technologies of emerging-pollutants- A critical review,” *TrAC - Trends Anal. Chem.*, vol. 122, 2020, doi: 10.1016/j.trac.2019.115744.

[4] S. Bagheri, A. Termehyousefi, and T. O. Do, “Photocatalytic pathway toward degradation of environmental pharmaceutical pollutants: Structure, kinetics and mechanism approach,” *Catal. Sci. Technol.*, vol. 7, no. 20, pp. 4548–4569, 2017, doi: 10.1039/c7cy00468k.

[5] M. Moghaddam, A.Khayatan, D.Esmaeili Fard Barzegar, P.Ranjbar, R.Yazdanian, M.Tahmasebi, E.Alam, H. Abbasi, K.Esmaeili Gouvarchin Ghaleh, and H.Tebyaniyan, *Biodegradation of pharmaceutical compounds in industrial wastewater using biological treatment: a comprehensive overview*, vol. 20, no. 5. Springer Berlin Heidelberg, 2023. doi: 10.1007/s13762-023-04880-2.

[6] P. Bottoni, S. Caroli, and A. B. Caracciolo, “Pharmaceuticals as priority water contaminants,” *Toxicol. Environ. Chem.*, vol. 92, no. 3, pp. 549–565, 2010, doi: 10.1080/02772241003614320.

[7] E. S. Okeke, A. Chukwudozie, Kingsley Ikechukwu Nyaruaba, Raphael Ita, Richard Ekeng Oladipo, O. Ejeromedoghene, E. O. Atakpa, and C. O. Agu, Chidozie Victor Okoye, *Antibiotic resistance in aquaculture and aquatic organisms: a review of current nanotechnology applications for sustainable management*, vol. 29, no. 46. Springer Berlin Heidelberg, 2022. doi: 10.1007/s11356-022-22319-y.

[8] X. Yue, Z. Li, and S. Zhao, “A new electrochemical sensor for simultaneous detection of sulfamethoxazole and trimethoprim antibiotics based on graphene and ZnO nanorods modified glassy carbon electrode,” *Microchem. J.*, vol. 159, no. April, p. 105440, 2020, doi: 10.1016/j.microc.2020.105440.

[9] J. Melo Henrique, J. Rocha Camargo, G. Gabriel de Oliveira, J. Santos Stefano, and B. Campos Janegitz, “Disposable electrochemical sensor based on shellac and graphite for sulfamethoxazole detection,” *Microchem. J.*, vol. 170, no. May, 2021, doi: 10.1016/j.microc.2021.106701.

[10] L. Wentland, C. Downs, and E. Fu, “Comparison of signal enhancement strategies for carbamazepine detection in undiluted human saliva using an electrochemical sensor with stencil-printed carbon electrodes,” *Anal. Methods*, vol. 14, no. 32, pp. 3103–3114, 2022, doi: 10.1039/d2ay00926a.

[11] A. R. Pruneanu, Stela Pogacean, Florina Biris, G. Ardelean, Stefania Canpean, Valentin Blanita, and A. S. Dervishi, Enkeleda Biris, “Novel graphene-gold nanoparticle modified electrodes for the high sensitivity electrochemical spectroscopy detection and analysis of carbamazepine,” *J. Phys. Chem. C*, vol. 115, no. 47, pp. 23387–23394, 2011, doi: 10.1021/jp206945e.

[12] Y. Ma, Yujie, Song and Q. Ma, Yunsu Wei, Fangdi Xu, Guanhong Cen, Yao Shi, Menglan Xu, Xiaoman Hu, “N-doped carbon dots as a fluorescent probe for the sensitive and facile detection of carbamazepine based on the inner filter effect,” *New J. Chem.*, vol. 42, no. 11, pp. 8992–8997, 2018, doi: 10.1039/c8nj00764k.

[13] E. Naghian, E. Marzi Khosrowshahi, E. Sohouli, F. Ahmadi, M. Rahimi-Nasrabadi, and V. Safarifard, “A new electrochemical sensor for the detection of fentanyl lethal drug by a screen-printed carbon electrode modified with the open-ended channels of Zn(ii)-MOF,” *New J. Chem.*,

vol. 44, no. 22, pp. 9271–9277, 2020, doi: 10.1039/d0nj01322f.

[14] M. Safaei and M. R. Shishehbore, “A review on analytical methods with special reference to electroanalytical methods for the determination of some anticancer drugs in pharmaceutical and biological samples,” *Talanta*, vol. 229, no. September 2020, p. 122247, 2021, doi: 10.1016/j.talanta.2021.122247.

[15] P. A. Datar, “Quantitative bioanalytical and analytical method development of dibenzazepine derivative, carbamazepine: A review,” *J. Pharm. Anal.*, vol. 5, no. 4, pp. 213–222, 2015, doi: 10.1016/j.jpha.2015.02.005.

[16] S. Chelly, M. Chelly, R. Zribi, R. Gdoura, H. Bouaziz-Ketata, and G. Neri, “Electrochemical Detection of Dopamine and Riboflavine on a Screen-Printed Carbon Electrode Modified by AuNPs Derived from Rhanterium suaveolens Plant Extract,” *ACS Omega*, vol. 6, no. 37, pp. 23666–23675, 2021, doi: 10.1021/acsomega.1c00793.

[17] V. Mariyappan, R. Sundaresan, S. M. Chen, and R. Ramachandran, “Ultrasensitive electrochemical sensor for the detection of carbamazepine based on gadolinium vanadate nanostructure decorated functionalized carbon nanofiber nanocomposite,” *Chemosphere*, vol. 307, no. P2, p. 135803, 2022, doi: 10.1016/j.chemosphere.2022.135803.

[18] N. Dhanalakshmi, T. Priya, and N. Thinakaran, “Highly electroactive Ce-ZnO/rGO nanocomposite: Ultra-sensitive electrochemical sensing platform for carbamazepine determination,” *J. Electroanal. Chem.*, vol. 826, no. June, pp. 150–156, 2018, doi: 10.1016/j.jelechem.2018.08.036.

[19] N. H. Qambrani, Nadeem Buledi, Jamil A. Khand and F. Solangi, Amber R. Ameen, Sidra Jalbani, Nida S. Khatoon, Amna Taher, Mohammad Ali Moghadam, F. H.Shojaei, Moein Karimi, “Facile Synthesis of NiO/ZnO nanocomposite as an effective platform for electrochemical determination of carbamazepine,” *Chemosphere*, vol. 303, no. P3, p. 135270, 2022, doi: 10.1016/j.chemosphere.2022.135270.

[20] P. M. Jahani and S. A. Ahmadi, “MnO2 nanorods modified screen-printed electrode for the electrochemical determination of Sudan dye in food sample,” *J. Electrochem. Sci. Eng.*, vol. 12, no. 6, pp. 1121–1131, 2022, doi: 10.5599/jese.1415.

[21] C. M. Miyazaki, N. Joshi, O. N. Oliveira, and F. M. Shimizu, *Metal Oxides and Sulfide-Based Biosensors for Monitoring and Health Control*. 2021. doi: 10.1007/978-3-030-63791-0_6.

[22] C. J. Makgopa, Katlego Ejikeme, Paul M. Jafta, M. Raju, Kumar Zeiger, and K. I. Presser, Volker Ozoemena, “A high-rate aqueous symmetric pseudocapacitor based on highly graphitized onion-like carbon/birnessite-type manganese oxide nanohybrids,” *J. Mater. Chem. A*, vol. 3, no. 7, pp. 3480–3490, 2015, doi: 10.1039/c4ta06715k.

[23] A. Sumboja, C. Y. Foo, J. Yan, C. Yan, R. K. Gupta, and P. S. Lee, “Significant electrochemical stability of manganese dioxide/polyaniline coaxial nanowires by self-terminated double surfactant polymerization for pseudocapacitor electrode,” *J. Mater. Chem.*, vol. 22, no. 45, pp. 23921–23928, 2012, doi: 10.1039/c2jm32456c.

[24] Y. Meng, W. Song, H. Huang, Z. Ren, S. Y. Chen, and S. L. Suib, “Structure-property relationship of bifunctional MnO2 nanostructures: Highly efficient, ultra-stable electrochemical water oxidation and oxygen reduction reaction catalysts identified in alkaline media,” *J. Am. Chem. Soc.*, vol. 136, no. 32, pp. 11452–11464, 2014, doi: 10.1021/ja505186m.

[25] A. O. Idris, P. J. Mafa, E. O. Oseghe, T. A. M. Msagati, U. Feleni, and B. B. Mamba, “A facile approach for the preparation of NiONPs@MnO2NRs nanocomposite material and its photocatalytic activity,” *J. Nanoparticle Res.*, vol. 23, no. 7, 2021, doi: 10.1007/s11051-021-05257-7.

[26] B. Cheng, Gao Yu, Lin Lan, Bang Sun, Ming Lin, Ting Fu, Zhiwei Su, Xiaohui Qiu, Minqiao Guo, Canhui Xu, “Controlled synthesis of α-MnO2 nanowires and their catalytic performance for toluene combustion,” *Mater. Res. Bull.*, vol. 75, pp. 17–24, 2016, doi: 10.1016/j.materresbull.2015.11.017.

[27] Z. U. H. Shah, Hidayat Ullah Wang, Fengping Javed, Muhammad Sufyan Ahmad, M. A. Saleem, Muhammad Zhan, Jinbing Khan and Y. Li, “In-situ growth of MnO2 nanorods forest on carbon textile as efficient electrode material for supercapacitors,” *J. Energy Storage*, vol. 17, no. April, pp. 318–326, 2018, doi: 10.1016/j.est.2018.03.015.

[28] J. Luo, Yongsong. Jiang, C. M. Zhou, Weiwei.Yang, Huanping Luo, Jingshan Qi, Xiaoying Zhang, Hua Yu, Denis Y.W. Li, and T. Yu, “Self-assembly of well-ordered whisker-like manganese oxide arrays on carbon fiber paper and its application as electrode material for supercapacitors,” *J. Mater. Chem.*, vol. 22, no. 17, pp. 8634–8640, 2012, doi: 10.1039/c2jm16419a.

[29] Z. Li, Y. Mi, X. Liu, S. Liu, S. Yang, and J. Wang, “Flexible graphene/MnO2 composite papers for supercapacitor electrodes,” *J. Mater. Chem.*, vol. 21, no. 38, pp. 14706–14711, 2011, doi: 10.1039/c1jm11941a.

[30] E. Kareem Jassem, A. Mustafa Abdul Majeed, and N. Mossa Umran, “The Effect of Temperature on Structural and optical properties of Manganese Oxide Nanoparticles,” *J. Phys. Conf. Ser.*, vol. 1279, no. 1, 2019, doi: 10.1088/1742-6596/1279/1/012004.

[31] Y. Zhao, Xiaoyu.Hou and Z. Wang, Yanfei Yang, Libin Zhu, Liang Cao, Ruge Sha, “Prepared MnO2 with different crystal forms as electrode materials for supercapacitors: Experimental research from hydrothermal crystallization process to electrochemical performances,” *RSC Adv.*, vol. 7, no. 64, pp. 40286–40294, 2017, doi: 10.1039/c7ra06369e.

[32] S. Chen, X. Shu, H. Wang, and J. Zhang, “Thermally driven phase transition of manganese oxide on carbon cloth for enhancing the performance of flexible all-solid-state zinc-air batteries,” *J. Mater. Chem. A*, vol. 7, no. 34, pp. 19719–19727, 2019, doi: 10.1039/c9ta05719f.

[33] Y. K. Hsu, Y. C. Chen, Y. G. Lin, L. C. Chen, and K. H. Chen, “Birnessite-type manganese oxides nanosheets with hole acceptor assisted photoelectrochemical activity in response to visible light,” *J. Mater. Chem.*, vol. 22, no. 6, pp. 2733–2739, 2012, doi: 10.1039/c1jm14355g.

[34] F. Paquin, J. Rivnay, A. Salleo, N. Stingelin, and C. Silva, “Multi-phase semicrystalline microstructures drive exciton dissociation in neat plastic semiconductors,” *J. Mater. Chem. C*, vol. 3, no. 207890, pp. 10715–10722, 2015, doi: 10.1039/b000000x.

[35] F. Paquin, J. Rivnay, A. Salleo, N. Stingelin, and C. Silva, “Multi-phase semicrystalline microstructures drive exciton dissociation in neat plastic semiconductors,” *J. Mater. Chem. C*, vol. 3, pp. 10715–10722, 2015, doi: 10.1039/b000000x.

[36] P. Wu, Yiyong. Deng and Q. Tian, Yaling Feng, Jinxia Xiao, Jingyun Li, Junhua Liu, Jun Li, Guangli He, “Simultaneous and sensitive determination of ascorbic acid, dopamine and uric acid via an electrochemical sensor based on PVP-graphene composite,” *J. Nanobiotechnology*, vol. 18, no. 1, pp. 1–13, 2020, doi: 10.1186/s12951-020-00672-9.

[37] M. Li, T. Zhang, and Y. Zhang, “Ultrasensitive electrochemical sensing platform for miRNA-21 detection based on manganese dioxide-gold nanoparticle nanoconjugates coupled with hybridization chain reaction and horseradish peroxidase signal amplification,” *Analyst*, pp. 2180–2188, 2023, doi: 10.1039/d3an00490b.

[38] M. Wang, Jiawei. Liao and B. Huang, Xinlin Li, Pengzhou Li, Jiaxin Ye, Lei Gao, Yue Peng, Huisheng Wang, “Enhanced cathode integrity for zinc-manganese oxide fiber batteries by a durable protective layer,” *J. Mater. Chem. A*, no. April, 2022, doi: 10.1039/d2ta00982j.

[39] M. A. Shah, Afzal.Malik, Maria Saleem Zahid, Anum Iftikhar, Faiza Jan Anwar, Ayaz Akhter, Mohammad Salim Shah, Muhammad Raza Zia, M. N. Ashiq, and A. H. Shah, “Carbamazepine coated silver nanoparticles for the simultaneous electrochemical sensing of specific food toxins,” *Electrochim. Acta*, vol. 274, pp. 131–142, 2018, doi: 10.1016/j.electacta.2018.04.096.

[40] M. Zahran, Z. Khalifa, M. A. H. Zahran, and M. Abdel Azzem, “Recent advances in silver nanoparticle-based electrochemical sensors for determining organic pollutants in water: A review,” *Mater. Adv.*, vol. 2, no. 22, pp. 7350–7365, 2021, doi: 10.1039/d1ma00769f.

[41] N. Qambrani *et al.*, “Facile Synthesis of NiO/ZnO nanocomposite as an effective platform for electrochemical determination of carbamazepine,” *Chemosphere*, vol. 303, no. P3, p. 135270, 2022, doi: 10.1016/j.chemosphere.2022.135270.

[42] S. S. Kalanur, S. Jaldappagari, and S. Balakrishnan, “Enhanced electrochemical response of carbamazepine at a nano-structured sensing film of fullerene-C60 and its analytical applications,” *Electrochim. Acta*, vol. 56, no. 15, pp. 5295–5301, 2011, doi: 10.1016/j.electacta.2010.08.071.

[43] S. Devaraj and N. Munichandraiah, “Electrochemical Supercapacitor Studies of Nanostructured α-MnO[sub 2] Synthesized by Microemulsion Method and the Effect of Annealing,” *J. Electrochem. Soc.*, vol. 154, no. 2, p. A80, 2007, doi: 10.1149/1.2404775.

[44] P. Senthil Kumar, B. S. Sreeja, K. Krishna Kumar, and G. Padmalaya, “Investigation of Nafion coated GO-ZnO nanocomposite behaviour for sulfamethoxazole detection using cyclic voltammetry,” *Food Chem. Toxicol.*, vol. 167, no. June, p. 113311, 2022, doi: 10.1016/j.fct.2022.113311.

[45] T. S. Martins, J. L. Bott-Neto, O. N. Oliveira, and S. A. S. Machado, “Paper-based electrochemical sensors with reduced graphene nanoribbons for simultaneous detection of sulfamethoxazole and trimethoprim in water samples,” *J. Electroanal. Chem.*, vol. 882, 2021, doi: 10.1016/j.jelechem.2021.114985.

[46] C. Chen, Y. C. Chen, Y. T. Hong, T. W. Lee, and J. F. Huang, “Facile fabrication of ascorbic acid reduced graphene oxide-modified electrodes toward electroanalytical determination of sulfamethoxazole in aqueous environments,” *Chem. Eng. J.*, vol. 352, no. May, pp. 188–197, 2018, doi: 10.1016/j.cej.2018.06.110.

[47] I. Cesarino, V. Cesarino, and M. R. V. Lanza, “Carbon nanotubes modified with antimony nanoparticles in a paraffin composite electrode: Simultaneous determination of sulfamethoxazole and trimethoprim,” *Sensors Actuators, B Chem.*, vol. 188, pp. 1293–1299, 2013, doi: 10.1016/j.snb.2013.08.047.

[48] Z. L. and N. H. Yang Zhao, Fang Yuan, Xie Quan, Hongtao Yu, Shuo Chen, Huimin Zhao, “An electrochemical sensor for selective determination of sulfamethoxazole in surface water using a molecularly imprinted polymer modified BDD electrode,” *Anal. Methods*, vol. 7, no. 6, pp. 2693–2698, 2015, doi: 10.1039/c4ay03055a.

[49] T. Rasheed, M. Bilal, F. Nabeel, M. Adeel, and H. M. N. Iqbal, “Environmentally-related contaminants of high concern: Potential sources and analytical modalities for detection, quantification, and treatment,” *Environ. Int.*, vol. 122, no. September 2018, pp. 52–66, 2019, doi: 10.1016/j.envint.2018.11.038.

[50] G. S. Tito, A. S. Abolanle, A. T. Kuvarega, B. B. Mamba, and U. Feleni, “Nickel Selenide Quantum dot Reactor for Electro-oxidation of Nevirapine in Wastewater,” *ChemistrySelect*, vol. 7, no. 40, 2022, doi: 10.1002/slct.202202294.

[51] N. Kaur, H. Thakur, R. Kumar, and N. Prabhakar, “An electrochemical sensor modified with poly(3,4-ethylenedioxythiophene)-wrapped multi-walled carbon nanotubes for enzyme inhibition-based determination of organophosphates,” *Microchim. Acta*, vol. 183, no. 7, pp. 2307–2315, 2016, doi: 10.1007/s00604-016-1871-y.

Chapter 5

Electro-oxidation of ibuprofen and metoprolol using manganese oxide platform

Summary

Pharmaceutical compounds, such as ibuprofen and metoprolol, are of increasing issue due to their persistence in the surrounding and potential negatively on human health. In this work, we developed an electrochemical detector system for the identification of ibuprofen and metoprolol based on a modified manganese oxide nanoparticle on a SPCE. The characterisation of MnO_2NPs modifier was investigated via FTIR, XRD, SEM, Raman spectroscopy techniques, uv/vis spectroscopy, and small-angle X-ray scattering spectroscopy. The electrochemical behaviour of the MnO_2NPs was studied involving DPV and CV techniques. By analysing the impact of pH on the CV reactions, electrolytes on the DPV reaction, and scan speeds on the CV reactions, the ideal conditions for testing were determined. The MnO_2NPs modified electrode demonstrated enhanced catalytic activity in the electro-oxidation of both ibuprofen and metoprolol. The oxidation peaks of Ibuprofen and Metoprolol were seen at +1.14 V and +1.46 V corresponding, for the MnO_2NPs/SPCE detector. The detector's limit of detection was 0.0004 µM and 0.005 µM respectively and its linear response was from 0.97–5.82 pM. In addition, durability and interfering investigations were carried out to assess the MnO_2NPs/SPCE sensor's efficiency under ideal circumstances, which produced an acceptable result. Using actual water samples, the suggested sensor was effectively applied to determine the levels of metoprolol and ibuprofen.

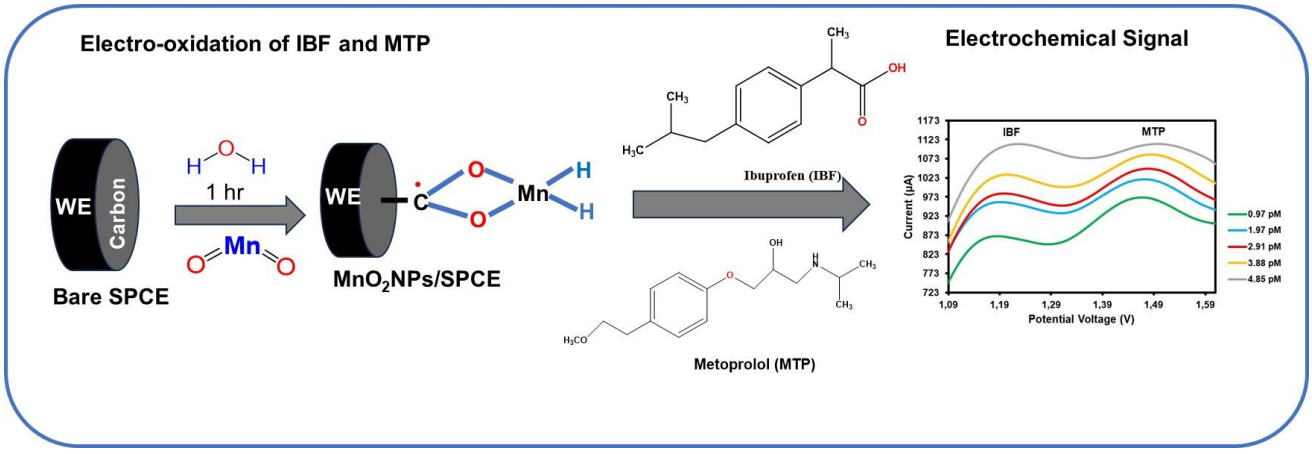

5.1 Introduction

Ibuprofen (IBU) and metoprolol (MP) belong to different classes of pharmaceuticals [1]. Ibuprofen involve NSAID, whereas metoprolol is a beta-blocker (as shown in Figure 5.1) [2,3,4]. Both medications have been detected in water bodies primarily as active pharmaceutical ingredients (APIs), which has raised environmental and health concerns [5]. The existence of APIs in water bodies can negatively impact marine habitats. Some APIs can interfere with marine creatures' hormonal balances, affect reproductive processes, and lead to imbalances in aquatic populations [6]. Ibuprofen is one of the most widely used and highest-selling drugs globally [7]. It is available over the counter, which means it can be purchased without a prescription, making it easily accessible to consumers [8]. Its effectiveness in relieving pain, reducing inflammation, and lowering fever has made preferred drug for a range of transient, non-specific headache indications, including headaches, muscle aches, menstrual cramps, and minor injuries [7]. This medicine is primarily processed in the liver, where about 90% of the drug undergoing metabolic transformations. These transformations result in the production

of hydroxy and carboxy metabolites of ibuprofen [8]. Only a small fraction, less than 10%, is excreted from the body unchanged in urine and bile [9].

While metoprolol is a selective β1 receptor blocker involve heal a range of cardiovascular conditions, most notably hypertension, angia pectoris, cardiac arrhythmia, and myocardial infarction [10]. Because of its extreme responsiveness, an excessive intake can result in sufficient inhibition from even a little ingested intake of the medication such a β-blocker can result in significant cardiac issues [11]. Because of MP's sedative effect, the International Olympic Committee has put it on the list of prohibited substances [10]. Both drugs can have negative impact on marine life [12]. Even at low concentrations, they may disrupt the marine species' hormonal systems, which impact their approach for growth and reproduction [13]. In the case of metoprolol, which is a beta-blocker, it may have effects on fish and other aquatic organisms sensitive to changes in heart rate [12]. These pharmaceuticals end up in our water bodies through several pathways such as hospital discharge, municipal discharge, domestic and industrial discharge, and many more [13]. Once these drugs enter wastewater systems, they undergo various levels of treatment at wastewater treatment plants. While some drugs may be removed during treatment, not all pharmaceutical residues are effectively eliminated, and they can still pass through the treatment process [14]. Consequently, treated wastewater may contain traces of pharmaceutical compounds, including ibuprofen and metoprolol [13]. Using a range of quantitative analytical techniques, ibuprofen, and metoprolol have been found in ambient samples [12]. These techniques include spectrofluorimetry [12], GC [15], spectrophotometry, LC-MS [12,15], planar chromatography, electrokinetic chromatography, and HPLC [16]. Therefore, many of these approach call for the utilization of expensive equipment, substantial outlays, and risky and toxic chemicals [15].

Electrochemical sensing is an alternative technique that has gained attention for detecting and quantifying pharmaceutical compounds like ibuprofen and metoprolol in various environmental samples, including water bodies [17]. Electrochemical sensors are low-cost, portable, and relatively simple to use, making them an appealing choice for monitoring use in both laboratory and field settings [15]. Amin et al (2014) developed a straightforward and accurate electroanalytical approach that uses electrochemically pretreated screen-printed graphite electrodes to measure the presence of ibuprofen in untreated wastewater. Koçak et al (2023) reported that the working electrode was altered with glutardialdehyde-ZnO suspension (GA_2–ZnO) for the detection of metoprolol. The modification of electrochemical sensors is an encouraging strategy to improving their effective for the identification of environmental contaminants containing pharmaceuticals [17]. In recent years, nanometal oxide MnO_2 has acquired significant interest from literature because to its unique properties [18]. MnO_2 nanoparticles have drawn notice for their outstanding optical features, extremely surface area, and good conductivity [19]. In this work, the aim is to develop a sensor that can detect two different compounds, Ibuprofen, and metoprolol, in wastewater samples. The sensor is intended to be simple, portable, low-cost, and reliable. To achieve this goal, the plan is to modify a screen-printed carbon electrode using manganese oxide nanoparticles (MnO_2NPs). The modified electrode will then be used as the sensing component of the device. Overall, the purpose of this work is to create a detector that can provide a quick and accurate way to detect the presence of these two compounds in wastewater samples, which can ultimately contribute to better management and treatment of wastewater.

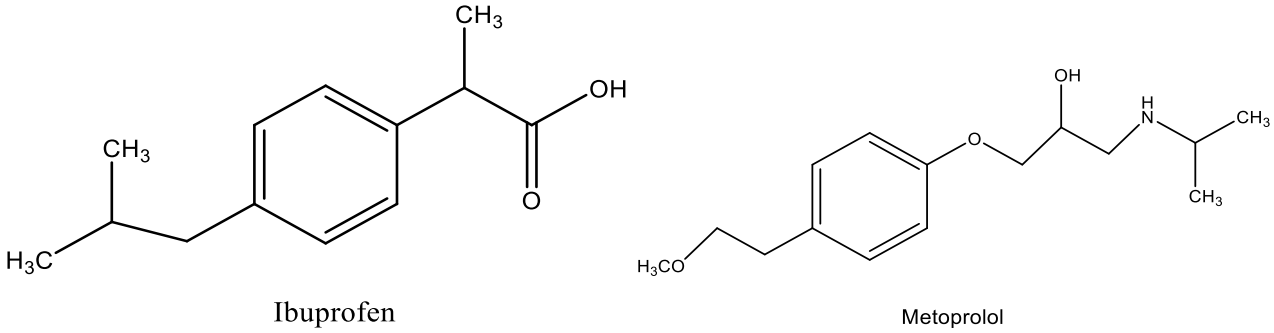

Figure 5.1: Structure of Ibuprofen and metoprolol.

5.2 Results and Discussion

5.2.1 Bandgap energy and UV/vis spectroscopy

UV-vis spectroscopy, as seen in Figure 5.2A, involves the investigation of the visual characteristics of MnO_2NPs and precursors. The spectra ranged from 280 to 800 nm. The optical features of the starting materials used were $MnSO_4$ and $KMnO_4$. The highest absorbing spectrum of MnO_2 was found to be approximately 305 nm, which could be related to the unique peak and the d–d transition of Mn^{4+} ions [33]. As illustrated in Figure 5.2B, absorbing is associated with the charge transfer of $O^{-2} \rightarrow Mn^{+4}$, which brings about attraction of electrons from the ground state to an excited state. The $KMnO_4$ can act as the oxidizing agent in the synthesis of the MnO_2NPs [20]. It can also exhibit strong absorption in the UV and visible regions due to electronic transitions. The absorption spectrum of $KMnO_4$ shows several peaks in the UV and visible range, with the primary one responsible for its purple colour [21]. The electronic structure of $KMnO_4$ involves the distribution of electrons in its constituent atoms. Manganese, in the +7-oxidation state, has a partially filled 3d subshell and exhibits complex electron configurations. Manganese can exhibit multiple oxidation states, including +2 and +3 [20]. In $MnSO_4$, manganese is in the +2-oxidation state, which is the oxidation state for manganese in its compounds. The optical band gap (Eg) for MnO_2 was measured involve the Tauc relation which is given in Eq 5.1:

$$\alpha hv = A(hv - Eg)^{n/2} \quad (5.1)$$

where n is a constant that is mostly dependent based on the substances' optical shift attributes, for instance as MnO_2NPs, and where α, h, A, Eg, and v are the coefficients of absorption, Planck's constant, constant, and bandgap incident light frequency. The value of n is 1 [21]. The band gap of a material determines its electrical conductivity and optical properties. Materials with smaller band gaps are generally better conductors of electricity, while those with larger band gaps are insulators [20]. The band gap also serves vital part in the absorption and emission of light. Photons with energies corresponding to the band gap can be absorbed by a material, promoting electrons from the valence band to the conduction band. When these excited electrons return to lower energy states, they emit photons, giving rise to the material's optical features [19]. As seen in Figure 5.2C the values of bandgap energy (Eg) of MnO_2NPs are identified by the linear extrapolation of the plot of $(\alpha hv)^2$ against (hv) to the energy axis. The obtained value of the optical band gap is 1.14 eV which indicates that the MnO_2NPs exhibit good electrical and optical properties.

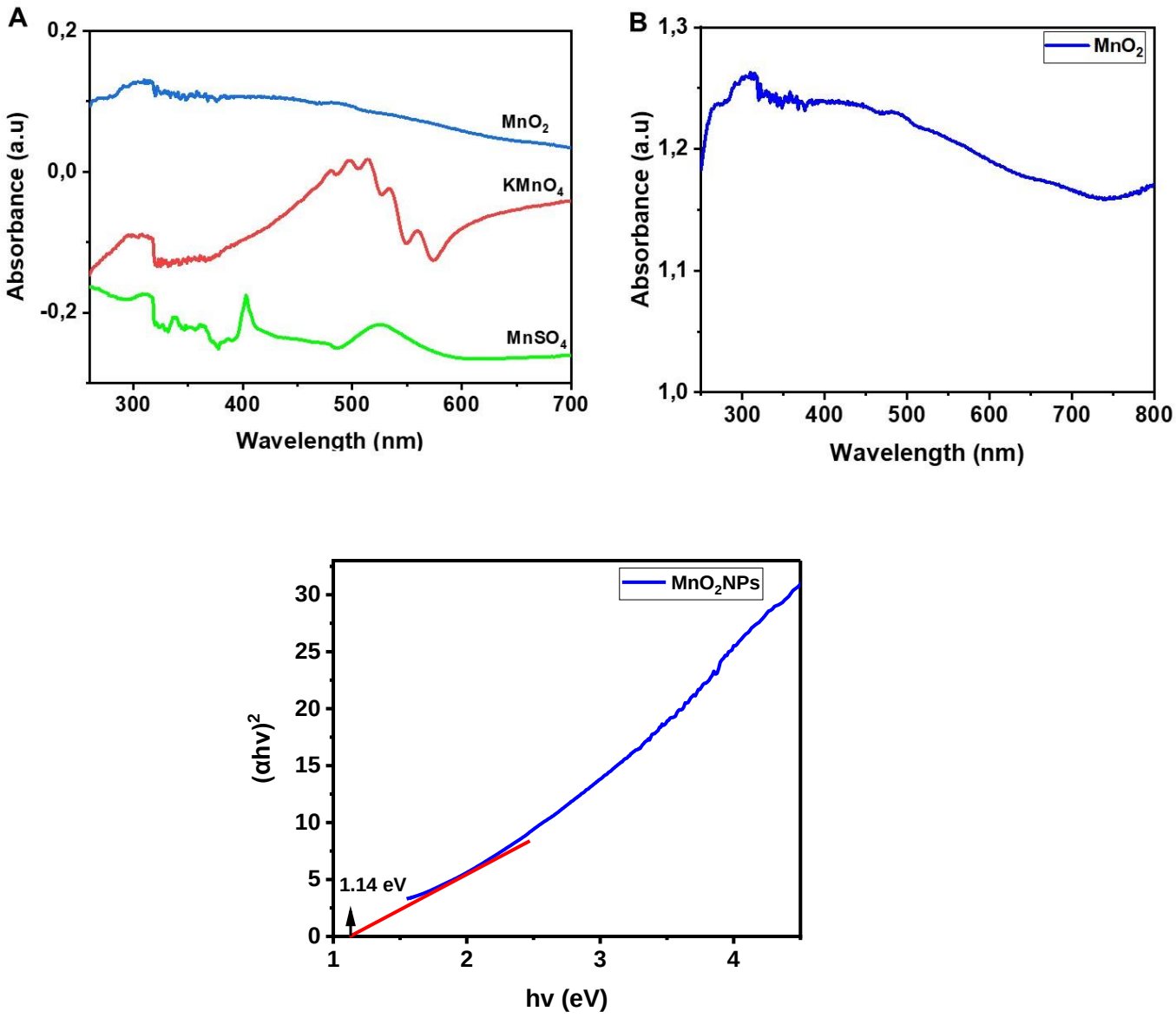

Figure 5.2: The absorption spectra of the (A) precursors, (B) MnO_2NPs, and the tauc plot of MnO_2NPs in UV light.

5.2.2 Small-angle X-ray scattering spectroscopy.

SAXS gives useful details about the general dimensions and forms of the nanoparticles as they are created. In Figure 5.3A shows the PDDF of MnO_2NPs which exhibits rod shaped arrangement, measuring 35 nm in radius and 86 nm in greatest diameter. The rod shape arises from the arrangement of manganese and oxygen atoms in one-dimensional tunnels within the crystal lattice [22]. This one-dimensional structure is responsible for the rod-like appearance of the nanoparticles. The rod shape of α–MnO_2NPs provides a substantial capacity to surface surface ratio [23]. This large area of surfaces makes them excellent candidates for catalytic reactions, where more active sites are accessible for reactants to interact with the catalyst [20]. The radius in SAXS does not typically refer to the physical size of the nanorods, but rather it provides information about the structural features of the sample. Specifically, the radius obtained from SAXS data provides information about the size and cross-sectional dimensions of the nanorods [23]. This can include details about their diameter or thickness, which is perpendicular to the rod's long axis. The breakdown of size by number is displayed in Figure 5.3B and indicates the existence of monodispersed molecule with the greatest length of radius of 6.5 nm. Which means that the MnO_2NPs was characterized by having uniform size and shape. Further, In Figure 5.3C, which shows the size distribution by volume with the maximum radius

of 10 nm. The plot shows the relatively narrow peak which indicates that MnO_2NPs synthesised have a consistent shape. In Figure 5.3D, provides valuable information about the structural characteristics of a sample. The plot displays the two peaks which have a radius at 47 nm and 69.5 nm. Both the peaks have a different value of intensity which suggest that the presence the presence of aggregated or clustered particles.

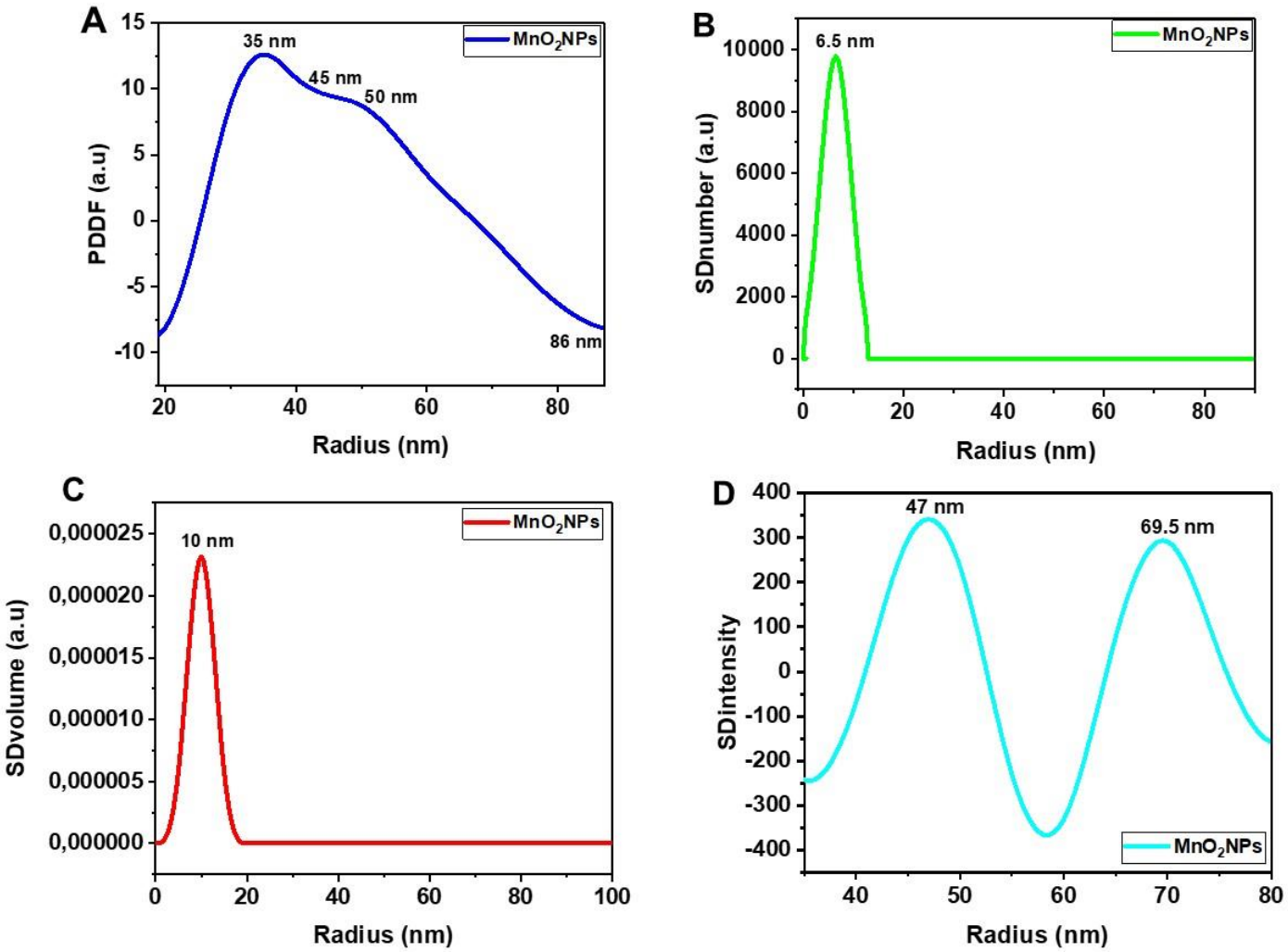

Figure 5.3: SAXS spectra of MnO_2NPs material (A) Pair distance distribution function (PDDF) for MnO_2NPs, (B) number weighted by size distribution function for MnO_2NPs (C) Volume weighted by size distribution function for MnO_2NPs (D) Intensity distribution function for MnO_2NPs.

5.2.3 MnO_2NPs/SPCE CV and EIS Studies

CV involving the bare and MnO_2NPs /SPCE in 1.0 mM $[Fe(CN)_6]^{4-}$ solution at the scan speed of 50 mV/s, as seen in Figure 5.4. The peak potential separation was calculated using the equation $\Delta Ep = (Epc - Epa)$ [24]. The CV curve illustrate a reversible electrochemical reaction of maximum potential separation for bare SPCE was obtained at 0.249 V, whereas 0.269 V was the greatest potential separation, this demonstrate that the electron transfer on the MnO_2NPs/SPCE was fast due to small peak potential separation, this suggests a rapid and efficient reaction at the electrode surface as contrasted to a bare electrode which indicated the slower electron transfer. The electrochemical response on a bare, a voltage reading was recorded with a peak potential of 180 mV and a modest oxidation current of 22.14 µA. On the other hand, MnO_2NPs/SPCE demonstrated a much-decreased over potential Ep = 199 mV along with an elevated abrupt anodic peak current (i_{pa} = 88.79 µA). From the observation, the MnO_2NPs/SPCE has a higher peak current, which indicates faster electron transfer rates due to efficient charge transfer between the electrode and the electroactive species. This outcome verified that the MnO_2NPs/SPCE increase the effectiveness of the altered electrode by

raising peak current. The peak from the MnO_2NPs/SPCE displays the nano-flower-like structure. The presence of two peaks in the solution, one for oxidation and one for reduction is consistent with the behaviour of ferrocyanide ions, which undergo reversible redox reactions [25].

Oxidation: $Fe(CN)_6^{4-} \longrightarrow Fe(CN)_6^{3-} + e^-$ (5.2)

Reduction: $Fe(CN)_6^{3-} + e^- \longrightarrow Fe(CN)_6^{4-}$ (5.3)

However, the characteristics of these peaks can be impacted by number variable factors, involve electrode surface modifications, solution composition, and experimental conditions. The modified electrode may enhance the electrochemical reaction kinetics, resulting in a well-defined peak, while the bare electrode might exhibit a less pronounced peak due to the absence of such enhancements [25].

The efficiency of electron transfer of bare SPCE and MnO_2NPs/SPCE involve by EIS, seen in Figure 5.4B. The Nyquist plots are seen with the real part (Z') on the X-axis and the imaginary part (−Z'') on the Y-axis [39, 41]. The bare and MnO_2NPs/SPCE was investigated in 1 mM $[Fe(CN)_6]^{4-}$ solution as seen in Figure 5.4B. The spectra show that the modified MnO_2NPs/SPCE exhibits improved conductivity compared to the bare SPCE. This conclusion is drawn based on the observation that the spectra of the bare SPCE show a semi-circular region, whereas the modified MnO_2NPs/SPCE exhibit a different behaviour. The presence of a semi-circular region in the spectra of the bare SPCE suggests higher charge transfer resistance, indicating less efficient electron transfer compared to the MnO_2NPs/SPCE. The modified MnO_2NPs/SPCE, on the other hand, exhibit low charge transfer resistance, indicating more efficient electron transfer and better conductivity. To further support this finding, fitted a circuit to obtain the charge transfer resistance values. The charge transfer resistance of the MnO_2NPs/SPCE was determined to be 86.9 Ω, while the bare SPCE had a higher charge transfer resistance of 3.95 kΩ. This comparison further confirms the enhanced conductivity and improved electron transfer efficiency of the MnO_2NPs/SPCE compared to the bare SPCE.

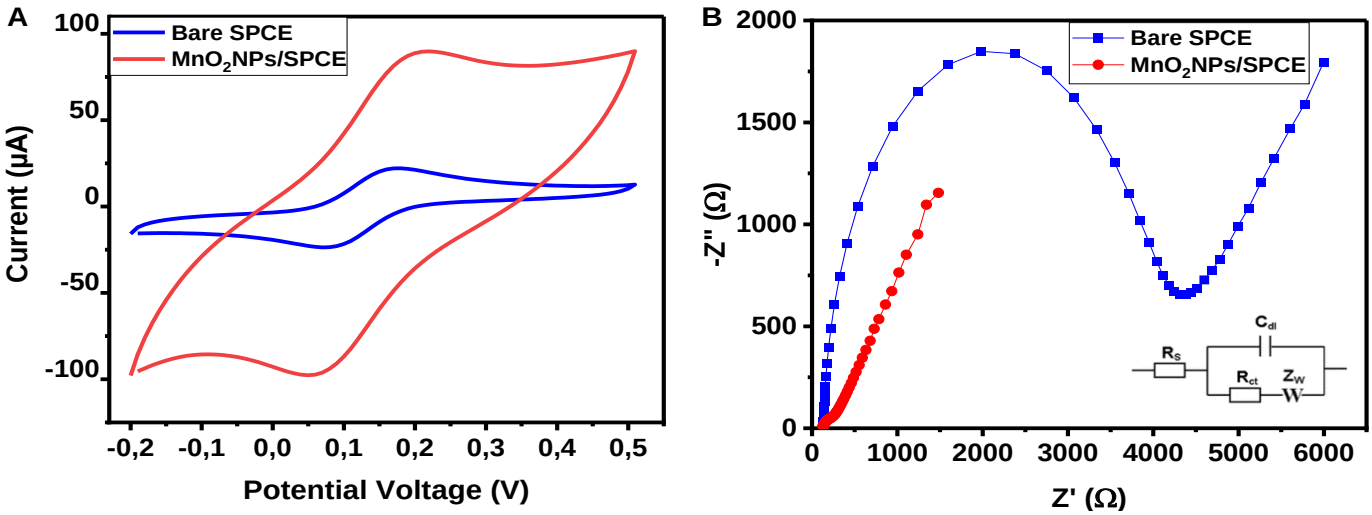

Figure 5.4: Modified MnO_2NPs/SPCE and bare SPCE cyclic voltammetry in a 1.0 mM $[Fe(CN)_6]^{4-}$ solution at a scan speed of 50 mV/s (A) CV (B) EIS.

5.2.4 Electrochemistry of MnO_2NPs/SPCE

Electrocatalytic features of bare electrode and MnO_2NPs/SPCE modified electrode in a PBS was investigated by CV as shown in Figure 5.5. As observed the presence of a peak during the reduction phase of cyclic voltammetry suggests that an electrochemical reduction process is occurring at the altered electrode surface. The reduction peak typically represents a reduction reaction where the substance gains electrons. It indicates that the MnO_2NPs are actively involved in the electrochemical reaction, possibly by serving as a catalyst or by

providing specific sites for the reduction process to occur [17]. The presence of the phosphate buffer is also significant. Phosphate buffers are known for their pH stability and compatibility with many electrochemical reactions. The peak observed during the reduction in the presence of the phosphate buffer can be considered a "signature" of the electrochemical behavior of the MnO_2NPs modified electrode [7]. MnO_2NPs is known to have catalytic activity for various electrochemical reactions. It can enhance the kinetics of reactions involving redox-active species, potentially leading to improved electrochemical performance [19].

The reason we have used the two electrolytes for the electrocatalytic study of bare and MnO_2NPs/SPCE electrode, due to that ferrocyanide solutions typically contain ferrocyanide ions $(Fe(CN)_6)^{4-}$ and are commonly used in electrochemical sensing as a model redox system [25]. They serve as a reference standard for electrochemical experiments and provide well-defined redox peaks. While phosphate buffer solutions are made by mixing phosphate salts and are often used as a pH buffer in electrochemical experiments. They help maintain a stable pH environment during electrochemical measurements [28].

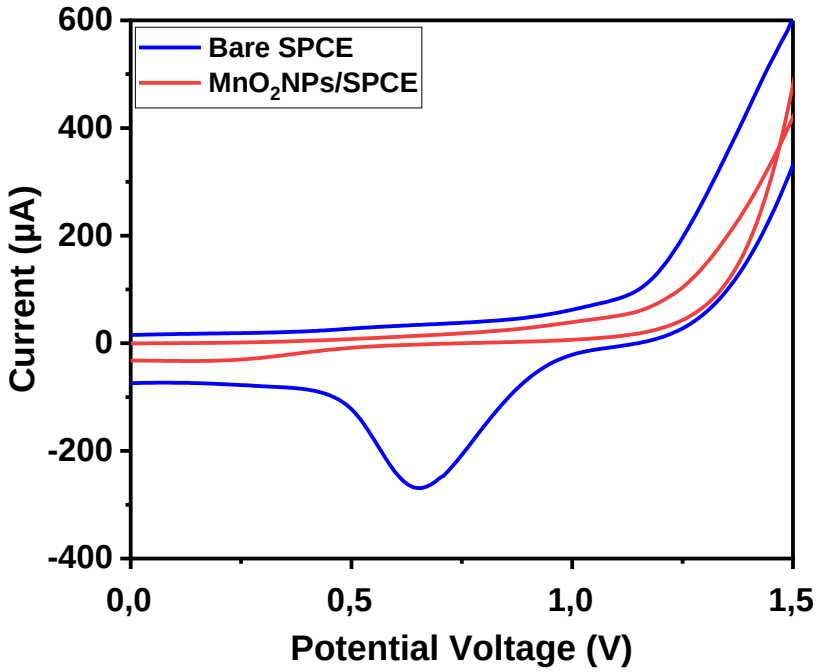

Figure 5.5: CV voltammograms of bare and MnO_2NPs/SPCE were taken at a scanning speed of 50 mV/s in 0.1 M PBS.

5.2.5 Scan rate studies

By applying the CV approach to the altered MnO_2NPs/SPCE with 100 pm IBU and MP in PBS solution, its impact of scan speed (v) was investigated in the range of 5 to 50 mV/s. As evidenced in Figure 5.6, the scan speed variation yields the obvious increase in the peak currents (Ip) of IBU. As illustrated in Figure 5.6A, in which two distinct peaks are observed. The peaks correspond to different substances or processes occurring at the electrode's surface. The first peak, the reduction peak, is associated with the existence of MnO_2NPs on the surface of the electrode. Reduction typically involves the gain of electrons or a decrease in oxidation state. The second peak corresponds to IBU. This peak likely represents an oxidation reaction, which typically involves the loss of electrons or an increase in oxidation state [15]. Figure 5.6B seen a linear plot of oxidation peak current and log scan speed, as well as the regression equation: I (µA)= 454.62 log (v) –193.4 with the (R^2 =0,9987). The plot shows a relationship where peak current rise as the logarithm of the scan speed rise. This relationship is characteristic of a diffusion-controlled process, where the speed of the electrochemical reaction is primarily influenced by the diffusion of species to and from the electrode surface [16]. The oxidation

peak of CBZ involve a maximum peak at a scan rate of 50mV/s, indicating the amplification of the MnO_2NPs/SPCE. The Randles-Sevcik Equation involves the compute the active surface area of an electrode:

$$i_p = 2.69 \times 10^5 (n^{3/2}) (A) (C) (D^{1/2}) (V^{1/2}) \quad \textbf{(5.4)}$$

where Ip is the maximum current, n is the total amount of transfers of electrons (2), A is the electrode's activated surface, D is the coefficient of the electroactive diffusion coefficient in the electrolyte (3.64×106 cm^2/s), C is the IBU concentration, and v is scanning speed. Figure 5.6C depicts the influence of scan speed on the oxidation reaction behaviour of MP in PBS (pH 7.0) at varied scanning speed ranging from 5 to 50 mV/s. The accompanying oxidation current rises as the scan speed increases, as does the potential movement of the oxidation potential in a positive direction. Figure 5.6D seen that the peak current of anodes inversely correlated the square root of the scan speed, with a correlation coefficient of 0.9983. This relationship implies that MP oxidation is a normal diffusion regulated process, which is consistent with earlier research. A maximum peak was seen at a scanning speed of 50 mV/s, indicating that the MnO_2NPs/SPCE on both graphs was enhanced.

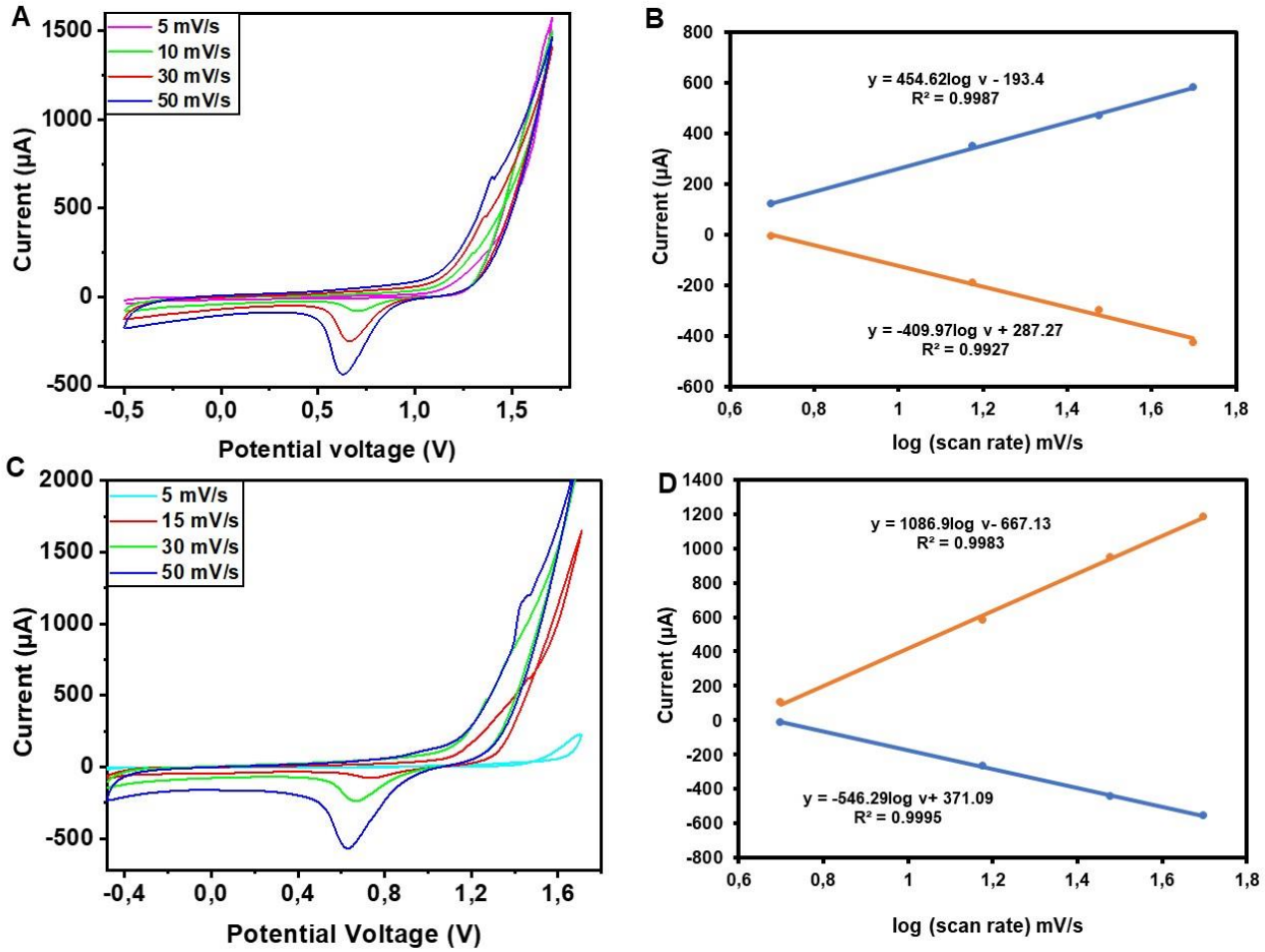

Figure 5.6: Cyclic Voltammetry of the MnO_2NPs/SPCE at varied scan rate range 5-50 mV/s and linear plot relationship (A-B) Ibuprofen (C-D) Metoprolol.

5.2.6 pH studies

The electrochemical procedure is typically influenced by the pH of a solution, which causes the redox potential to move in either a more positive or negative direction with varied redox peak currents [15]. Consequently, at low peak potentials, an ideal pH is needed to boost the vitality of the oxidative peak currents. In Figure 5.7A, demonstrates how pH affects IBU redox process with MnO_2NPs/SPCE. in the pH range of 5.0–8.0. The CVs of the MnO_2NPs/SPCE showed a strong dependence on the pH values of solutions. The peak currents increased significantly when pH values increased from 5.0 to

7.0, and then decreased when the pH exceeded 7.0. These responses might be due to the structural changes in the –OH and –$NHCOCH_3$ groups of IBU with respect to pH. At pH 7.0, charge neutrality of IBU may be responsible for the best response. Thus, the PBS of pH 7.0 was selected as the electrolyte pH in the following experiments. The pH studies of MP in the 0.1 phosphate buffer using a MnO_2NPs/SPCE involve investigating the behaviour and stability of MP at different pH levels within a PBS. For an electrode reaction with protons involved, pH had an important influence on its redox peak current. When pH = 7.0, MP indicate the strongest CV response. So, pH = 7.0 was selected as the optimal acidity for MP identification.

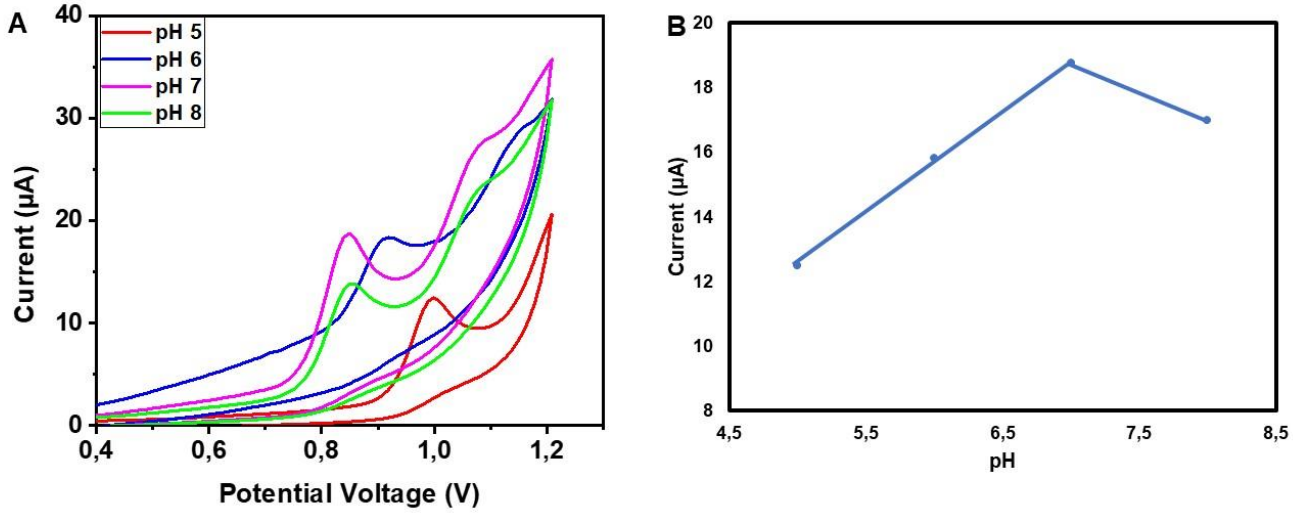

Figure 5.7: CV response of the IBU at MnO_2NPs/SPCE at different pH range 5-8 of 0.1 M PBS and a plot of current vs pH.

5.2.7 Electrolytes studies

Electrolytes are essential in the electrochemical sensing process [29]. The MnO_2NPs/SPCE electrode was utilized to investigate a variety of electrolytes at a rate of 50 mv/s as determined by DPV, including 0.1 M NaCl, KCl, ferrocyanide $[Fe(CN)_6]^{4-}$, and PBS in the existence of IBU (Figure 5.8). The results showed that PBS was the optimum electrolyte for detecting IBU, while NaCl, KCl, and Ferrocyanide did not provide a signal for IBU. This is because phosphate buffers have been recognized for retaining their chemical properties throughout an extensive temperature and condition region [30]. This stability is crucial for maintaining the integrity of the electrolyte solution during electrochemical experiments. The stable pH of the PBS likely played a significant role in obtaining consistent and reliable electrochemical signals [29]. Phosphate buffers are often biologically compatible, which makes them suitable for applications involving biological samples. In this context, the compatibility of PBS with the IBU or the electrode's surface may have contributed to a successful signal. Phosphate ions in the PBS solution might have a specific interaction with IBU that enhances the electrochemical response. This interaction may be related to the chemical structure of IBU and the behaviour of phosphate ions [30]. The characteristics of PBS may have led to a favourable interface, improving the electrode's performance in detecting IBU. The option of electrolyte is a critical factor in electrochemical sensing and can significantly impact the effectiveness and specify of the detector, as demonstrated in this study. Same response was observed with the detection of MP.

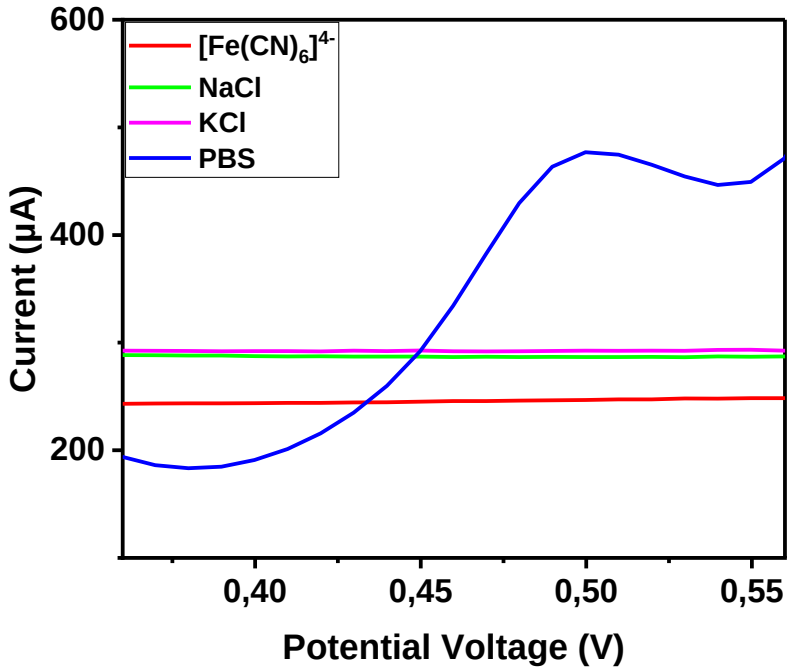

Figure 5.8: DP voltammograms for 0.1 µm different electrolyte (NaCl, KCl, PBS, and $[Fe(CN)_6]^{4-}$ on MnO_2NPs/SPCE in the existence of IBU at 50 mV/s.

5.2.8 Electrochemical behavior of IBU on MnO_2NPs/ SPCE

Based on these experimental findings, the produced MnO_2NPs/SPCE as the proposed sensor was developed to quantify IBU. Figure 5.9 illustrates the investigation of Bare SPCE and Modified SPCE in a 0.1 M PBS electrolyte under ideal conditions at various concentrations ranging from 0.97 to 5.82 pM. The electrical current response was concentration dependent. Figure 5.9C depicts a well-distributed signal as compared to Figure 5.9A (bare electrode), this is because of the good electrical properties of the material. The oxidation peak was seen at +1.14 V for the MnO_2NPs/SPCE detector. Relation linearity between the peak current and the IBU concentrations in the domain 0.97 to 5.82 pM is obtained for the modified electrode as seen in Figure 5.9D. The equation of the calibration curve is $I(\mu A) = 29.886\,[IBU] + 483.79$ (R^2= 0.9981). From the calibration curve, the LOD was calculated. The values of LOD (0.0004 µM) indicated that the sensor developed in this study has improved its performance when compared to the LOD of the bare electrode (5.50 pM) with the (R^2=0.9964) as shown in Figure 5.9B.

A comparison between the proposed sensor and previous studies is shown in Table 5.1. In comparison to previous investigations for the identification of ibuprofen, the LOD value for the MnO_2NPs/SPCE detector was reported to be lower at 0.0004 µM. It is possible to say that the altered electrode containing MnO_2NPs is an appropriate foundation for the analysis identification of IBU. These previous investigations provide important information about the material that was employed as a substrate on the electrode's interface for IBU identification and the distinct LOD values that were obtained [31]. Ibuprofen was detected in urine by Maleh et al using the same technique with the linearity range of 1–40 µM and a modified Ag/MWCNT/MPAC/GCE electrode to obtain the threshold of detection of 0.4 µM. Hu et al demonstrated the identification of Ibuprofen by involving the modified GO/AgNPs/SPCE with the differential pulse voltammetry technique with the PBS electrolyte at pH 7.0 within the linearity range of 0.1–40 µM, yielding a 0.028 µM threshold of detecting. Figure 5.10 depicts the mechanism of IBU electrochemical oxidation. The first single-electron oxidation produces benzyl radical and carboxyl radical after deprotonation. By removing CO_2 from both radicals, a common benzyl radical is formed. Its subsequent (second) single-electron oxidation yields benzyl cation, which serves as the substrate for the formation of the final products: reaction with water followed by deprotonation yields alcohol, and in situ formation of the alcohol to the carbocyanine yields symmetrical ether. In parallel,

the addition of oxygen to the benzyl radical results in the creation of the labile hydroperoxide, which creates a disproportionate amount of alcohol and ketone [17].

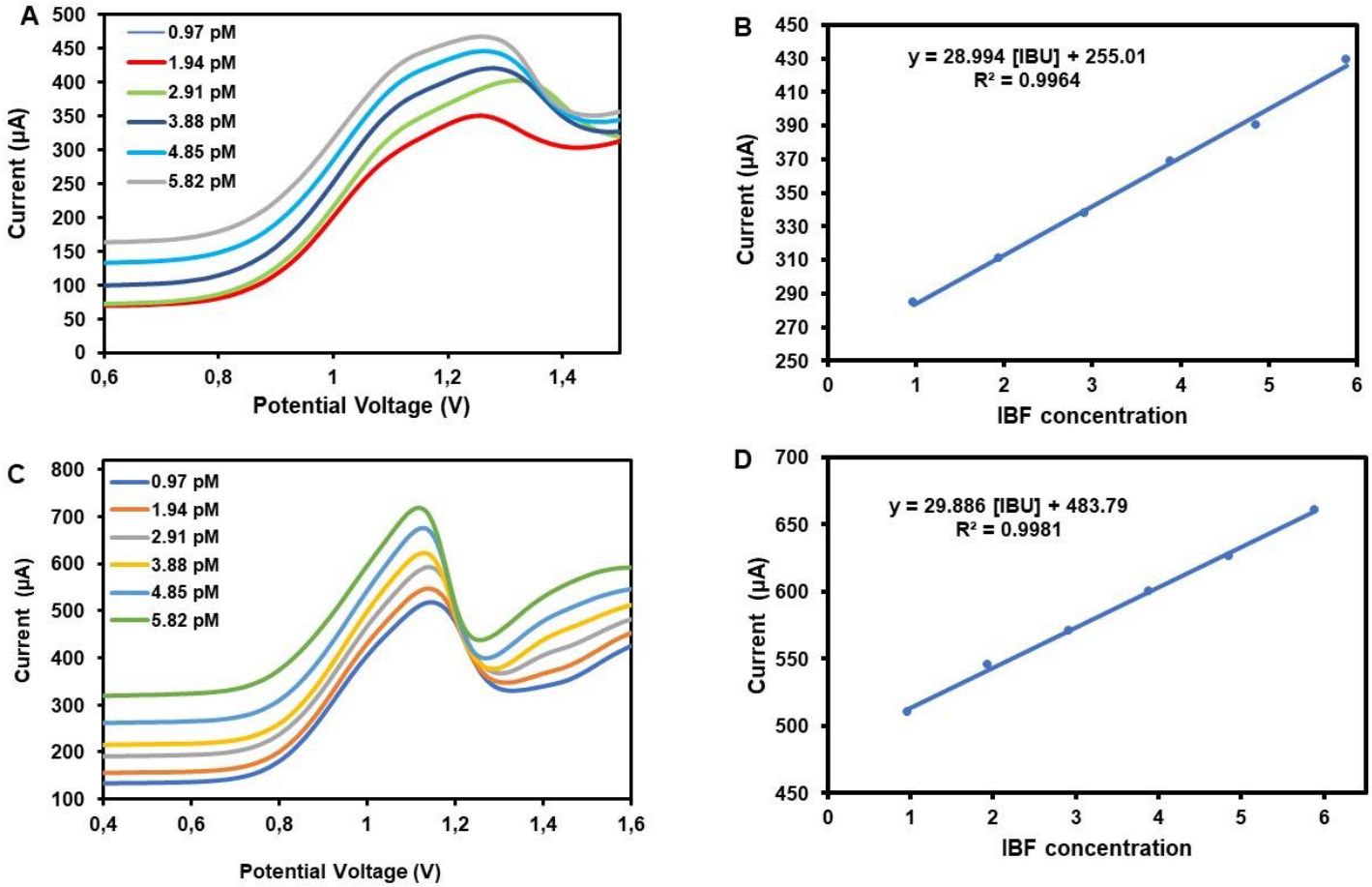

Figure 5.9: DPV indicators of (A) bare SPCE used to calculate IBU from 0.97 to 5.82 pM in pH 7.0 (0.1 M PBS). (B)The simple linear of IBU anodic peak currents vs concentrations. (C) modified MnO_2 SPCE to determine IBU concentrations ranging from 0.97 to 5.82 pM in pH 7 (0.1 M PBS) and (D) Simple linear of IBU anodic peak currents vs concentrations.

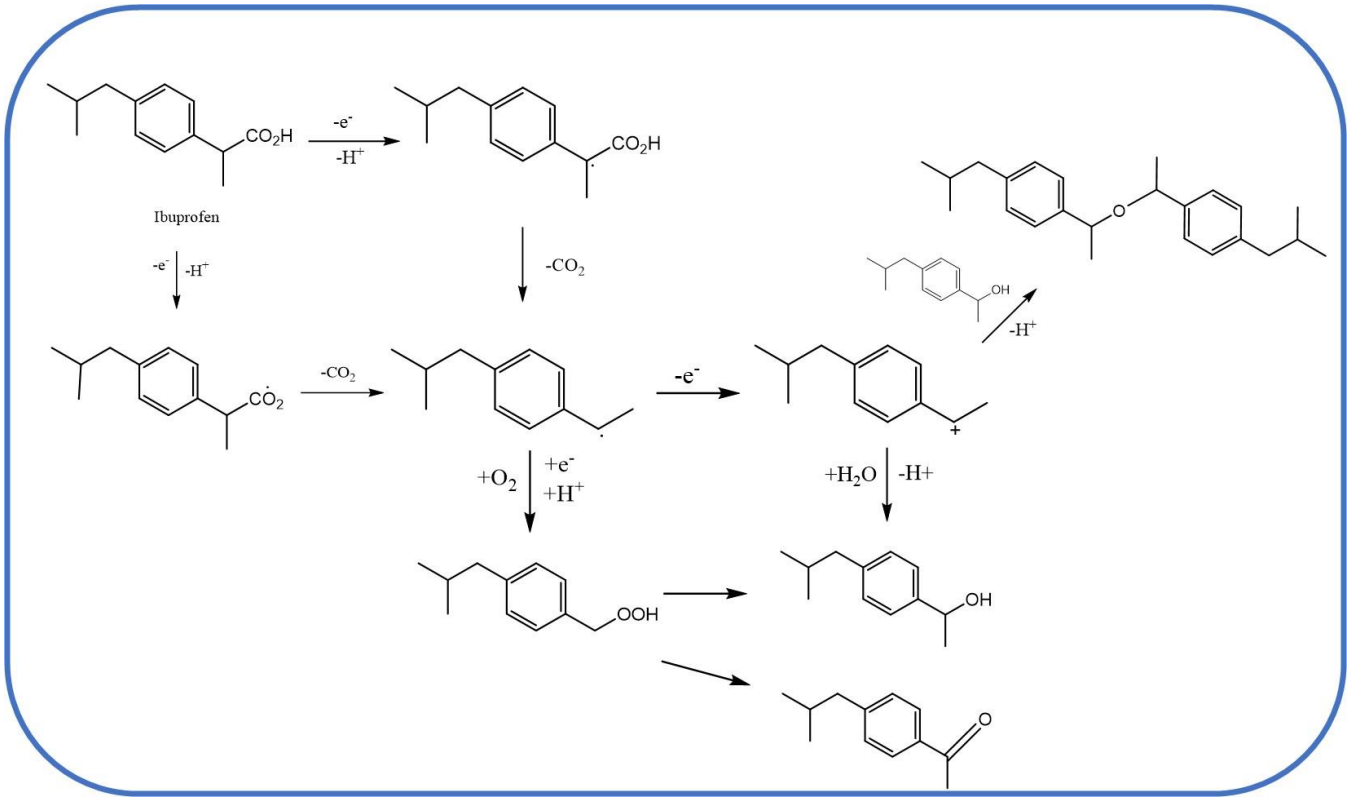

Figure 5.10: Schematic proposed mechanism of electrochemical oxidation of Ibuprofen on MnO_2NPs/SPCE.

Table 5.1: Qualities of comparable approaches for determining IBU.

Material	Technique	Linearity range (μM)	LOD (μM)	Ref
Apt/AuNPs/GCE	DPV	0.005–7	0.0005	[23]
Apt/CdTeQD/GCE	CV	0.05–20.00	0.016	[1]
GO/AgNPs/GCE	DPV	0.1–40	0.028	[3]
rGO/PdNPs/GCE	SWV	1–40	0.4	[3]
AuNPs/MWCNTs/GCE	CV	1–100	0.55	[85]
Ag_2MWCNT/GCE	SWV	5–25	1.5	[52]
AuNPs@N-GQDs/GCE	FiA.AMP	10–1000	1.95	[53]
MnO_2NPs/SPCE	DPV	0.010–0.006	0.0004	This work

Note: *These values were converted to μM. Aptasensor based gold nanoparticle-glassy carbon electrode (GCE), graphene oxide-silver nanoparticles (Ag) nanocomposite, reduced graphene oxide-lead nanoparticles nanocomposite, gold nanoparticles (AuNPs)-multiwalled carbon nanotubes (MWCNTs), Aptasensor based cadmium telluride quantum dots (CdTeQD), nitrogen doped graphene quantum dots (N-GQDs).*

5.2.9 Application of IBU in Wastewater effluent

The investigated detector was utilized to identification IBU in wastewater effluent samples and to evaluate its practicability and reliability. The sample solutions were prepared by the approach as shown in experimental section. The good IBU recoveries were attained at between 105% and 122%, indicating that the MnO_2NPs/SPCE sensor had strong potential to enable applications in environmental monitoring. The %RSD value was found to be 0.151 which indicates less variability and higher precision. A low %RSD suggests that the sensor provides consistent and reproducible results, increasing confidence in its accuracy and precision.

Table 5.2: IBU measurement in wastewater samples.

Effluent	[added] (pM)	[Found] (pM)	% Recovery
1	1.94 ± 2.02	2.05 ± 2.82	105%
2	2.91 ± 2.02	3.05 ± 2.82	106%
3	5.82 ± 2.02	7.36 ± 2.82	122%

5.2.10 Electrochemical behavior of MP on MnO_2NPs/ SPCE

The electrochemical behavior of the anodic peak potentials for MP involves both bare and modified electrodes in 0.1 M PBS at the pH of 7.0 at the optimum condition of the scan rate. The experiment was investigated using various concentrations ranging from 0.97– 4.85 pM. As seen in Figure 5.11A, the peak potential of the bare electrode does not produce a significant signal while detecting MP. This is because the bare electrode may not be sensitive enough to identify the low levels of MP present in the sample. MnO_2NPs/SPCE was employed as a modified electrode under ideal circumstances to improve the detection of MP. An effectively improved signal for the oxidation peak, which was seen at 1.46V, was shown in Figure 5.11C. As the concentration rises, the current response similarly rises, demonstrating a direct proportion, as seen in Figures 5.11A–C. The linear regression equation for the calibration curve for MP, demonstrate a linear relationship between current and concentrations on MnO_2NPs/SPCE.

$$\mathrm{I}(\mu\mathrm{A}) = 33.706\,[\mathrm{MP}] + 950.09 \qquad R^2 = 0.9983$$

where, [MP] is MP concentration (mol L^{-1}) and, I the anodic peak current (μA). The limit of detection (LOD) was obtained 0.005 μM. It is significantly lower than that of some other previous electrochemical methods for determination of MP [32]. The analytical performance results of the proposed sensor were found superior to the previous similar reports as shown in Table 5.3 [33]. According to Table 5.3, Using a modified Ga_2-ZnO/BDDE electrode, differential pulse voltammetry was used by Berk et al. to illustrate the detection of metoprolol. The electrolyte was PBS at pH 7.0., obtaining a threshold of detection of 7.53 M within the linearity range of 9.99–3.38 μM. Zorluogh et al. used urine to detect the metoprolol using the same technique. Figure 5.12 illustrates this observation, which shows that two electrons and two protons are involved in the electron transfer phase of the electro-oxidation of MP. At this time, we might speculate that the potential oxidation site of MP is the secondary alcohol group. The electro-oxidations of atenolol and propranolol, two more anti-hypertensive drugs with related chemical structures, showed comparable results. In each instance, the hydroxyl(–OH) group of MP underwent electro-oxidation by the transfer of protons and electrons [34].

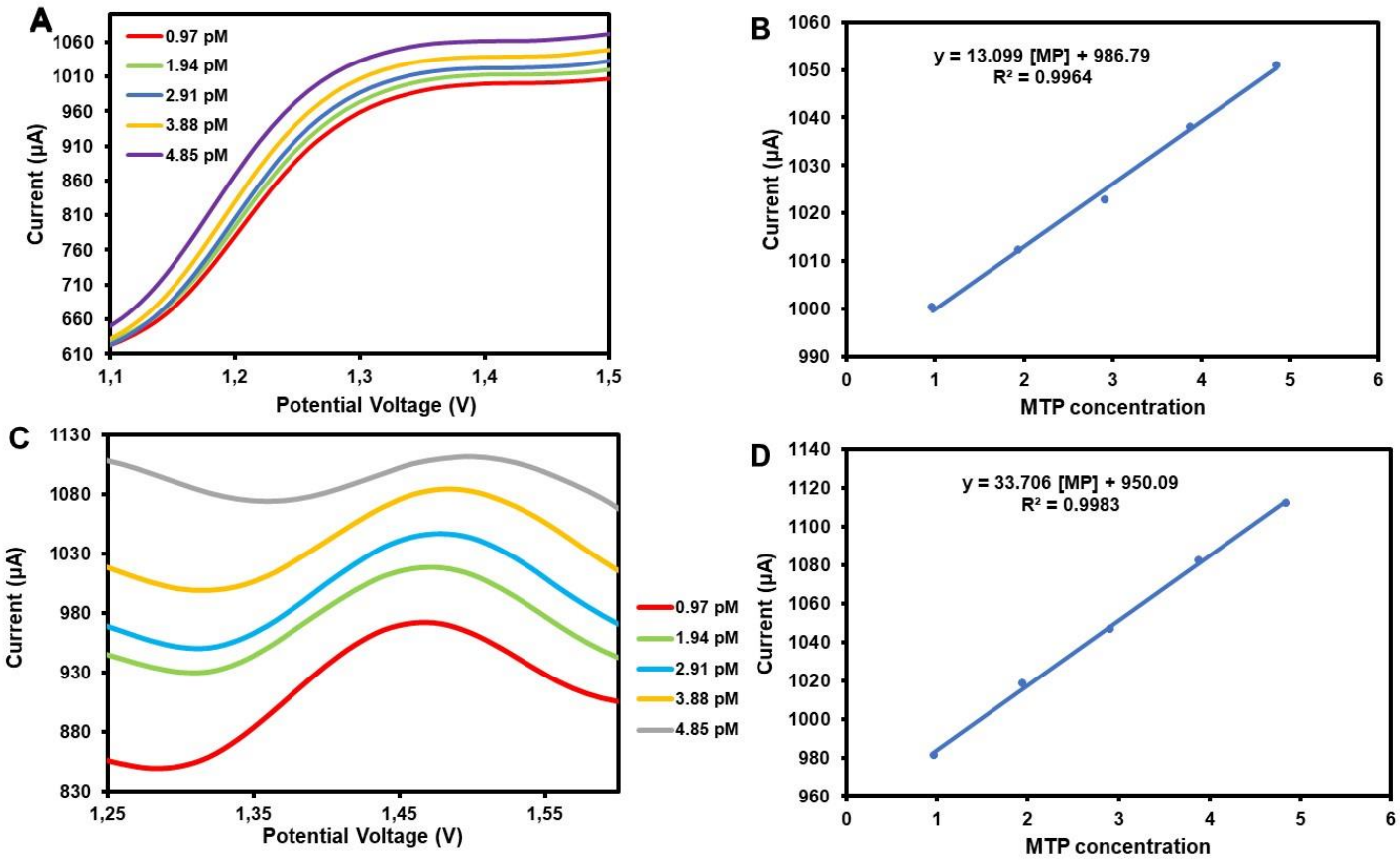

Figure 5.11: DPV outputs of (A) bare SPCE used to calculate MP from 0.97 to 4.85 pM in pH 7.0 (0.1 M PBS). (B)The linear plot of IBU anodic peak currents vs concentrations. (C) modified MnO_2 SPCE for determining MP levels ranging from 0.97 to 4.85 pM in pH 7.0 (0.1 M PBS) and (D) Linear plot of MP levels versus anodic peak currents.

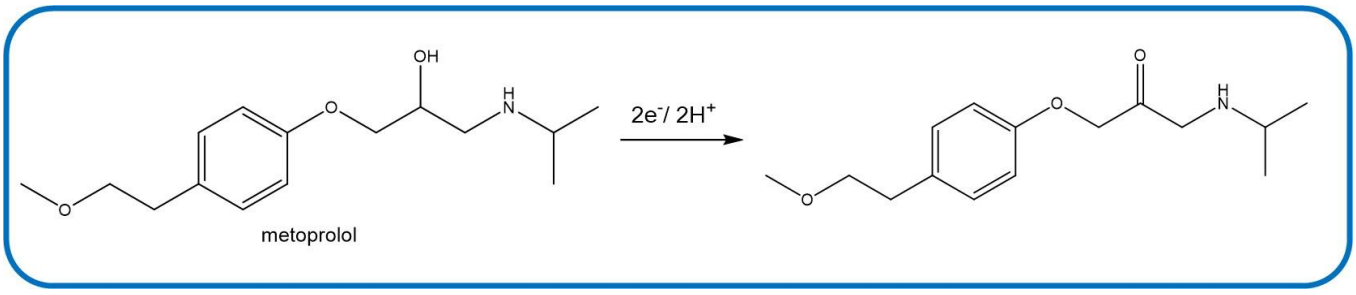

Figure 5.12: Schematic proposed mechanism for electro-oxidation of MP on MnO_2NPs/SPCE.

Table 5.3: Qualities of related approaches for determining MP.

Material	Technique	Linearity (μM)	LOD (μM)	Ref
Ga_2-ZnO/BDDE	DPV	9.99–3.38	7.53	[32]
MIP/MWCNTs/PGE	SWV	0.06–490	2.9	[34]
GCE	DPV	0.07–90	35.1	[34]
HDME	DPV	0.95–9.45	0.29	[33]
Nafion-CNT	DPV	0.07–90	35.1	[32]
PVC-membrane graphite	SWV	0.2–800	0.126	[32]
GRE/PtNPs/NFN	Ads DPV	0.014–0.75	4.3	[34]
MnO_2NPs/SPCE	DPV	0.010–0.006	0.005	This work

Note: *These values were converted to μM. Glassy carbon electrode (GCE), Carbon nanotube (CNT), multiwalled carbon nanotube (MWCNTs), gallium-zinc oxide boron doped diamond electrode (Ga_2-ZnO/BDDE), graphene/platinum nanoparticle nafion composite, hanging mercury drop electrode (HDME), molecularly imprinted polymer-pencil graphite electrode, SWV, square wave stripping voltammetry, LSV, Linear sweep voltammetry, DPV differential pulse voltammetry.*

5.2.11 Application of MP in Wastewater

The MP concentration in wastewater samples was measured to assess the proposed sensor's effectiveness. Specific MP levels were added to these samples. and analysed using the MnO_2NPs/SPCE based electrochemical sensor Table 5.4 displays the percentages of recoveries, which range from 99 to 115%. The findings reveal that the MP measurement utilizing the MnO_2NPs/SPCE detector is not significantly impacted by the matrix of the actual samples. As an outcome, there is great potential for the created sensor to analyze MP in real samples, including wastewater samples.

Table 5.4: Determination of MP in wastewater.

Samples	[added] (pM)	[Found] (pM)	% Recovery
1	1.94 ± 0.97	1.92 ± 1.27	99%
2	2.91 ± 0.97	3.05 ± 1.27	104%
3	3.88 ± 0.97	4.45 ± 1.27	115%

5.2.12 Interference studies

The performance and accuracy of MnO_2NPs/SPCE sensors must be subjected to interference tests to determine how various chemicals might affect the sensor's operation [33]. The selectivity, dependability, and robustness of the sensor are determined by these investigations, particularly when it comes to detecting target drugs like IBU and MP in the existence of potentially interfering substances. In this investigation, the capacity of the modified MnO_2NPs/SPCE electrode to detect IBU and MP in the existence of common possible interfering species involving Diclofenac (DCF), Naproxen (NPX), and Nevirapine (NVP) was assessed. Diclofenac, naproxen, and nevirapine are all pharmaceutical drugs used for different medical purposes. Diclofenac and naproxen are NSAIDs used primarily for pain relief and anti-inflammatory purposes, whereas nevirapine is an antiretroviral

medication used specifically for the treatment of HIV infection [35]. These chemicals (DCF, NPX, and NVP) were discovered to be degraded at distinct potentials and so are not interfering with IBU and MP detection, implying that during electrochemical sensing employing MnO_2NPs/SPCE, the oxidation processes of these compounds occur at distinct electrical potentials. The ability to distinguish between the electrochemical signals produced by the oxidation of DCF, NPX, and NVP and the oxidation signals of IBU and MP is made possible by this differential in oxidation potentials [36]. The existence of the identical functional group, such as imine (C=N) or methyl (CH_3), structure chemical homology, or comparable characteristics may all be responsible for the slight enhancement of the DPV signal that was observed. Figure 5.13A and Figure 5.13B both show that the enhancement rises when the interfering species are included in the detection of IBU and MP. This demonstrates the suggested sensor's suitability for accurate, interference-free sensing.

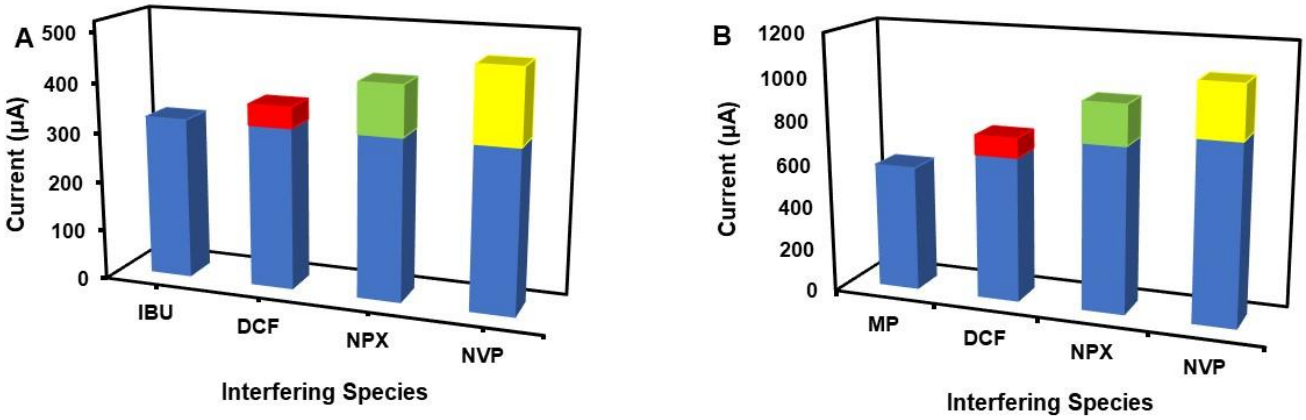

Figure 5.13: Peak current responses of (A) 20 pM IBU in the presence of interfering species (20 pM DCF, 20 pM NPX, and 20 pM NVP), (B) 20 pM MP in the presence of interfering species (20 pM DCF, 20 pM NPX and 20 pM NVP).

5.2.13 Stability studies

DPV in 0.1 M PBS with 20 μM Ibuprofen and metoprolol was used to test the durability of storage of the MnO_2NPs/SPCE sensor. Two conditions of storage were investigated. The sensor was kept within RT for 9 days in the original test, and the data displayed in Figure 5.14A illustrate that the maximum current of the detector dropped to 68% of the original reaction. Pleasantly, the sensor kept 84% of its original reactivity after 9 days of preservation within 4 °C, as shown in Figure 5.14B. Therefore, storing the sensor in a fridge is preferred because it preserves the sensor's viability. The storage reliability of metoprolol was examined under identical circumstances as ibuprofen, and Figure 5.14C shows that the maximum current of the drop decreased to 57% of the original reaction at ambient temperature. In Figure 5.14D, we saw 85% of its first response. According to this information, the sensor was robust for Ibuprofen and metoprolol.

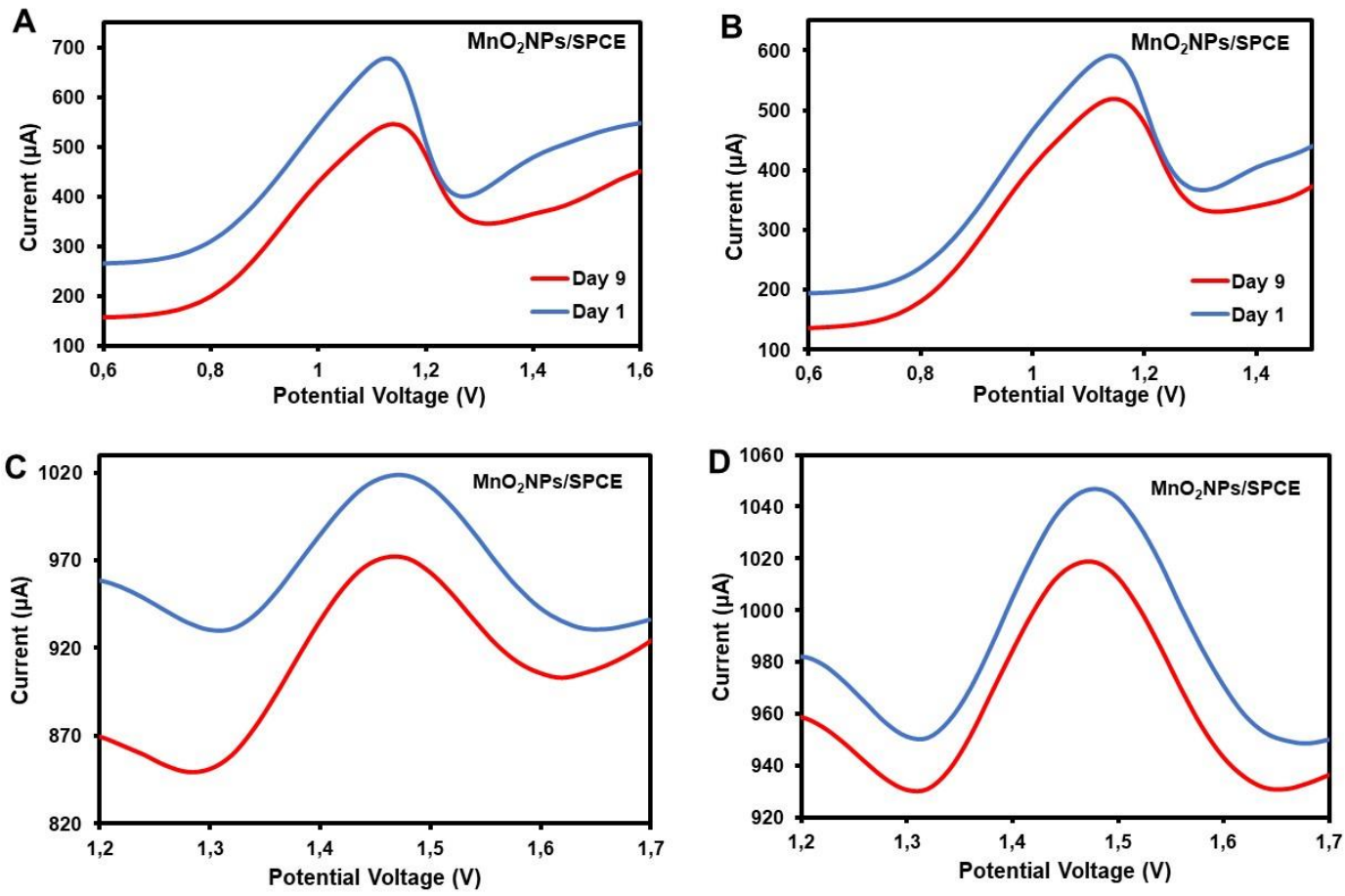

Figure 5.14: Pulse differential MnO_2NPs/SPCE voltammetry reactions to 20 µM Ibuprofen (IBU) and metoprolol (MP) on day 1 and day 9 following preservation (A-C) at room temperature (B-D) at 4°C.

5.2.14 Simultaneously detection of IBU and MP on MnO_2NPs/SPCE sensor

Further testing was done to determine how well MnO_2NPs/SPCE performed in determining IBU and MP simultaneously in 0.1 M PBS (pH 7.0). Their DPV oxidation peak currents increased proportionally with their concentrations, as seen in Figure 5.15, when the concentrations of IBU and MP were simultaneously increased. The potential window of the analytes identified individually to simultaneous remains unaltered by the simultaneous detection of IBU and MP utilizing MnO_2NPs/SPCE. At 1.1 V and 1.45 V, correspond, the oxidation peaks for IBU and MP can be seen. This behaviour suggests that the sensor exhibits greater precision and accuracy.

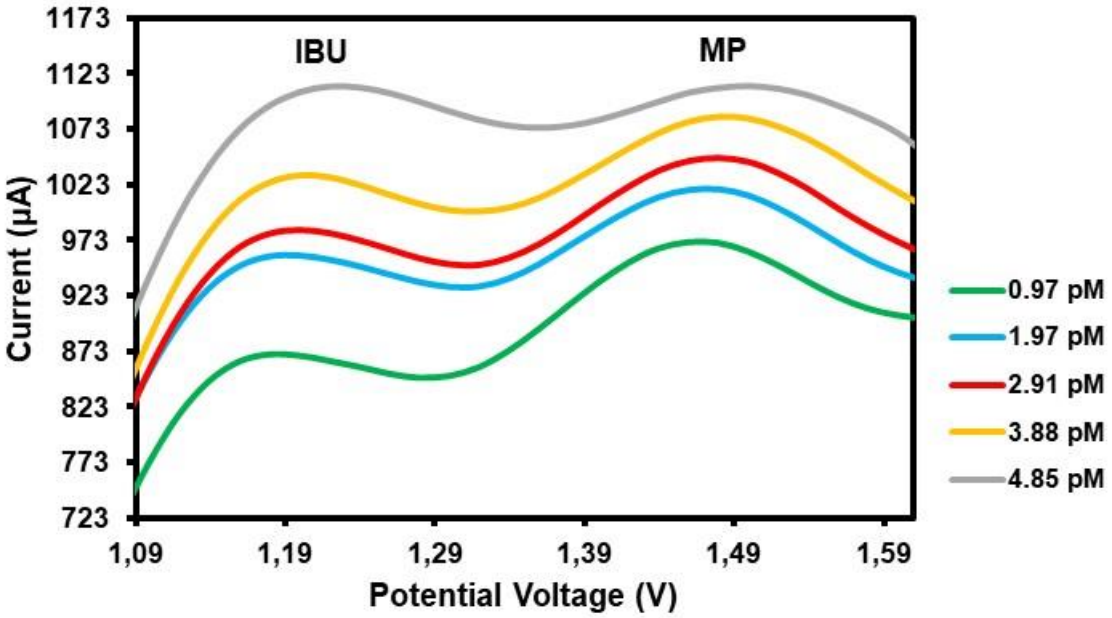

Figure 5.15: DPV voltammograms of MnO_2NPs/SPCE in pH 7.0 (0.1 M PBS) with optimized settings for the concurrent identification of IBU and MP.

5.3 Conclusion

The described electrochemical detector also has several benefits, including affordability, specificity, and simple manufacture. MnO_2NPs was successfully synthesised and characterised using analytical techniques such as XRD, SEM, UV/Vis, SAXS, FTIR and Raman spectroscopy which has a good yield. MnO_2NPs/SPCE was used as a modifier on the surface of the electrode which exhibited excellent electrochemical effectiveness. From the observation, the MnO_2NPs/SPCE has a higher peak current, which indicates faster electron transfer rates due to efficient charge transfer between the electrode and the electroactive species. The offered protocol's quantitative effectiveness was evaluated using the adjusted experimental variables for both differential pulse approach with the confirmation variable such as LOD at 0.0004 µM and 0.005 µM respectively, linear concentration range of 0.97–5.82 pM. The improved electrochemical sensor displayed excellent accuracy, rigidity, specificity, and durability. As a result, MnO_2NPs/SPCE provides a suitable electrochemical sensing platform for determining IBU and MP in real-world samples.

Reference

[1] B. Mutharani and A. Ranganathan, Palraj, Chen, Shen-ming, Chen, Tse-wei Ali, M Ajmal, Hossam, “Ultrasonics - Sonochemistry Sonochemical synthesis of novel thermo-responsive polymer and tungsten dioxide composite for the temperature-controlled reversible ‘ on-o ff ’ electrochemical detection of β -Blocker metoprolol,” *Ultrason. - Sonochemistry*, vol. 64, no. February, p. 105008, 2020.

[2] K. Wei, H. Guo, F. Fang, and X. Y. Qian, “Giant right sinus of Valsalva aneurysm led to proximal right coronary artery occlusion,” *Anatol. J. Cardiol.*, vol. 23, no. 6, pp. 350–353, 2020.

[3] D. Morales, “Quantifying the risk of beta-blockers and non-steroidal anti-inflammatory drugs in asthma,” 2014, [Online]. Available: http://hdl.handle.net/10588/56ca8828-73f6-47cc-b919-6e3e78e11a7b

[4] Simon, “Effects of the anti-inflammatory drug diclofenac and the,” 2018.

[5] K. Kümmerer, “The presence of pharmaceuticals in the environment due to human use - present knowledge and future challenges,” *J. Environ. Manage.*, vol. 90, no. 8, pp. 2354–2366, 2009, doi: 10.1016/j.jenvman.2009.01.023.

[6] S. Y. Wee, D. E. M. Haron, A. Z. Aris, F. M. Yusoff, and S. M. Praveena, “Active pharmaceutical ingredients in Malaysian drinking water: consumption, exposure, and human health risk,” *Environ. Geochem. Health*, vol. 42, no. 10, pp. 3247–3261, 2020, doi: 10.1007/s10653-020-00565-8.

[7] A. Q. Dao, D. M. Nguyen, and T. T. T. Toan, “The Modified Glassy Carbon Electrode by MWCNTs-PLL to Detect Both Paracetamol and Ibuprofen in Human Biological Fluid,” *J. Electrochem. Soc.*, vol. 169, no. 5, p. 057525, 2022, doi: 10.1149/1945-7111/ac6f89.

[8] A. Singh and S. Saluja, “Microbial Degradation of Antibiotics from Effluents,” no. July, pp. 389–404, 2021, doi: 10.1007/978-981-16-0518-5_15.

[9] S. Chopra and D. Kumar, “Ibuprofen as an emerging organic contaminant in environment, distribution and remediation,” *Heliyon*, vol. 6, no. 6, p. e04087, 2020, doi: 10.1016/j.heliyon.2020.e04087.

[10] A. Pathak and S. Mrabeti, “β-Blockade for Patients with Hypertension, Ischemic Heart Disease or Heart Failure: Where are We Now?,” *Vasc. Health Risk Manag.*, vol. 17, pp. 337–348, 2021, doi: 10.2147/VHRM.S285907.

[11] S. Habib, M. Alam, M. Mustafa, and A. Verma, “Role of Beta-Blockers as an Effective Cardio protective Agents, an insight in to Tackling with Cardiovascular Diseases (CVDs) and Hypertension,” *Researchgate.Net*, no. September, 2021, [Online]. Available: https://www.researchgate.net/profile/Abhishek-Kumar-Verma-2/publication/354694288_Role_of_Beta-Blockers_as_an_Effective_Cardio_protective_Agents_an_insight_in_to_Tackling_with_Cardiovascular_Diseases_CVDs_and_Hypertension/links/6148083f519a1a381f6fce3c/Ro

[12] M. Patel, R. Kumar, K. Kishor, T. Mlsna, C. U. Pittman, and D. Mohan, “Pharmaceuticals of emerging concern in aquatic systems: Chemistry, occurrence, effects, and removal methods,” *Chem. Rev.*, vol. 119, no. 6, pp. 3510–3673, 2019, doi: 10.1021/acs.chemrev.8b00299.

[13] J. Świacka, Klaudia, Michnowska, Alicja, Maculewicz, M. Caban, and K. Smolarz, “Toxic effects of NSAIDs in non-target species: A review from the perspective of the aquatic environment,” *Environ. Pollut.*, vol. 273, 2021, doi: 10.1016/j.envpol.2020.115891.

[14] H. Wang, Huan, Xi, M. Xu, LinlingJin, and H. Zhao, Wenlu, Liu, “Ecotoxicological effects, environmental fate and risks of pharmaceutical and personal care products in the water environment: A review,” *Sci. Total Environ.*, vol. 788, p. 147819, 2021, doi: 10.1016/j.scitotenv.2021.147819.

[15] B. M. Ţuchiu, R. I. Stefan-van Staden, and J. (Koos) F. van Staden, “Recent Trends in Ibuprofen and Ketoprofen Electrochemical Quantification–A Review,” *Crit. Rev. Anal. Chem.*, vol. 0, no. 0, pp. 1–12, 2022, doi: 10.1080/10408347.2022.2050348.

[16] O. Swiech, M. Majdecki, and R. Bilewicz, “PEGylated Network Nanostructured by Gold Nanoparticles for Electrochemical Sensing of Aromatic Redox and Nonredox Analytes,” *ACS Appl. Polym. Mater.*, 2022, doi: 10.1021/acsapm.2c01451.

[17] M. Roushani and F. Shahdost-fard, “Applicability of AuNPs@N-GQDs nanocomposite in the modeling of the amplified electrochemical Ibuprofen aptasensing assay by monitoring of riboflavin,” *Bioelectrochemistry*, vol. 126, pp. 38–47, 2019, doi: 10.1016/j.bioelechem.2018.11.005.

[18] G. Qu, Shaohua, Wu, D. Fang, Jianwu, Zang, and H. Xing, Hui, Wang, Liuding, Wu, *Dielectric and Magnetic Loss Behavior of Nanooxides*, vol. 2, no. December. 2017. doi: 10.1016/B978-0-323-46140-5.00011-X.

[19] D. Zhuang, Xuming.Chen, H. Wang, Shengnan.Liu, and L. Chen, “Manganese dioxide nanosheet-decorated ionic liquid-functionalized graphene for electrochemical theophylline biosensing,” *Sensors Actuators, B Chem.*, vol. 251, pp. 185–191, 2017, doi: 10.1016/j.snb.2017.05.049.

[20] I. Khan, M. Sadiq, I. Khan, and K. Saeed, “Manganese dioxide nanoparticles/activated carbon composite as efficient UV and visible-light photocatalyst,” *Environ. Sci. Pollut. Res.*, vol. 26, no. 5, pp. 5140–5154, 2019, doi: 10.1007/s11356-018-4055-y.

[21] R. Manjula, M. Thenmozhi, S. Thilagavathi, R. Srinivasan, and A. Kathirvel, “Green synthesis and characterization of manganese oxide nanoparticles from Gardenia resinifera leaves,” *Mater. Today Proc.*, vol. 26, pp. 3559–3563, 2019, doi: 10.1016/j.matpr.2019.07.396.

[22] M. Zhang, Jinyue, Jin, L. Park, Yong Il, Jin, and B. Quan, “Facile synthesis of ultra-small hollow manganese silicate nanoparticles as pH/GSH-responsive T1-MRI contrast agents,” *Ceram. Int.*, vol. 46, no. 11, pp. 18632–18638, 2020, doi: 10.1016/j.ceramint.2020.04.175.

[23] C. Nolly, P. Ikpo, Chinwe O. Ndipingwi, Miranda M. Ekwere, and E. I. Iwuoha, “Pseudocapacitive Effects of Multi-Walled Carbon Nanotubes-Functionalised Spinel Copper Manganese Oxide,” *Nanomaterials*, vol. 12, no. 19, 2022, doi: 10.3390/nano12193514.

[24] P. Wu, Yiyong. Deng and Q. Tian, Yaling Feng, Jinxia Xiao, Jingyun Li, Junhua Liu, Jun Li, Guangli He, “Simultaneous and sensitive determination of ascorbic acid, dopamine and uric acid via an electrochemical sensor based on PVP-graphene composite,” *J. Nanobiotechnology*, vol. 18, no. 1, pp. 1–13, 2020, doi: 10.1186/s12951-020-00672-9.

[25] M. H. Cheah and P. Chernev, “Electrochemical oxidation of ferricyanide,” *Sci. Rep.*, vol. 11, no. 1, pp. 1–7, 2021, doi: 10.1038/s41598-021-02355-3.

[26] M. Li, T. Zhang, and Y. Zhang, “Ultrasensitive electrochemical sensing platform for miRNA-21 detection based on manganese dioxide-gold nanoparticle nanoconjugates coupled with hybridization chain reaction and horseradish peroxidase signal amplification,” *Analyst*, pp. 2180–2188, 2023, doi: 10.1039/d3an00490b.

[27] M. Wang, Jiawei. Liao and B. Huang, Xinlin Li, Pengzhou Li, Jiaxin Ye, Lei Gao, Yue Peng, Huisheng Wang, “Enhanced cathode integrity for zinc-manganese oxide fiber batteries by a durable protective layer,” *J. Mater. Chem. A*, no. April, 2022, doi: 10.1039/d2ta00982j.

[28] M. Sanchez-Amaya and E. R. Bárcena-Soto, Maximiliano A-L, René R-L, Aaron Barragan, Jose Angel, Gutierrez-Becerra, Alberto L-Durán, “Effect of Wide Ranges of Polarization and Concentration on the Behavior of Ferricyanide/Ferrocyanide Systems Studied Through Electrochemical Measurements,” *Int. J. Electrochem. Sci.*, vol. 17, no. 1, p. 22016, 2022, doi: 10.20964/2022.01.11.

[29] T. Adam, Hussaini, Gopinath, Subash C.B., Md Arshad, M. K. Ramanathan, S A and U. Azan, M Isa Ahmad Adam, Tijjani, Hashim, “Fabrication of gold nanorod–zinc oxide nanocomposite on gap-fingered integrated interdigitated aluminum electrodes and their response to electrolytes,” *Appl. Phys. A Mater. Sci. Process.*, vol. 125, no. 12, pp. 1–11, 2019, doi: 10.1007/s00339-019-3106-7.

[30] B. Xiong, W. Zhao, L. Chen, and J. Shi, “One-Step Synthesis of W2C@N,P-C Nanocatalysts for Efficient Hydrogen Electrooxidation across the Whole pH Range,” *Adv. Funct. Mater.*, vol. 29, no. 31, pp. 1–9, 2019, doi: 10.1002/adfm.201902505.

[31] K. Tyszczuk-Rotko, J. Kozak, and A. Węzińska, “Electrochemically activated screen-printed carbon electrode for determination of ibuprofen,” *Appl. Sci.*, vol. 11, no. 21, 2021, doi: 10.3390/app11219908.

[32] B. Koçak, Y. İpek, and A. Keçeci, “A novel electrochemical sensor for metoprolol analysis based on glutardialdehyde–zinc oxide modified boron doped diamond electrode,” *Diam. Relat. Mater.*, vol. 131, no. November 2022, 2023, doi: 10.1016/j.diamond.2022.109558.

[33] M. R. J. Sarvestani, T. Madrakian, and A. Afkhami, “Developed electrochemical sensors for the determination of beta-blockers: A comprehensive review,” *J. Electroanal. Chem.*, vol. 899, no. July, p. 115666, 2021, doi: 10.1016/j.jelechem.2021.115666.

[34] D. Silva, Mariana, Morante-Zarcero, Sonia, Pérez-Quintanilla and I. Sierra, “Simultaneous determination of pindolol, acebutolol and metoprolol in waters by differential-pulse voltammetry

using an efficient sensor based on carbon paste electrode modified with amino-functionalized mesostructured silica," *Sensors Actuators, B Chem.*, vol. 283, no. December 2018, pp. 434–442, 2019, doi: 10.1016/j.snb.2018.12.058.

[35] L. M. Madikizela and L. Chimuka, "Occurrence of naproxen, ibuprofen, and diclofenac residues in wastewater and river water of KwaZulu-Natal Province in South Africa," *Environ. Monit. Assess.*, vol. 189, no. 7, 2017, doi: 10.1007/s10661-017-6069-1.

[36] Ľ. Švorc, I. Strežová, K. Kianičková, D. M. Stanković, P. Otřísal, and A. Samphao, "An advanced approach for electrochemical sensing of ibuprofen in pharmaceuticals and human urine samples using a bare boron-doped diamond electrode," *J. Electroanal. Chem.*, vol. 822, no. March, pp. 144–152, 2018, doi: 10.1016/j.jelechem.2018.05.026.

Chapter 6

Conclusion and recommendations

Based on the material that has been given, this chapter draws conclusions and makes suggestions for additional research.

6.1 Conclusion

The study concludes with the description of a remarkably reactive, precise, and specific MnO_2NPs/SPCE sensor for the identification of multidrug such metoprolol, carbamazepine, sulfamethoxazole, and ibuprofen. The manganese oxide nanoparticle was successfully synthesized using the hydrothermal method that yields larger quantity product. The synthesis was performed on the aqueous environment with advantages such as high purity and uniform particle size and distribution. In the synthesis, the $KMnO_4$ precursor functions as a potent oxidizing agent include its effectiveness in controlled oxidation reactions, versatility, ease of handling, availability, and its ability to facilitate the formation of specific manganese oxide phases with tailored properties. MnO_2 nanoparticle and precursors were successful characterised to evaluate the optical traits of the material involve Uv/vis spectroscopy at the spectra range from 280 to 800 nm. Further, we evaluated the band separation of the MnO_2 nanoparticle, obtained to be 1.14 eV indicates that the MnO_2NPs exhibit good electrical and optical properties. The FTIR and Raman analysis were conducted to confirm the functionality of the MnO_2NPs, which successfully displayed peaks that correspond to the material. We further evaluated the crystallinity of the material using the XRD instrument. It was discovered that the MnO_2 nanoparticles' XRD distribution and the XRD standard card (JSPDF 44-0141) agreed quite well. SEM was used to look at the MnO_2NPs' form. Utilizing the SAXS approach, the size and shape variation of the MnO_2NPs material was examined. The MnO_2NPs' PDDF, which has an average width of 86 nm and an outer diameter of 35 nm, has a rod-shaped form. MnO_2NPs served as a foundation for SPCE. Due to exceptional properties of MnO_2NPs's chemical durability and substantial surface area, the electrochemical analysis was examined. The electrochemical study was conducted for bare and modified electrode involving CV and EIS. The outcome obtained demonstrated that the CV curve showed a reversible electrochemical response of peak potential separation for bare SPCE was obtained at 0.249 V whereas the peak potential separation was 0.269 V, this suggests that the MnO_2NPs/SPCE electron exchange was rapid due to small peak potential separation, this suggests a rapid and efficient reaction at the electrode surface in comparison to an electrode that is bare which indicated the slower electron transfer. Furthermore, the EIS showed that the modified MnO_2NPs/SPCE, on the other hand, exhibits low charge transfer resistance, indicating more efficient electron transfer and better conductivity. Study was done on the optimization variables such pH, scan speed, and electrolytes. The optimum parameters used are as follows pH 7.0, 50 mV/s and PBS for the investigation electrochemical detection of the analytes. The electrochemical behaviour of CBZ, SMX, IBU and MP on MnO_2NPs/SPCE were investigated. The values of limit of the detection obtained were 0.0005 μM, 0.0002 μM, 0.0004 μM and 0.005 μM in the linear range from 0.010–0.006 μM respectively. As compared to the previous studies of the electrochemical performance, the LOD shows an accurate, precise, and sensitive response of the MnO_2NPs/SPCE sensor. The wastewater samples were analysed for the application of MnO_2NPs/SPCE sensor. Between 95% and 11% of the samples showed significant CBZ turnarounds, suggesting that the MnO_2NPs/SPCE sensor had considerable potential for environmental monitoring applications. With yields of recovery ranging from 90 to 105%, the suggested electrochemical detector can reliably and accurately measure the amounts of SMX in effluent samples. Through the assessment of the interfering species and the sensor's stability analysis, the electrochemical efficiency of the MnO_2NPs/SPCE sensor was investigated. The outcome obtained for the interfering studies was that the interfering species were oxidized at different potentials, indicating that their oxidation did not overlap with the potential range used for the detection of the CBZ

same observation for SMX. Furthermore, CBZ and SMX were simultaneously detected using the MnO_2NPs/SPCE sensor.

6.2 Recommendations for future study

Below is a study of additional research on MnO_2NPs-based electrochemical sensors and their uses.

- Investigate different synthesis methods such as hydrothermal, sol-gel, co-precipitation, and chemical vapour deposition to determine their impact on the properties of MnO_2.
- Fine-tune parameters such as temperature, pH, precursor concentration, and reaction time to achieve the desired crystallinity, particle size, and morphology of MnO_2.
- Examine the influence of MnO_2 morphology (e.g., nanowires, nanoparticles, nanosheets) on the sensor's sensitivity, selectivity, and response time.
- Investigate the role of different crystal facets of MnO_2 in catalytic and sensing activities. Surface engineering can expose specific facets that are more reactive and enhance sensor performance.
- Use advanced characterization techniques like high-resolution transmission electron microscopy (HRTEM) and X-ray photoelectron spectroscopy (XPS) to gain insights into the structural and chemical properties of MnO_2.
- Test the optimized MnO_2 sensors in real-world conditions to evaluate their performance, stability, and reliability.
- Investigate the long-term stability and repeatability of MnO_2 sensors to ensure they can maintain performance over extended periods.
- Explore the integration of the MnO_2NPs-based electrochemical sensor with passive sampling techniques. This integrated system could provide a thorough method for actual time monitoring of specific analytes in various environmental or biological samples, providing a more accurate representation of the target analyte concentrations.